Modelling of roll compaction process by finiite element method

Alon Mazor

Université Fédérale

Toulouse Midi-Pyrénées

THÈSE

En vue de l'obtention du

DOCTORAT DE L'UNIVERSITÉ DE TOULOUSE

Délivré par

IMT - École nationale supérieure des Mines d'Albi-Carmaux

Présentée et soutenue par

Alon MAZOR

le 1er décembre 2017

Modelling of roll compaction process by finite element method

---

École doctorale et discipline ou spécialité :

MEGEP : Génie des procédés et de l'Environnement

Unité de recherche :

Centre RAPSODEE, UMR CNRS 5302, IMT Mines Albi

Directeurs de thèse :

Abderrahim MICHRAFY

Alain DE RYCK

Membres du jury :

Jean-Yves DELENNE, Directeur de Recherche, INRA *(Président)*

Chuan-Yu WU, Professeur, Université de Surrey *(Rapporteur)*

Olivier BONNEFOY, Professeur, Mines Saint-Étienne *(Rapporteur)*

Christine ESPINOSA, Maître de Conférences, Université de Toulouse *(Examinateur)*

Abderrahim MICHRAFY, Ingénieur de recherche, CNRS, IMT Mines Albi (Directeur)

Alain DE RYCK, Professeur, IMT Mines Albi (Co-directeur)

Contents

This page intentionally left blank.

Abstract

In the pharmaceutical industry, dry granulation by roll compaction is a process of size enlargement of powder into granules with good flowability for subsequent die compaction process. Understanding the roll compaction process and optimizing manufacturing efficiency is limited using the experimental approach due to the high cost of powder, time-consuming and the complexity of the process.

In this work, a 3D Finite Element Method (FEM) model was developed to identify the critical material properties, roll press designs and process parameters controlling the quality of the product. The Drucker-Prager Cap (DPC) model was used to describe the powder compaction behavior and was determined based on standard calibration method. To overcome the complexity involving two different mechanisms of powder feeding by the screw and powder compaction between rolls, a novel combined approach of the Discrete Element Method (DEM), used to predict the granular material flow in the feed zone and the Finite Elements Method (FEM) employed for roll compaction, was developed. Lastly, for a more realistic roll compaction modelling, allowing the fluctuation of the gap between rolls, a Coupled-Eulerian Lagrangian (CEL) approach was developed.

FEM simulation results clearly show the effect of different process parameters on roll pressure and density distribution in the compaction zone of powder between the rolls. Moreover, results show that using a cheek-plates sealing system causes a nonuniform roll pressure and density distribution with the highest values in the middle and the lowest at the edges. On the other hand, the resultant pressure and density distributions with the rimmed-roll obtained higher values in the edges than in the middle and overall a more uniform distribution. The combined DEM-FEM methodology clearly shows a direct correlation between the particle velocity driven by the screw conveyor to the feed zone and the roll pressure, both oscillating in the same period. This translates into an anisotropic ribbon with a density profile varying sinusoidally along its length. To validate the results, the simulations are compared with literature and experimentally measured values in order to assess the ability of the model to predict the properties of the produced ribbons.

This page intentionally left blank.

Resumé

Dans l'industrie pharmaceutique, la granulation sèche par compactage à rouleaux est un procédé d'agglomération de poudres en granulés pour améliorer les propriétés d'écoulement nécessaire pour le procédé de compression en matrice. Comprendre le procédé de compactage à rouleaux et optimiser l'efficacité de production est limitée par l'utilisation de l'approche expérimentale à cause du coût élevé des poudres, le temps des essais et la complexité du procédé.

Dans ce travail, une méthode d'éléments finis en 3D, est développée dans le but d'identifier les paramètres critiques du matériau et du procédé pour le contrôle de la qualité de la production. Le modèle de comportement de Drucker-Prager Cap est utilisé pour décrire le comportement en compression de poudres et sa calibration est déterminée à partir des essais standard. Pour surmonter la complexité liée à l'existence de deux mécanismes différents, l'alimentation en poudre par une vis sans fin et le compactage entre les rouleaux, une nouvelle méthode d'interfaçage entre la méthode des éléments discrets (DEM) employée pour décrire l'écoulement dans l'alimentation et la méthode des éléments finis (FEM) utilisée pour le compactage entre les rouleaux est développée. Enfin, pour une modélisation de compactage de rouleaux plus réaliste, prenant en compte la variation de l'entrefer entre les rouleaux, une nouvelle approche de couplage Euler-Lagrange est proposée.

Les résultats de simulations par éléments finis montrent clairement l'effet des différents paramètres du procédé sur les distributions de pression et de densité dans la zone de compactage. En outre, les résultats montrent que l'utilisation de plaques de confinement de la poudre entre les rouleaux, développe une distribution de pression et de densité non homogène dans le compact, avec une densité plus élevée au centre et plus faible aux bords. D'autre part, l'utilisation de rouleaux dont l'un est surmontée d'une jante de confinement, a montré une distribution de propriétés globalement plus uniforme sur la largeur du compact avec des valeurs légèrement plus élevées aux bords qu'au centre. La méthodologie combinant les méthodes DEM & FEM montre

clairement une corrélation directe entre la vitesse des particules entraînées par la vis dans la zone d'alimentation et la pression du rouleau. Tous les deux oscillent avec la même période. Cela se traduit par un compact anisotrope avec un profile de densité variant de manière sinusoïdale le long de sa largeur. Afin d'étudier la capacité du modèle à prédire les propriétés des compacts produits par compactage à rouleaux, les prédictions par simulations numériques sont comparées aux données de la littérature et validées par des mesures spécifiques.

Acknowledgments

I would like to express my appreciation and gratitude to the main supervisor of this Ph.D. study, Dr. Abderrahim Michrafy, for his guidance and support during the term of my candidature. Without his valuable assistance, such as academic supervision, administrative support, and friendship, this work would not have been completed. On the same note, I would also like to thank the co-supervisor of this work, Prof. Alain deryck.

In fact, I wish to thank all of the Research Centre on Particulate Solids, Energy and Environment (RAPSODEE) of the École des Mines d'Albi. In particularly, special thanks goes to my colleague, Dr. Lucia Perez-Gandarillas for all her support and friendship throughout my period in Albi.

Most importantly, I would like to thank my lovely wife Liza, for her unconditional support and encouragement towards obtaining scientific achievements and success.

This page intentionally left blank.

Introduction

In the pharmaceutical industry, the roll compaction process is used for dry granulation, densifying fine powders into large dense granular thus improving flowability for direct compression and minimizing dust problems[1]. Densifying the powder is done by passing between two counter-rotating rollers, which applies mechanical pressure on the powder. The friction between the feed material and roller surface pushes the powder to a narrow gap, where the powder is subjected to high stresses leading to the formation of compacted ribbons. The roll pressure in the gap region during roll compaction has the most significant impact on the porosity of the ribbons. Ribbon's density, i.e., solid fraction, is one of the critical quality parameter of the roll compaction process that influences the compactibility of granules during tablet formation. The roll compaction system design and operating conditions have a direct effect on the produced ribbon's quality. In order to ensure the consistency, reproducibility and quality of the final dosage form, it is important to ensure the quality and avoid heterogeneity of the produced ribbon.

Numerous studies have already been performed to investigate the roll compaction process. However, this is mainly done by experimental trial-and-error, which uses valuable human resource, machine and material cost. For this, several analytical models have been developed and able us to have a better understanding of the process. These analytical models are still limited and this gave way to more complex mathematical modelling of the process.

Over the past two decades, Finite Elements Method (FEM) modeling were adopted and further developed to simulate pharmaceutical forming processes. FEM models of powder roll compaction process which started considering a plane strain two-dimensional case[2, 3, 4, 5], founded to be comparable and more accurate than the one-dimensional analytical Johanson[6] and Slab method[7, 8] models. With the increasing computational power in the last years, the development of three-dimensional models provided greater insight on the pressure and density distribution during the roll compaction processes[9, 10, 11].

Objective and scope

The aim of this work is to investigate by FEM modelling the roll compaction process and the effect of both the process parameters and the system design, such as sealing system and screw conveyor. More specifically, the objectives of this thesis include:

- Characterizing the microcrystalline cellulose (Avicel PH 101) powder in a continuous manner by the Drucker-Prager Cap constitutive model, with density-dependent properties. Following by three-dimensional FEM modelling to study the effect of different process parameters and to validate the models based on previous studies in the literature.

- Studying the effect of sealing system design (Rimmed-roll or cheek-plates) based on current FEM approach and validates the results experimentally.

- Developing new approaches of a combined DEM-FEM and Coupled-Eulerian Lagrangian (CEL) methods in order to investigate the effects of screw conveyor and floating roll, respectively, on the roll compaction process. These approaches can be very useful in modelling a continuous process, which has a great interest nowadays in order to replace the more conservative batch process.

Outline

The following outline gives an overview of the main points discussed and studied in this thesis.

Introduction of roll compaction as part of the dry granulation process and its functionality. A short description of the process itself is described together with emphasizing the lack of knowledge still exists in this field, which needs to be further studied. This follows by the objective and the outline of the thesis work.

Chapter 1 starts by a short history briefing roll compaction and its relatively recent application in the pharmaceutical industry as part of the dry granulation process. Then, the theoretical background and the effect of roll compaction process conditions on the resulted ribbons are presented. Lastly, the chapter describes numerical approaches used to investigate the process including, theoretical background, recent advances and current modelling limitations.

Chapter 2 elaborates the material and methods used in order to model the roll compaction process using the finite element method. This includes a description of the roll compactors and powder used in this work. Most importantly, the procedure of modelling the roll compaction process using FEM including characterizing and implementing the powder as continuous material was described extensively.

Chapter 3 is divided into two main parts. First, Three dimensional FEM analysis of the effect of different process and simulation parameters on roll compaction is conducted widely and further discussed. The second part of this chapter focuses on modelling the effect of different sealing system design (rimmed-roll and cheek plates) on the process, which was compared and validated experimentally

Chapter 4 introduces a novel three dimensional modelling of the entire roll compaction process by including both the screw feeding and roll compaction unit in a combined DEM & FEM modelling approach.

Chapter 5 describes a newly developed Coupled Eulerian-Lagrangian (CEL) approach for a more realistic roll compaction modelling. In this method, a floating roll and the ejection and production of final ribbon product can be modelled.

General conclusions and perspectives part discusses and concludes the main results obtained in the thesis, finalizing with few perspectives in order to motives current and future scientists and researchers to continue developing this field of study.

This page intentionally left blank.

Chapter 1

Background

Abstract

This chapter starts with a brief history on the roll compaction process and its development throughout the last two decades. The use of trial and error was routinely employed to understand the roll compaction process and to solve the quality by design in the manufacturing process. The effect of process parameters, bulk powder properties, sealing and feeding systems on the roll compaction process are investigated numerously in the literature and presented in this chapter. Nonetheless, the overall understanding of roll compaction process has not yet been fully achieved. The second part of this chapter describes analytical models, followed by more sophisticated computer modelling approaches using the Finite Element Method (FEM) for a better understanding of the roll compaction process. Lastly, the theoretical background of this FEM modelling approach is introduced and summarized.

Resumé

Ce chapitre introduit un bref historique sur le processus de compactage à rouleaux et son développement au cours des deux dernières décennies. Pour répondre à la qualité du produit par la conception du procédé de compactage à rouleaux, les tests essai-erreur sont classiquement utilisés. Dans ce chapitre, on présente l'état de l'art de la littérature sur l'effet des paramètres du procédé, des propriétés de la poudre, des systèmes de confinement des rouleaux et du système d'alimentation sur le processus de compactage par presse à rouleaux. Il découle de cette revue que, la compréhension du processus de compactage à rouleaux est loin d'être achevée. La seconde partie de ce chapitre décrit les apports des approches analytiques et les approches numériques basées sur la méthode des éléments finis pour une meilleure compréhension du procédé. Enfin, un résumé des bases théoriques de cette approche numérique est présenté.

1.1 History of roll compaction

The first roll compaction process of producing a metal strip by powder was accidentally discovered by the English inventor and Engineer, Sir Henry Bessemer in 1843 when he was trying to make brass flake pigment from brass powders [12]. Henry Bessemer did not pursue this work, and it was not until 1902 that a patent application for making tantalum strip from powder was filed in Germany and was granted to Siemens and Halske [13]. Patents were also issued by Hardy (1938)[14] and Marvin (1941)[15] for rolling of metal powder fed horizontally and vertically, respectively. The real stimulus to develop roll compaction of powders for making metal strip came only after the publication of the classic paper by Naeser and Zirm in 1950 [16], in which they described a powder rolling process for making iron strip from iron powders. Evans and Smith at the University of Cambridge and Franssen in Germany showed that copper powder can also be processed into strip in a similar manner. A detailed evaluation of the process was published in 1959. The engineering and economic aspects of the process started attracting attention from research workers in the late 1950s.

During the 1960s, dozens of theoretical and experimental studies on roll compaction of metallic powders were conducted in the Soviet Union [17]. During the same period, Tundermann and Singer [18] at the University College of Swansea, UK, and Kimura et al. [19] at the Toyota research center, Japan, carried out a detailed and systematic investigation on the various aspects of roll compaction. By 1968, roll compaction had gained sufficient importance among the new processes developed by that time, and was the main topic of a conference held in Swansea on 'Powder rolling and associated new techniques of powder production'.

In the past 50 years, roll compaction has been widely used as part of the dry granulation process in the pharmaceutical industry [1]. However, only recently it has been subjected to an extensive study and investigation.

1.2 Dry granulation

As introduced previously, in the pharmaceutical industry, the roll compaction process is used for dry granulation, densifying fine powders into large granular, thus improving flowability for direct compression and minimizing dust problems[1].

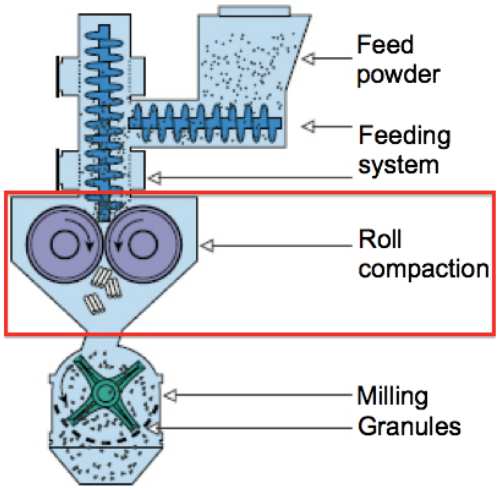

Figure 1.1: Scheme of a typical dry granulation process [20]

The dry granulation process includes several sub-processes in which powder is being fed to the roll compaction unit, resulting in dense ribbons, which will be milled into large granules. These granules are larger than the original feed powders and exhibit better flowability. This is necessary, as the granules will be filled into a die and will be compacted to produce tablets (i.e. oral dosage forms).

Understanding the roll compaction process is essential in optimizing manufacturing efficiency and product quality.

1.2.1 Roll compaction overview

Roll compaction is a continuous process for densifing powder by passing between two counter-rotating rolls, which applies mechanical pressure on the powder. The compactor typically consists of a screw feeding system, two rolls and a sealing system (Fig. 1.2).

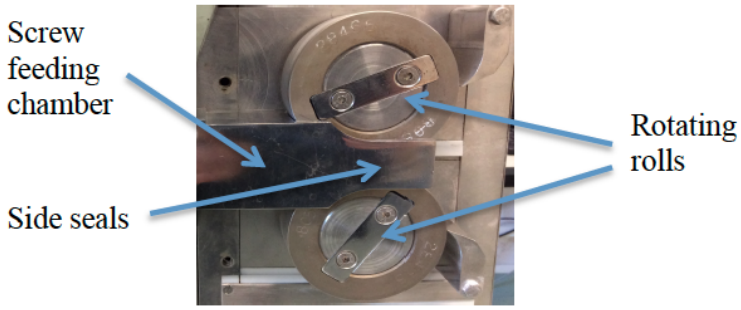

Figure 1.2: Side view of roll compactor Komarek B050H

The roll compaction system design and operating conditions have a direct effect on the produced compacted ribbon's quality. Understanding fully the process and its variables assists in controlling the process parameters and raw material specification. Thus ensuring the consistency, reproducibility and quality of the produced ribbons. There are several known common problems in the roll compaction process. Heterogeneity of the produced ribbon due to the screw feeding and sealing system, uncertainty in the scaleability of the process due to a wide range of process parameters and a strong dependency on the feed powder properties.

Roll compactors can be found in different designs that differ between suppliers. The designs have a direct effect on the produced ribbon quality. There are different sizes of rolls and mounting position on the press: horizontal, vertical or inclined. Both of the rolls may be fixed or one fixed and one movable roller. The surface of the roll can be smooth, knurled or pocket design (Fig. 1.3) in order to alter the interaction between powder and rolls[1-3]. As the roll compaction press applies pressure on the powder only from the rolls, a sealing system is mounted in order to

avoid material lose. Another source of leakage is the production of excessive fines in the compaction process due to powder feed variability at the nip and in the roll gap regions. The most commonly used sealing system is the side seals (chick plates), which are fixed and positioned in between the rolls. The use of side sealing showed that the powder is not adequately and uniformly delivered to the gripping and compaction zone. This occurred as the side seals preventing the powder flow and causes an uneven compaction across the ribbon's width. Moreover, side seals may have a negative effect on the ribbon with fractured or incomplete compacted edges [4-6]. In order to avoid the problems caused by side seals, some roll compactors such as Gerties® Minipactor have a rim-roll sealing system. The rim-roll is basically a ring, which is mounted on the bottom roll and acts as a sealing in the compaction region.

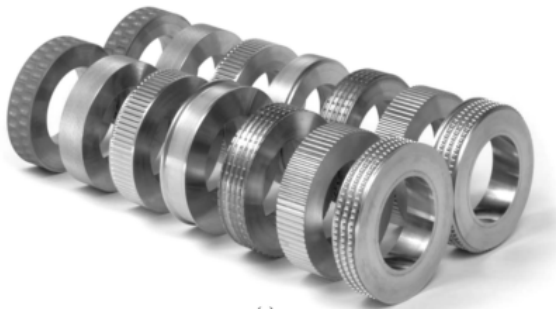

Figure 1.3: Different possible roll surfaces [The Fitzpatrick Company]

As mentioned, uneven powder feed causes leakage, i.e, uncompacted powder particles. Therefore, it is often needed to recycle the uncompacted powder or fines which increases the production time and cost. In order to achieve a uniform and consistent produced ribbon, it is important to control the compaction process by setting a constant powder feeding rate. Controlling the powder feed can be done either by using multiple horizontal feed screws, providing more uniform feeding or by variating some of the process parameters until reaching the desired roll separation force.

In conclusion, the different roll compactors not only differ in their design, they are also offer different critical processing variables that control the quality of the

produced ribbon. The main processing variables are: compaction pressure/force (per cm), screw feeding speed, roller speed, roller surface, roll gap and deareation capability with vacuum.

1.2.2 Powder compaction theory

Powder compaction depends on several physico-chemical properties. Except for particle properties such as size, shape and surface texture, the inherent ability of the powder to reduce its volume during compression could affect the amount of interparticulate attraction in the final compact. A decrease in compact porosity with increasing compression load is normally attributed to particle rearrangement, elastic deformation, plastic deformation and particle fragmentation [21]:

- Particle rearrangement - occurs initially in the feeding zone as powder fills void spaces. Air leaves the powder interstitial spaces and the particles move closer together which leads to an increase in density. Particle shapes and sizes are the dominant factor in this stage.

- Particle deformation - both elastic and plastic deformations occurs with increasing compressional forces leading to an increase in contact points between particles.

- Particle fragmentation - at higher compressional forces, particles fracture thus creating multiple new surface sites and contact points. When the applied pressure is further increased, the smaller particles formed could again undergo deformation.

- Particle bonding - once the plastic deformation and fragmentation occurs, particles bond by van der Waals forces and mechanical interlocking.

The Bonding surface area can be regarded as the effective area that is involved in the interaction between particles. The surface area changes due to fracture and flow and is dependent on the material's porosity. The particle size, shape and surface

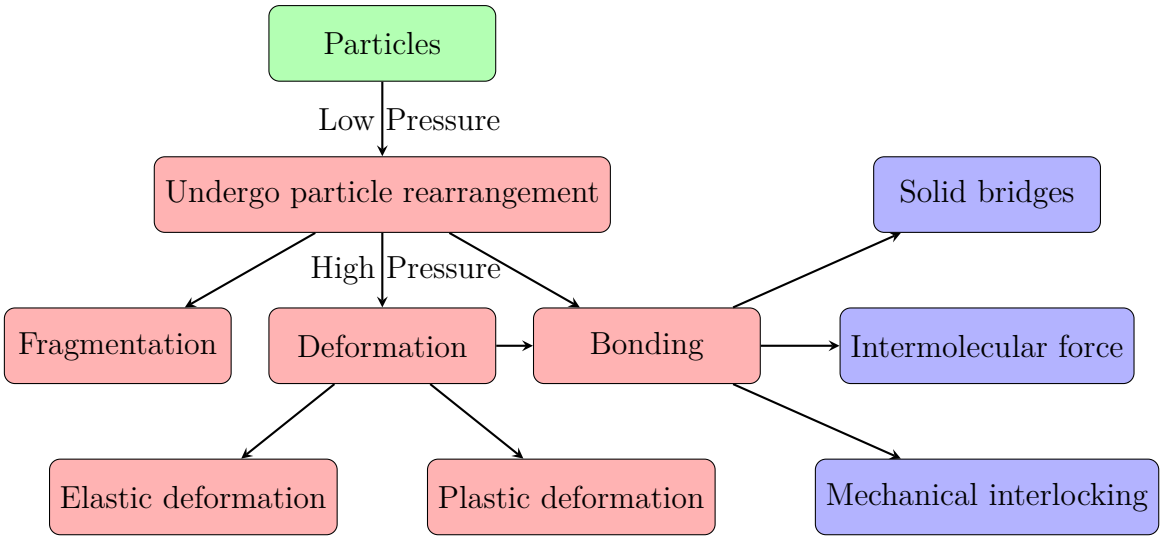

Figure 1.4: Flowchart of powder compaction

energy along with understanding the compaction mechanism gives the information for powder compaction. An appearance of respectively large forces joining individual grains is the necessary condition of formation a stable agglomerate. Rumpf H. [22] divided the mechanisms of grains binding into 5 categories.

- **Solid bridges** - formed between two particles by process such as crystallization of amorphous portions of solid, sintering, or chemical reactions.
- Movable liquids - related to surface tension forces and is more dominated with presence of high moisture content.
- Non-freely movable binders - Viscous binders and adsorption layers used in wet granulation process.
- **Attraction between solid particles** - Intermolecular forces include van der Waals forces, hydrogen bonding and electrostatic forces, created during the plastic deformation or fragmentation of particles [23].

- **Mechanical interlocking** - between irregular shaped particles and is mainly depends on the size and shape of the particles.Smooth spherical particles will have little tendency to interlock, whereas irregularly shaped particles might be expected to do so [24].

While all these binding mechanisms can be regarded as of significance, in the case of compaction of dry, crystalline powder, it has been suggested that solid bridge formation, intermolecular forces and mechanical interlocking are dominant [25]. Solid bridges correspond to the strong bonding mechanism, having a contact at an atomic level between adjacent surfaces. The intermolecular forces include the more dominant van der Waals interaction and the mechanical interlocking corresponds to the more weaker bonds, acting over distances.

The mechanism of compaction not only depends on the powder properties [26] but is also affected by particle size [27], shape [28], moisture content [29] and experimental conditions, e.g. applied pressure [30] and velocity of compaction [31]. In addition, the properties of the resulting compact can be influenced by the presence of a lubricant and binder [32].

1.2.3 Description of roll compaction process

Rolling compaction of powder, unlike sheet metal, results in a varying of yield stress and therefore it is difficult to determine the area of contact in between the powder and rolls. Evans et al. [33] was the first to investigate the powder compaction behaviour in roll press. He describes the process by dividing the zone between the rolls into two regions. In the beginning, powder is fed in between the rolls and slip occurs between particles at least up to an angle α on the roll surface, named as the gripping angle (or nip angle). An illustrated description of the process is shown in Fig. 1.5. Where zone 1 contains the powder from the feeding angle θ to the point where it begins to be gripped by the rolls. Zone 2 contains the powder between this point and the minimum gap region.

Obtaining the value of gripping angle is done by stopping the process before all the fed powder is compacted and removing the uncompacted powder. Evans noticed

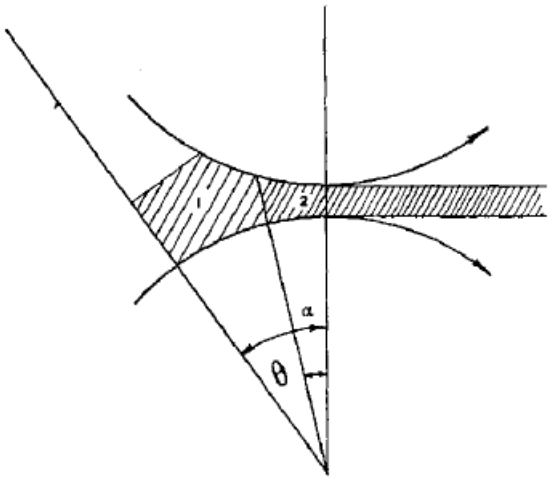

Figure 1.5: Schematic representation of roll compaction. Zone 1: incoherent powder; zone 2: coherent powder [33].

that the gripping angle varies for different particle shapes, which suggest that slipping of particles plays and important part in powder roll compaction. This variation in the gripping angle with particle shape, may be attributed to particle/roll friction, since particles of the same general shape by different mean particle sizes showed the same gripping angle. Furthermore, even when the powder has passed the point of gripping, its yield stress varies and increases as the bonding between particles increases and work-hardening proceeds. The increased bonding reduces the possibility of relative particle movement. Increasing the roll/powder friction, results in an increasing gripping angle, α. The factors mostly likley to affect roll/particle friction are: (a) roll surface roughness, (b) Temperature of rolling, (c) Feeding pressure of powder to the rolls, and (d) the roll speed. Later it was found that the gripping angle decreases with increasing roll speed and with increasing roll gap [34].

Later on, a deeper investigation of the roll compaction process was conducted and founded that the powder behaviour under the rolls may be divided into three zones [17]. In fact this was only due the division of the second zone described earlier into two different regions, defined by the neutral angle (or axis) β. In this description, the nip region ends at the neutral angle where the roll pressure reaches a maximum value

and the frictional shear stress at the roll surface reverses direction. After the neutral angle, the release region begins and the pressure decreases rapidly. In most cases, the neutral angle does not coincide with the minimum roll gap and is a function of material properties.

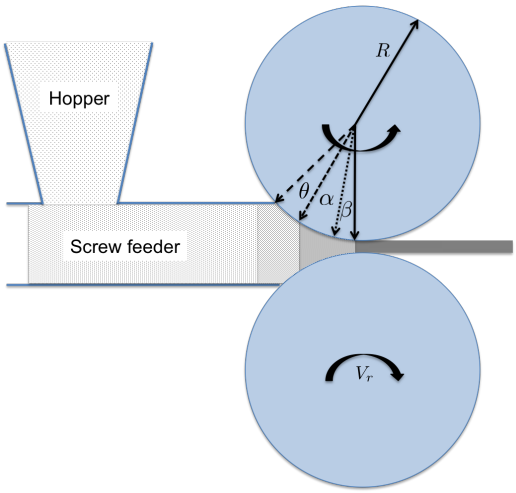

Figure 1.6: Schematic representation of roll compaction represented by three angles under the rolls.

1.2.4 Experimental studies of roll compaction

First experimental studies of pharmaceutical roll compaction process were conducted in 1966 by Cohn et al. and Jaminet and Hess. Cohn et al. [35] investigated the effect of oil pressure on the amperage of roll compaction, amount of non-compacted material and hardness of the tablet. It was found that the leakage of powder cause large problems and that there is no simple relationship between the input variables and output variables. However, an optimal setting of the output variables were found. Jaminet and Hess [36] investigated the effect of different binders on the properties of briquettes, granules and tablets. The most important findings that was obtained is that roll compaction process parameters and briquettes strength strongly determined the particle size distribution of the granules. The use of trial and error was routinely employed to understand the roll compaction process and to solve the

quality by design in the manufacturing process. The effect of process parameters, bulk powder properties, sealing and feeding systems on the roll compaction process were investigated.

1.2.4.1 Effect of powder properties and process parameters

As mentioned, Jaminet and Hess [36] were one of the first experimental team working on roll compaction process. Several important finding were obtained. The addition of binders to lactose starch mixtures resulted in the significant decrease of non compacted material. Moreover, the addition of small amount of water decreased the amount of non compacted material and weakened the briquettes. Inghelbrecht and Remon [37] evaluated the effect of process parameters on the granule properties. It was reported that roll hydraulic pressure had the most significant influence on the granules, followed by roll speed and horizontal screw speed. The powder type, particle size and density determined the design space of the roll compaction process parameters, where usually the best compaction quality was achieved at high roll pressures and low screw speeds. Mansa et al. [38] investigated the effect of roll speed and gap width on the compaction behavior of MCC 101, DCPA and their mixtures. It was found that an increase in the effective friction angle and cohesion of the feed powder resulted in an increase of the nip angle, whereas, an increase in the roll speed resulted in a decrease of nip angle. The ribbon's relative density increased with increasing roll pressure at low roll speeds (1-3 rpm), especially for the MCC. Bindhumadhavan et al. [39] investigated the effect of gap width on the compaction behavior of MCC 102 using a gravity fed roll compactor. They found that the maximum pressure was quite sensitive to the variation of the flow properties of the feed powders, and increased with increasing wall friction between powder and roll surface. Miguelez-Moran et al. [40] exmined the effect of lubrication during roll compaction of MCC using magnesium stearate (MgSt). It was observed that wall lubrication did not affect the average ribbon density. On the other hand, bulk lubrication resulted in lower maximum pressure and nip angle.

1.2.4.2 Effect of sealing system

The roll compactors are constructed with a sealing system, limiting the loss of powder from the sides[1]. However, the sealing system may result in unwanted non-uniform properties along the ribbon's width and may also exhibit fractured or incomplete compacted edges. Numerous experimental studies were conducted in order to evaluate the density distribution of roll compacted ribbons using destructive and non-destructive methods. The studies were conducted on pharmaceutical powders using laboratory roll compactors integrated with fixed side seals (cheek plates), evaluating the density distribution (Fig. 1.7) by micro-indentation[40], ultrasonic[41], x-ray tomography [41, 40], near infrared chemical imaging[42, 43] and pressure gauges[10, 44]. Results showed non-uniformity along the ribbon's width with lower densification at the edges and higher at the middle of the produced ribbon.

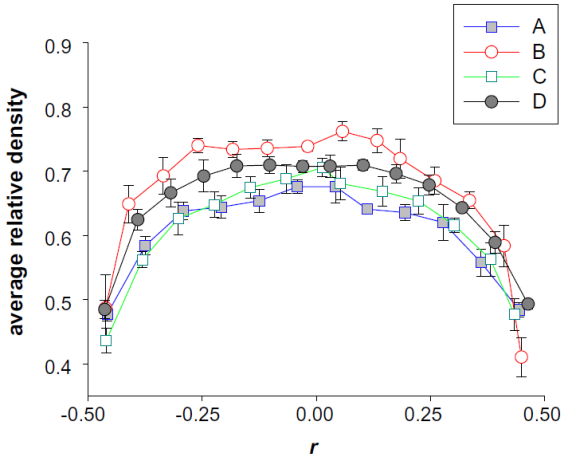

Figure 1.7: Density variation along the ribbon width obtained using micro-indentation with different roll gap (1mm (A,C,D) and 0.9 (B)) and roll speed (6 rpm (A,B) and 3 rpm (C,D) [40]

Moreover, cheek plates may also have a negative effect on the ribbon with fractured or incomplete compacted edges. Funakoshi [45] developed a roll compactor with concave-convex roll pair in order to avoid the loss of powder and to reduce the ribbon's heterogeneity. The compaction pressure distribution obtained for convaco-convex rolls showed an overall uniform distribution compared to the flat rolls which

obtained a higher compaction pressure at the middle and lower at the edges. Based on the same mechanics, several roll compactors offers a rimmed-roll sealing system in order to reduce the cheek plates unwanted effects.

1.2.4.3 Effect of feeding system

The conveying of powder in between rolls have a large influence on the roll compaction process. Experimental work showed that the delivery of powder by a screw feed is linearly related to the screw speed [9, 46, 47]. Once reaching a certain minimum screw speed the powder is fed sufficiently to the rolls, assuring a proper compaction. At higher screw speeds, the throughput is lower then the theoretical screw conveying throughput(without rolls) as shown in Fig.1.8. This may indicate that the conveyed powder exhibit a counter pressure from the roll, thus limiting the throughput.

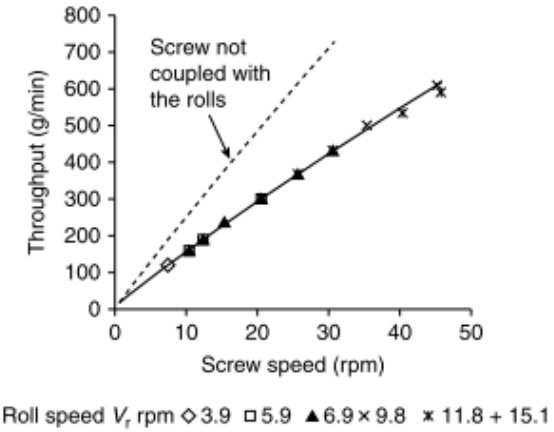

Figure 1.8: Screw throughput as a function of screw speed [47]

Simon and Guigon [47] also showed that by using a single feed screw, the resultant compacted ribbon was neither homogeneous on the ribbon width nor with time. They characterize the heterogeneity using light transmission through a sodium chloride compacted ribbon (Fig.1.9). Moreover, this fluctuation have the same period of the screw rotation.

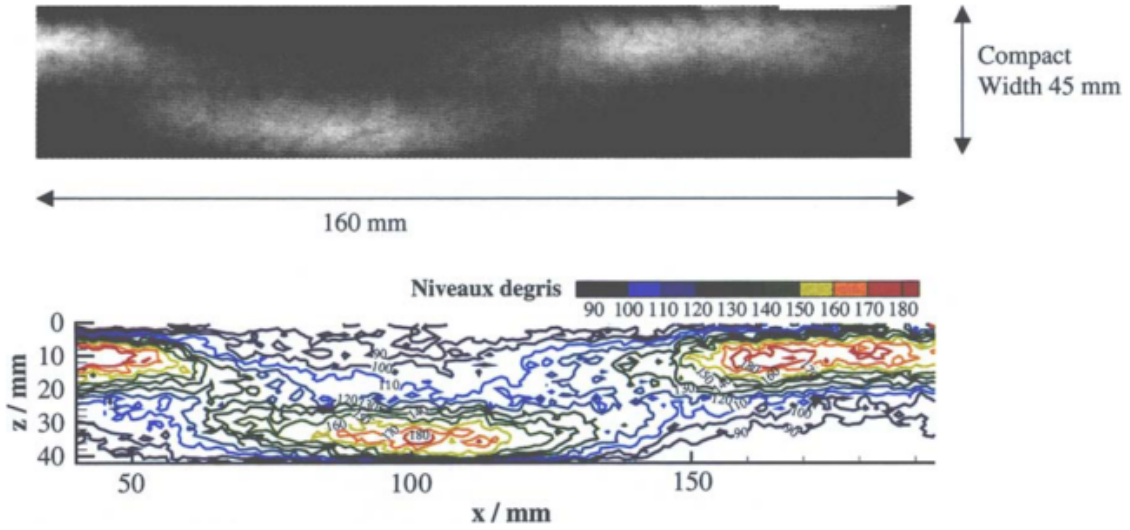

Figure 1.9: Light transmission through a sodium chloride ribbon (top) and iso-levels of the light transmission (bottom) [47]

Michrafy et al. ([9]) found similar ribbon heterogeneity for a screw feeding. They performed roll compaction experiments on MCC (Avicel PH 102) using a vertical-layout roll compactor combined with a horizontal feeding screw. They analysed the density homogeneity of the ribbons also using light transmission (Fig. 1.10) and mercury porosimetry measurements. Both approaches resulted in heterogeneity of the density across ribbon width: the light transmission revealed periodic heterogeneity shown by darker and lighter zones of the compacted strip as in the work of Simon and Guigon. On the other hand, the mercury porosimetry showed higher densities at the central part of the compact and lower densities at the sides.

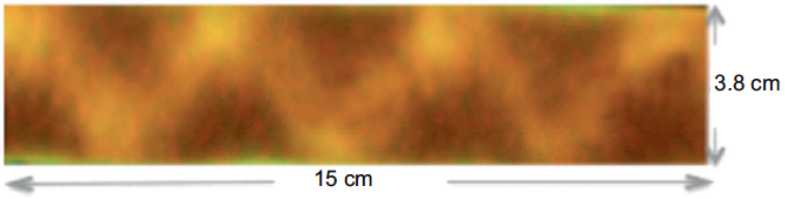

Figure 1.10: Results of light transmission through the depth of MCC ribbon [9]

On the contrary, Lecompte et al. [48] did not observed this variation due to the screw feeding rotation, using a similar roll compactor and instrumentation. It was suggested that increasing the distance between the last flight of the screw and the rolls reduce the unwanted effect of the screw rotation. It was also observed that using different combination of process parameters (screw speed,roll speed and gap) may help homogenize the power feeding. Increasing the amount of powder entering the nip angle by increasing the screw speed, reducing roll speed and using a narrow gap will result in a more evenly distributed powder along the ribbon width.

1.2.4.4 Effect of powder de-aeration

One of the key factors limiting compaction quality and throughput, although often neglected in studies, is the air entrapment during roll compaction process. In rolling, the air or other gases evolved during compaction passes through the powder mass, fluidize the powder feed, and thereby restrict velocity. The air entrapped in the powder mass can be escaped by two paths only. Either through the powder in a direction counter-current to the feed, and/or through the gap between the rolls and the cheek plates. Certain amount of air can also be compressed inside the compact itself, without being escaped. This results in limiting the compaction throughput, as well as non-uniformity in the ribbon density. Moreover, entrapped air may result in ribbons bursting, breakage or irregularly shape pieces and is usually associated with a popping sound [49].

Worn and perks [50] found that when rolling was carried out under different gas atmospheres, it could be shown that the lower the viscosity of the gas, the greater was the flow rate of powder to the compaction zone. It was also established that strip thickness and density were affected by varying the gas pressure. Vinogradov and Fedorchenko [51] conducted tests in vacuum (10-3- 10-4rp.m Hg), which produced strip of increased thickness and density. They maintained that the use of vacuum in rolling removes the counterflow effect and increases inter-particle friction and friction between the powder and the roll surfaces. It was demonstrated that a

$44\mu m$ iron powder, which could not be rolled under atmospheric conditions, could be rolled under 150 mm Hg air pressure, or under a vacuum of 1 mm Hg. Rolling powder under vacuum produced thicker and denser ribbons than could be obtained from coarse powder rolled under the same conditions. As would be expected, the disturbance caused by gas evolution increases as the rolling speed is increased [52].

Johanson et al. [53] analyzed the effects of roller speed and permeability on air pressure in the compacted sheet using a roll compactor with screw feeder (Fig.1.11). It was shown that air entrainment does not limit roller speed for coarse granular material, and only insignificantly influences the choice of roller speeds for moderately permeable coarser powder, but leaves only a small range of very low speeds for impermeable fine powders [49].

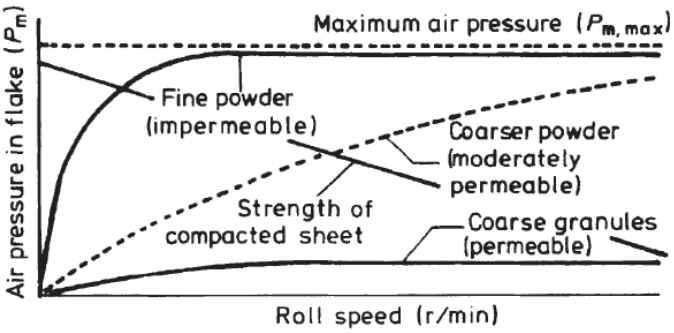

Figure 1.11: Effect of roller speed and permeability on air pressure in compacted sheet [53]

Modelling such complex multi-physic problem is challenging due to the coupling of solid-gas phases. Esnault et al., [54] further developed the analytical modelling introduced by Johanson in order to establish the operating conditions based on the material properties and process parameters, that can lead to an improvement in manipulating and handling the roll compactor, thus improving production efficiency and quality.

1.2.5 Analytical models

Analytical and computational models are capable of accurately predict the significant parameters in powder roll compaction process. Among those significant parameters are, the forces and torques acting on the rolls, the "nip" angle (the angle at which the powder no longer slips against the rolls) and the compacted ribbon's density distribution.

Understanding the factors that influence these parameters and quantitatively predicting their values, gives important information for improving the design and operation of the roll compaction process. The process parameters show a strong dependency on the properties of powder, which makes the process difficult for understanding. In the process, the deformation of powder by drawing and densifying between rolls involves various complex mechanisms. Therefore, such analytical and computational models for the roll compaction process are being developed.

1.2.5.1 Johanson model

As did Evans et al. [33], Johanson divided the zone between the rolls into two regions[6]. Slip region where the slips occurs along the roll surface and nip region where no-slip boundary conditions applies. Taking into account press dimensions and material characteristics, the model analytically determines some of the process parameters: the nip angle, pressure distribution above the nip area, pressure in the nip region and roll force and torque.

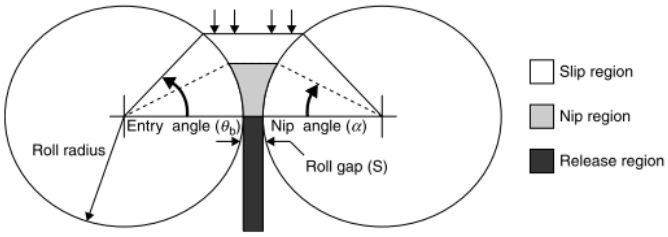

Figure 1.12: Schematic diagram of a typical roll compaction design [6]

Johanson model includes several assumptions:

- Material is isotropic, frictional, and cohesive and obeys the Jenike-Shield effective yield criterion.
- Rolls are rigid and the gap between them is fixed.
- The model is one-dimensional.
- Gravity effect is negligible when using forced feeding.

Johanson expressed the pressure gradients both for the slip and non-slip regions. Assuming slip conditions, based on Jenike-Shield yield criterion the pressure gradient along the roll surface is:

$$\frac{d\sigma}{dx} = \frac{4(\frac{\pi}{2} - \theta - \nu)}{\frac{D}{2}(1 + \frac{S}{D} - cos\theta)[cot(A - \mu) - cot(A + \mu)]} \tag{1.1}$$

Where x, θ , S and D are respectively the distance from the gap, the roll angle, the gap size and the roll diameter. The parameters A , ν and μ are constants. The pressure gradient when slip does not occur along roll surface is:

$$\frac{d\sigma}{dx} = \frac{K\sigma_\theta(2cos\theta - 1 - \frac{S}{D})tan\theta}{\frac{D}{2}[(1 + \frac{S}{D} - cos\theta)cos\theta]} \tag{1.2}$$

The angle in which the pressure gradients intersect is the nip angle:

$$\left(\frac{d\sigma}{dx}\right)_{slip} = \left(\frac{d\sigma}{dx}\right)_{nip} \tag{1.3}$$

From the above equations, it can be seen that the nip angle is mainly dependent on the material properties; compressible constant, effective angle of friction and the wall friction.

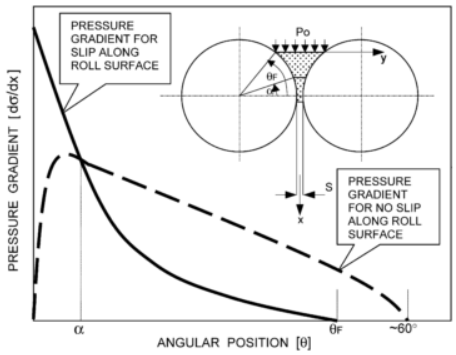

Figure 1.13: Vertical pressure gradient vs. angular position in roll bite [6]

Once the nip angle is known, the pressure distribution between the roll can be obtained. The pressure σ_θ at any $\theta < 0$ can be determined as a function of the pressure σ_α at $\theta = \alpha$ by the pressure-density relationship.

$$\sigma_\theta = \sigma_\alpha \left(\frac{\rho_\theta}{\rho_\alpha}\right)^K = \sigma_\alpha \left(\frac{V_\theta}{V_\alpha}\right)^K \tag{1.4}$$

By defining the geometry of each volume, the resulting pressure distribution equation for $\theta \leq \alpha$ is obtained:

$$\sigma_\theta = \sigma_\theta \left[\frac{\left(1 + \frac{S}{D} - \cos\alpha\right)\cos\alpha}{\left(1 + \frac{S}{D} - \cos\theta\right)\cos\theta}\right]^K \tag{1.5}$$

Once obtaining the pressure distribution between the rolls, the total separation force can be calculated as:

$$RF = \int_{\theta=0}^{\theta=\theta_h} P_\theta W \frac{D}{2} \cos\theta d\theta = \frac{P_{max} W D F}{2} \tag{1.6}$$

Where the roll force, F is:

$$F = \int_{\theta=0}^{\theta=\alpha} \left[\frac{S}{D\left(1 + \frac{S}{D} - \cos\theta\right)\cos\theta} \right]^K \cos\theta d\theta \tag{1.7}$$

Although the Johanson model is able to predict the nip angle and the roll pressure distribution, it has some major limitations:

- Does not take into account the roll speed.
- Does no take into account the case of over/under feeding of powder.
- Assumes that the maximum roll normal stress occurs at the minimum gap width.
- Follows the simple yield criterion of Jenike-Shield.
- The model is one-dimensional.

1.2.5.2 Extension of Johanson model

One of the main limitation of the classical Jonanson model is that it does not take into account the screw speed. Therefore, Reynolds et al. [55] extended this analytical

model. Firstly, a relationship between the ribbon relative density and the peak pressure is obtained by the simple powder law relationship:

$$Rd = Rd_0 P_{max}^{\frac{1}{K}} \tag{1.8}$$

From Eqs. 1.6 - 1.8, we now can obtain a relationship between the the process parameters, press geometry and material properties to the resultant ribbon relative density:

$$Rd = Rd_0 \left(\frac{2RF}{WD \int_{\theta=0}^{\theta=\alpha} \left[\frac{S}{D\left(1+\frac{S}{D}-\cos\theta\right)\cos\theta} \right]^K \cos\theta d\theta} \right)^{\frac{1}{K}} \tag{1.9}$$

In order to introduce the screw speed process parameters in the above equations, several steps need to be taken first. For the screw conveyor, the inlet mass flow rate is usually proportional to the screw rotation rate and written as: $\dot{m}_s = c_s N_s$. The outlet mass flow rate can be written as: $\dot{m}_r = \rho_{true} RdWSD\pi N_r$. Where W is the roll width, D is the roll diameter, S is the roll gap and Rd is the ribbon relative density. Assuming no leakage from the side seals, all the powder entering the rolls by the screw conveyors should pass out of the rolls. Therefore, from the inlet and outlet mass flow rate, the following relationship is obtained:

$$\frac{N_s}{N_r} = \frac{\pi}{c_s} \rho_{true} RdWSD \tag{1.10}$$

Where c_s is the screw constant which is obtained experimentally by the relationship between the mass throughput and the screw/roll speed ratio.

Now the relationship between screw speed, roll speed and gap can be introduced into Eq. 1.9 by replacing the term of roll gap, S using Eq. 1.10:

$$Rd = Rd_0 \left(2RF\right)^{\frac{1}{K}} \left(WD \int_{\theta=0}^{\theta=\alpha} \left[\frac{c_s N_s}{\pi \rho_{true} RdWD^2 N_r \left(1 + \frac{c_s N_s}{\pi \rho_{true} RdWD^2 N_r} - \cos\theta\right) \cos\theta} \right]^K \cos\theta d\theta \right)^{-\frac{1}{K}} \tag{1.11}$$

1.2.6 Numerical (Computer) modeling of roll compaction process

G. Ya. Gun et al. [56, 57] was the first to introduce mathematical modelling for the roll compaction process of metallic powders, dating back to 1983. A Boundary Value Problem (BVP) was used to model the steady-state plane plastic flow of powder in the densification (compaction) zone during symmetrical rolling.

As the powder is fed vertically into the rolls, the inlet boundary S_1 is governed solely by the weight of the powder above the densification zone. On the other side of the rolls (surface S_4), powder is free to flow out without front tension. The boundary surface S_2, which represents the contact between powder and roll, obeys the laws of coulomb friction. Figure 1.14a, illustrates the geometry and marks the boundary regions used to solve this model.

Assuming the values of the neutral angle and rotation speed of rolls are known, together with the law of mass conservation, the initial velocity of powder V_0 at the boundary S_1 can be determined. With the above mentioned boundary conditions, the boundary-value problem is solved using the approximative Galerkin's method. The resultant distribution of the intensity of shear deformation rates (Fig.1.14b) is reflected in changes in powder density (Fig.1.14c) over the thickness of the densification zone.

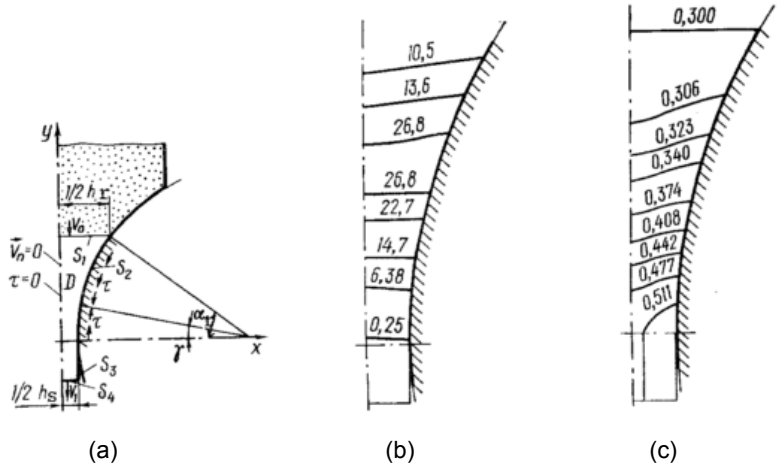

Figure 1.14: BVP solved by G. Gun et al, starting from a) describing the problem and obtaining the resultant field of isolines of b) deformation rate intensity and c) relative density [57].

Over the past two decades, Finite Elements Method (FEM) modeling using commercial softwares were adopted and further developed to simulate pharmaceutical forming processes. FEM models of powder roll compaction process which started considering a plane strain two-dimensional case[2, 3, 4, 5], founded to be comparable and more accurate than the one-dimensional analytical Johanson[6] and Slab method[7, 8] models. With the increasing computational power in the last years, the development of three-dimensional models provided greater insight on the pressure and density distribution during the roll compaction processes[9, 10, 11].

1.2.6.1 Two-dimensional FEM model

Dec et al. [2] firstly introduced a two-dimenstional FEM modelling of the roll compaction process. The model consisted of a simplified Drucker-Prager Cap model, assuming zero cohesion and a constant friction angle of 65°. The resultant roll pressure profiles as a function of feed stress and coefficient of friction are shown in Fig. 1.15a and 1.15b. The nip angle was defined as a value of the rolling angle in which

the linear velocity of the roll surface is equal to the velocity of contacting material. The neutral angle was defined as the angle in which the frictional shear stress at the roll surface reverses direction. The results, as anticipated, distinguish between two regions of slip in the feed zone and sticking in the nip region.

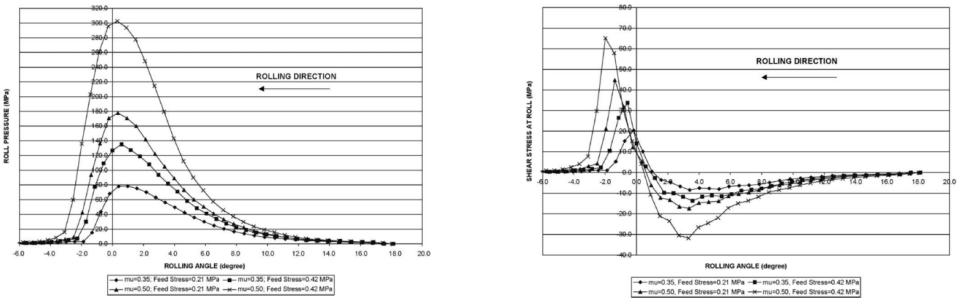

(a) Effect of friction on feed pressure on roll pressure

(b) Effect of friction on feed pressure on roll shear stress

Figure 1.15: Two-dimensional FEM simulation results by Dec et al. [2]

The roll force, roll torque, and material relative density at the roll gap increase with increasing feed pressure or powder-roll friction coefficient. The nip angle, however, was largely unaffected by changes in feed pressure, but increased with an increase in powder-roll friction coefficient. Michrafy et al. [4] developed a two-dimensional FEM model to study the roll compaction process and the influence of material properties. Firstly, the material density and velocity versus the rolling angle were plotted (Fig.1.16b and 1.16a, respectively). The predicted velocity of the powder in the roll direction distinguish two different regions: the first region, where the powder has lower velocity than the roll (slip region) and a second region, where the powder and the roll are moving together with the same velocity (stick region). The angle in which the powder starts to have the same velocity of the roll is determined as the nip angle.

The effect of material rigidity on the roll compaction process was studied as well, by varying the Young's Modulus and the Cap eccentricity. Increasing the Young's modulus will, as expected, result in an increase of the maximum roll pressure (Fig.1.17a). Decreasing the cap eccentricity from 1 to 0.4 resulted in an increasing

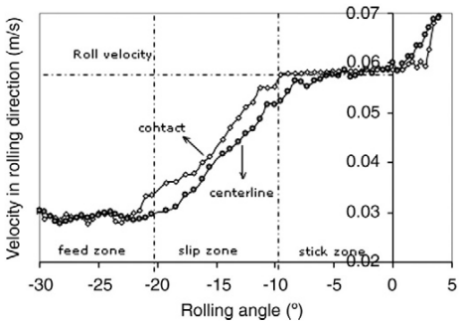

(a) Velocity in rolling direction

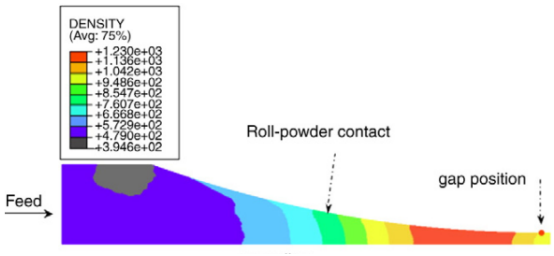

(b) Density distribution in rolling direction

Figure 1.16: Two-dimensional FEM simulation results by Michrafy et al. [4]

of the maximum roll pressure, nip angle and maximum relative density (1.17b).

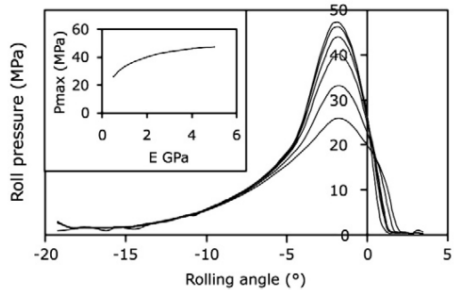

(a) Roll pressure in rolling direction

Eccentricity (R)	Maximum roll pressure (MPa)	Nip angle (degree)	Maximum relative density
0.4	120.2	12.39	0.81
0.5	78.79	9.55	0.79
0.6	47.2	9.56	0.76
0.7	31.9	8.99	0.74
0.8	23.3	8.43	0.7
0.9	18.5	7.88	0.68
1	16.17	7.35	0.65

(b) Cap eccentricity effect on roll compaction process

Figure 1.17: Material properties effect on FEM modelling of roll compaction process

Cunningham et al. [3] evaluated the effects of feed stress, roll friction on roll force, profiles of roll pressure and roll shear stress, nip angle and relative density of the compacted powder. The relative density showed an increase with powder entry angle, assuming all other process parameters are kept constant (Fig. 1.18a). The value of nip angle was nearly unaffected and showed a slight increase with the entry angle. The effect of constant feed stress can be observed in the level of pre-densification in the feeder before the powder contacts the rolls (Fig. 1.18b). Higher feed stress increases the density of the powder in the feeder and consequently resulting in higher final densification. On the other hand, the nip angle is unaffected by the variation in feed stress.

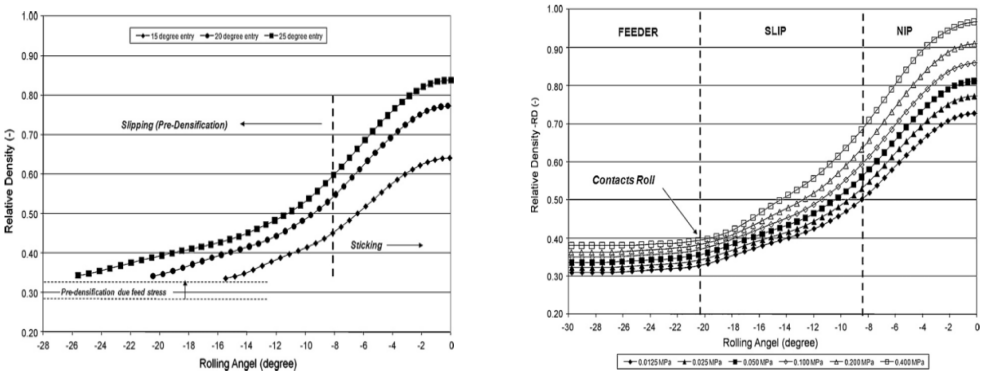

(a) Effect of powder entry angle on relative density in rolling direction

(b) Effect of inlet feeding pressure on relative density in rolling direction

Figure 1.18: Two-dimensional FEM simulation results by Cunningham et al. [3]

As observed in Table 1.1, the nip angle, maximum roll pressure and maximum relative density increase as the coefficient of roll/powder friction increases. These results are in agreement with the previous results Dec et al. [2] obtained. Increasing the roll friction will result in earlier gripping of powder and therefore, greater densification is obtained in the nip region with higher values of roll pressure developed.

Effect of roll friction coefficient on nip angle, maximum roll pressure and relative density at exit.

Roll friction coefficient	Nip angle (°)	Maximum roll pressure (MPa)	Relative density at exit
0.30	7.0	35	0.71
0.35	8.2	50	0.78
0.40	10.0	75	0.81
0.50	13.5	130	0.89
0.60	14.5	210	0.91

Table 1.1: Effect of friction coefficient on roll compaction process using FEM [3]

Muliadi et al. [5] compared the predicted nip angle, maximum roll normal stress, and maximum ribbon's relative density using the Johanson model [6] and two-dimensional FEM model. Results show similar trends to those using the Johanson model, except the fact that the nip angle decreases with increasing effective friction angle. Moreover, Simulation results obtained lower values of relative density and normal pressure than the Johanson model.

1.2.6.2 Three-dimensional FEM model

In order to study the effect of the fixed sealing system and the screw feeding on the resultant ribbon non-uniformity, three-dimensional FEM models have been used. Michrafy et al. [9] examined the uniformity of the pressure and density across the ribbon's width for the two boundary conditions of either constant feed pressure or feed velocity using a three-dimensional FEM model. The simulation results show a uniform pressure and density distribution along the ribbon's width by using a constant feeding pressure as inlet boundary condition. However, a constant inlet feeding velocity resulted in a non uniform distribution, where the higher pressure and density obtained in the middle of the ribbon and lower at the edges. Cunningham et al. [10] compared a uniform inlet feeding velocity to a variable inlet feeding velocity where the highest value in the middle and lowest at the sides which represent the non-uniform behavior of screw feeding. In the case of uniform inlet feeding velocity, the maximum roll pressure and relative density was the same along the ribbon's width. Using a non-uniform inlet feeding velocity,the powder is fed more in the middle than the edges and, as expected, it results in higher maximum roll pressure (Fig. 1.19a), shear stresses (Fig. 1.19b), and relative density (Fig. 1.20) in the middle of the ribbon than the edges. It is also noticed that the nip angle remains the same along the ribbon's width.

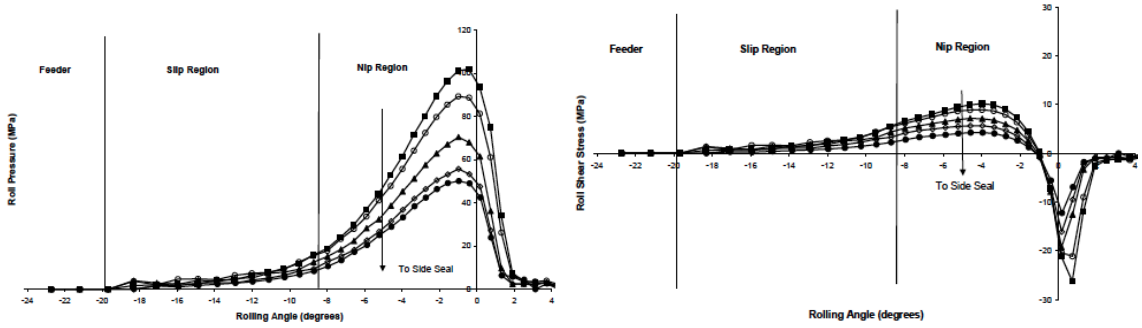

(a) Roll pressure distribution (b) Roll shear stress distribution

Figure 1.19: Three-dimensional FEM simulation results by Cunningham et al. [3]

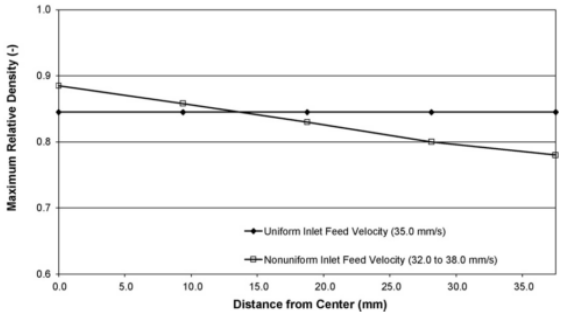

Figure 1.20: Density distribution along the ribbon width for two cases of inlet feeding velocity[3]

Muliadi et al. [11] presented a similar and validated simulation results of a roll compaction process using a piston instead of screw feeder (Fig. 1.21). Results using both the a non-uniform inlet velocity and non-zero friction between the powder and the side seals, indicates that both effects in the roll compaction process may contributed to the inhomogeneous produced ribbons.

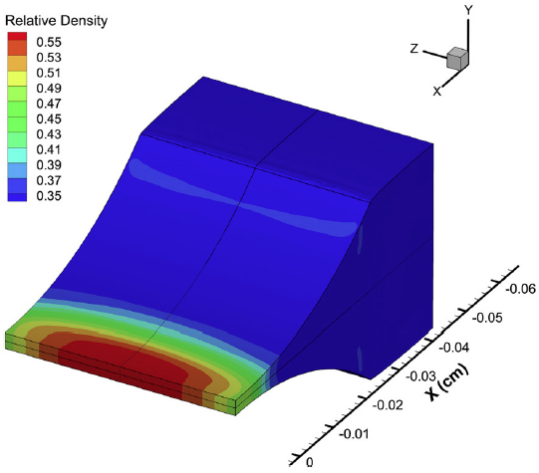

(a) Density from FEM modelling

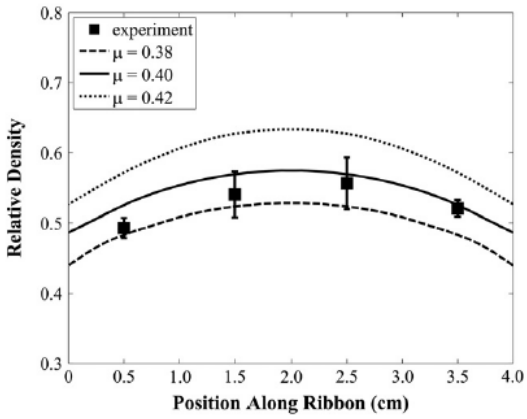

(b) Comparison between relative density obtained numerically and experimentally

Figure 1.21: Three-dimensional FEM simulation results by Muliadi et al. [11]

1.3 Theoretical aspects of Finite Elements Method (FEM)

The Finite Element Method (FEM), applied to structural models, can be defined as a numerical technique to approximate the solution of partial differential equations, which composes an analytical model to describe the structural behavior, the physical problem. The structure shall be divided into elements, i.e. a finite number of degrees of freedom, in order to represent the continuum. As an engineering analysis, the results are evaluated and modifications are made in the definition of the physical problem, analytical model or the finite element procedure. For instance, in this present project, the FE model of the roll compaction is first built with assumptions, which are furthermore evaluated and used in order to improve the FE model. In the following sections the main methods covered on this project are hereafter presented, such as the basic theory of the FEM and nonlinear analysis.

The general formulation, displacement-based FEM, is explained according to the reference where the displacements are the unknowns to be calculated. As illustrated on figure 1.22, the FE model of a real structure consists in an assembly of individual finite elements, where at the element level, the stiffness matrices are calculated and the global stiffness matrix is then formulated by adding these element stiffness matrices. As a result, the global displacements can be calculated by solving the equilibrium equations of the model. Thus the element displacements and stresses can be evaluated.

To begin with, for a case of a static linear-elastic analysis conditions, the strain vector $\{\epsilon\}$ can be obtained by the general elasticity problem, where the interpolation functions $[N]$, represent the relations between the displacement vector at any point in the element,$\{U\}$, and the nodal displacements, $\{u\}$. Thus, it should satisfy the compatibility condition, where the displacement field is continuous and fulfills the displacement boundary conditions. Hence, the strain vector as a nodal displacement function is obtained through the strain-displacement matrix $[B]$.

The principal of virtual displacements, also known as principle of virtual work,

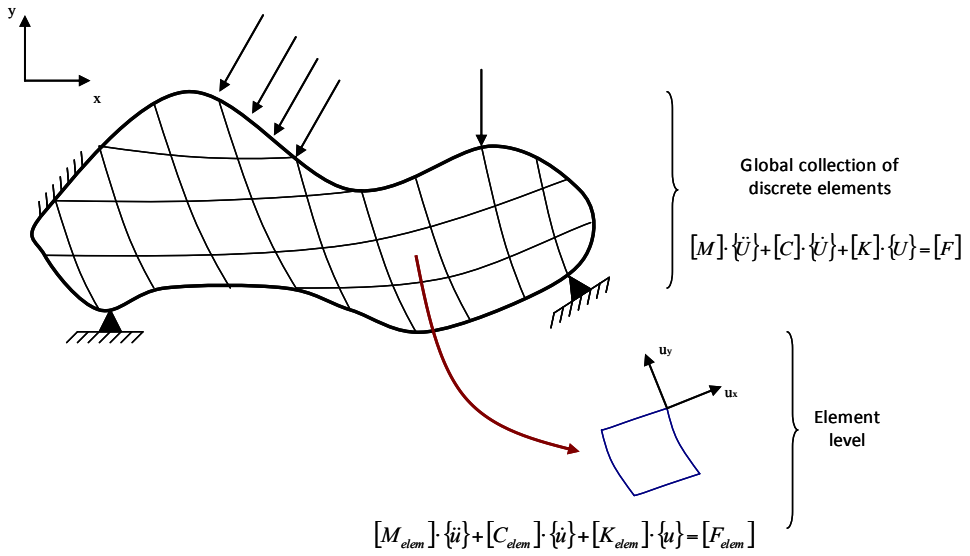

Figure 1.22: FEM global and element level relation

is the main idea of the displacement-based FEM and states that, in the equilibrium configuration of a body, the total internal work, δW_{int} , is equal to the total external work, δW_{ext} [58]. Therefore, the general differential equilibrium equation (Eq. 1.12) is achieved, and its assemblage form is:

$$[M] \cdot \{\ddot{U}\} + \underbrace{[K] \cdot \{U\}}_{\text{Internal forces}} = \underbrace{[F]}_{\text{External loads}} \tag{1.12}$$

Thus, the force matrix for element assemblage is:

$$[F] = \sum_{elem} \sum^{n} [N_{elem}]^T \cdot [F_{elem}] \tag{1.13}$$

The stiffness matrix for element assemblage (total stiffness of the body) is:

$$[K] = \sum_{elem} [K_{elem}] = \sum_{elem} \int_{Velemt} [B_{elem}]^T \cdot [E] \cdot [B_{elem}] \cdot dV_{elem} \tag{1.14}$$

$[M]$ is the mass matrix, for element assemblage:

$$[M] = \sum_{elem} \int_{Velemt} [N_{elem}]^T \cdot \rho_{elem} \cdot [N_{elem}] \cdot dV_{elem} \tag{1.15}$$

1.3.1 Explicit dynamic integration scheme

For nonlinear problems, only numerical solutions are possible. Abaqus/Explicit uses the central difference scheme to integrate the equation of motion. For explicit scheme, the equation of motion is evaluated at the old time step t_n, whereas implicit method use the equation of motion at the new time step t_{n+1}.

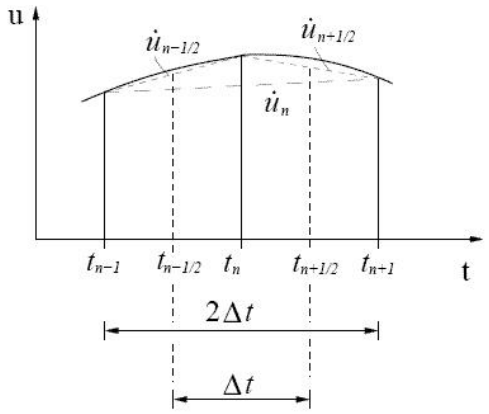

Figure 1.23: The Central difference scheme

Typical for the central difference method is that the displacement $\{\tilde{u}\}$ and acceleration $\{\ddot{\tilde{u}}\}$ are evaluated at whole time steps t_{n-1}, t_n, t_{n+1}, and so on while velocities $\{\dot{\tilde{u}}\}$ are evaluated at the midpoints of the time intervals, i.e. at $t_{n-\frac{1}{2}}$ and $t_{n+\frac{1}{2}}$.

Acceleration:

$$\begin{aligned}\{\ddot{\tilde{u}}\} &= \frac{1}{\Delta t}\left(\{\dot{\tilde{u}}\}_{n+\frac{1}{2}} - \{\dot{\tilde{u}}\}_{n-\frac{1}{2}}\right) \\ &= \frac{1}{\Delta t}\left(\frac{\{\tilde{u}\}_{n+1} - \{\tilde{u}\}_n}{\Delta t} - \frac{\{\tilde{u}\}_n - \{\tilde{u}\}_{n-1}}{\Delta t}\right) \\ &= \frac{1}{(\Delta t)^2}\left(\{\tilde{u}\}_{n+1} - 2\{\tilde{u}\}_n + \{\tilde{u}\}_{n+1}\right)\end{aligned} \tag{1.16}$$

Velocity:

$$\{\dot{\tilde{u}}\} = \frac{1}{2\Delta t}\left(\{\tilde{u}\}_{n+1} - \{\tilde{u}\}_{n-1}\right) \tag{1.17}$$

The dynamic equilibrium equations at time t_n can be written as

$$[M] \cdot \{\ddot{\tilde{u}}\}_n + [C] \cdot \{\dot{\tilde{u}}\}_n = \{f_{ext}\}_n - \{f_{int}\}_n \tag{1.18}$$

Substituting acceleration equation by the velocity equation and rearranging yields:

$$\{\ddot{\tilde{u}}\}_n = [M]_n^{-1}\left(-[C]\{\dot{\tilde{u}}\}_{n-\frac{1}{2}} + \{f_{ext}\}_n - \{f_{int}\}_n\right) \tag{1.19}$$

$$\{\dot{\tilde{u}}\}_{n+\frac{1}{2}} = \{\dot{\tilde{u}}\}_{n-\frac{1}{2}} + \Delta t\{\ddot{\tilde{u}}\}_n \tag{1.20}$$

$$\{\tilde{u}\}_{n+1} = \{\tilde{u}\}_n + \Delta t\{\dot{\tilde{u}}\}_{n+\frac{1}{2}} \tag{1.21}$$

It is important to mention, that for this study, the contribution of damping matrix $[C]$ either from the roll press or the material behavior was not considered.

The explicit method can be summarized into the following steps:

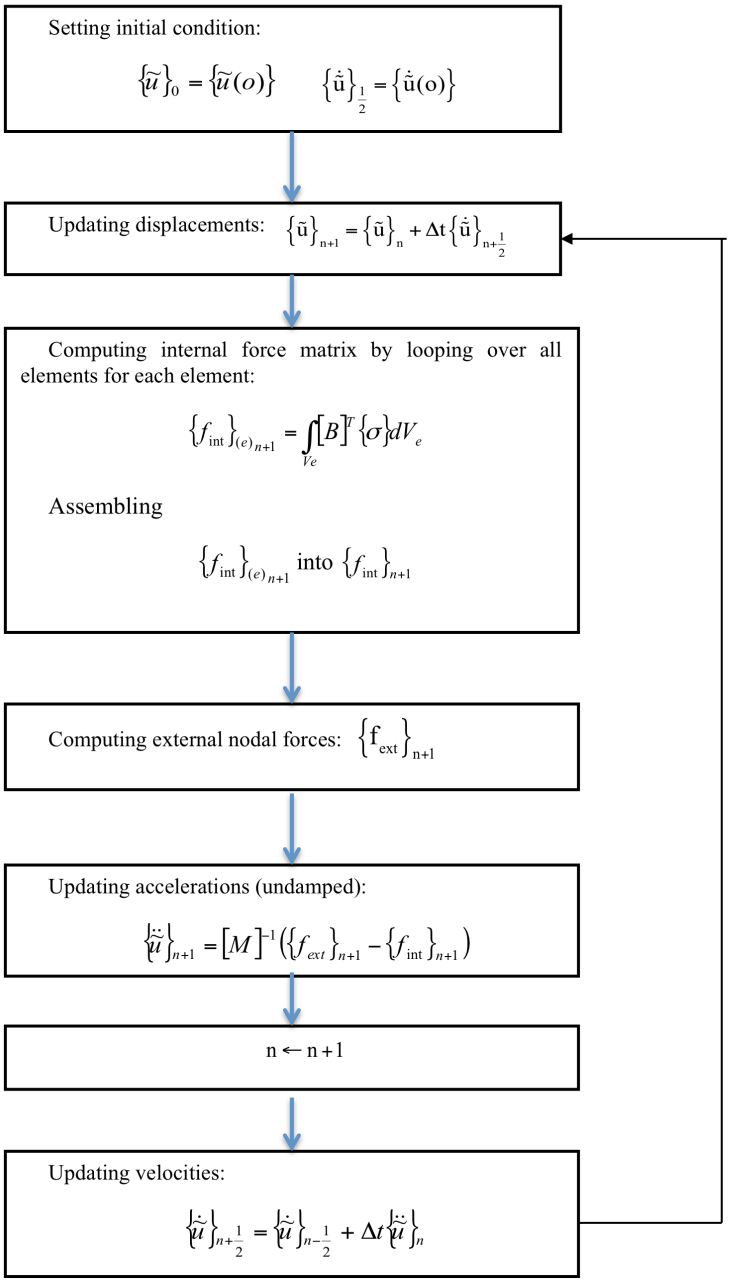

Figure 1.24: Flow chart for explicit integration scheme

1.3.2 Time integration

The solution of displacement at time t_{n+1} only depends on the displacement of the known states at times t_n and t_{n-1}, this discretization scheme is named as dynamic explicit integration of the equation of motion. In the case of the implicit integration methods, the solution depends also on the displacements of the unknown state at time t_{n+1}, which is usually expressed as dependency of the stiffness term on the unknown displacements.

The time step should be smaller than a critical time step Δt_{cr}, which is:

$$\Delta t_{cr} = \frac{T}{\pi} = \frac{2}{\omega} = 2\sqrt{\frac{m}{k}} \tag{1.22}$$

Where T is the eigen-period of the system to satisfy the condition for convergence.

The explicit algorithm integrates through time by using small time increments. The central difference operator is conditionally stable as already pointed out and the stability limit for the operator, excluding damping is simplified to:

The Maximum eigen-frequency is determined by the smallest element in the FE-mesh. Using Courant condition, the time step can be written as:

$$\Delta t \leq \frac{l}{c} \tag{1.23}$$

Where, c is the speed of sound in the material and l is a characteristic length of the smallest element. The speed of sound for porous media is approximately:

$$c \approx \sqrt{\frac{E}{\rho}} \tag{1.24}$$

The time step should be small enough that information does not propagate across more than one element during a single time step.

1.3.3 Mass scaling

Sometimes, short elements edge lengths in a mesh are unavoidable. Using mass scaling can increase the solving solution speed. Mass scaling changes the speed of sound in a particular element by increasing the density in that element. The resulting slower sound speed increases Δt_{cr} for the particular element.

The shortfall of mass scaling is that artificial mass is added to the system. As mentioned previously, sound speed, c, is approximately $c \approx \sqrt{E/\rho}$ where E is Young's modulus and ρ is mass density. Applying mass scaling to the mesh below (Fig.1.25), to get the left mesh CPU time to match the right mesh (Δt_{cr} left=Δt_{cr} right), would require increasing the pink element (smallest) density by about 25 times, the yellow element density by about 16 times, and the green & orange element density by about 10 times and so on. Note the total mass of the left mesh would increase.

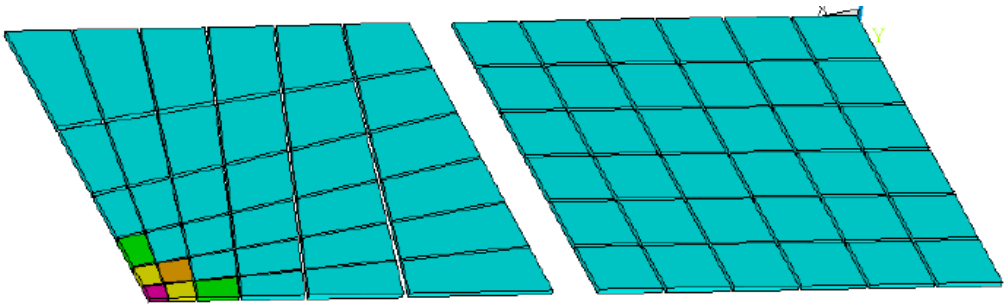

Figure 1.25: Different element sizes influence on mass scaling

Anytime you add nonphysical mass to increase the time step in a dynamic analysis, you affect the results. Sometimes the effect is insignificant and in those cases adding nonphysical mass is justifiable. Examples of such cases is the addition of mass in quasi-static simulations where the velocity is low and the kinetic energy is very small relative to the peak internal energy

As mentioned, Mass-scaling is a term that is used for the process of scaling the element's mass in explicit simulations to adjust its time step. The primary motivation is to change (usually increase) the global compute time step, which is limited by the Courant's stability criteria.

1.3.4 Eulerian and Lagrangian formulation

One of the major problems in FEM modelling of roll compaction of pharmaceutical powders is avoiding the mesh distortion during the mechanical process. The pharmaceutical powder is in fact a porous media, which is highly compressed during the roll compaction process. Basically, there are three different ways to model the Roll Compaction process in Abaqus/Explicit:

1. All the mesh is constructed with Lagrangian elements. This is typically used for transient analysis and where the mesh does not encounter severe distortion.

2. All the mesh is constructed with Eulerian elements. This method also name as "Coupled-Eulerian-Lagrangian (CEL)", where the Eulerian elements represent a fluid or highly distorted elements and the tools (such as rolls) are meshed with Lagrangian elements.

3. A combination of both Eulerian and Lagrangian elements in the same mesh is called the "Arbitrary Lagrangian Eulerian (ALE)" method, where some areas of the mesh considered as Eulerian (usually the inlet/outlet surfaces) and some as Lagrangian (having contact with tools). The ALE is typically used for steady state analysis, where the mesh is fixed for the entire simulation and using inlet/outlet Eulerian boundary conditions.

For FEM modelling of mechanically processing highly compressible materials such as porous medias, the ALE method is considered as the best option. The ALE uses the advantages of both Eulerian and Lagrangian elements and is cost effective.

Arbitrary Lagrangian Eulerian (ALE)

The arbitrary Lagrangian Eulerian description is an extension of both classical Lagrangian and Eulerian ones. The grid points are not constrained to remain fixed in space (as in the Eulerian description) or to move with material points (as in Lagrangian description), but have their own motion governing equations.

In the ALE description, three different configurations are considered; the material domain Ω_X, spatial domain Ω_x and the arbitrary reference domain Ω_ζ, which is called the ALE domain [59]. In such a description, material points are represented by a set of Lagrangian coordinates $\overrightarrow{X}$,spatial points with a set of Eulerian coordinates $\overrightarrow{x}$ and reference points (grid points) with a set of arbitrary coordinates $\overrightarrow{\zeta}$ as shown in Fig.1.26.

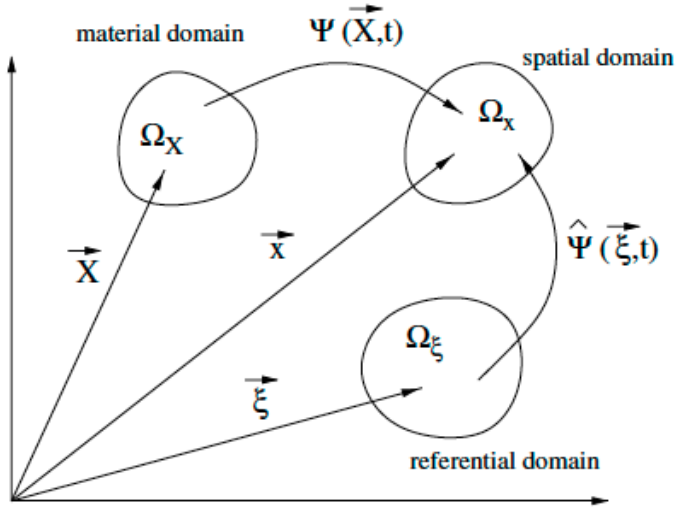

Figure 1.26: Arbitrary Lagrangian Eulerian description

The most common way to implement the ALE equations, is the operator split. In this approach, the calculation, for each time step is divided into two phases.

First, a Lagrangian phase is performed, in which the mesh moves with the material. In this step, the displacements are computed using the explicit integration scheme described previously (Ch. 1.3.2). In the second phase, the solution from the Lagrangian step is being mapped (convected) to the reference grid and the trans-

port of mass, energy and momentum across element boundaries are computed. Here, remapping the displaced mesh at the Lagrangian phase back to its original for Eulerian formulation or arbitrary position for ALE formulation using smoothing algorithms. This second advection (or Eulerian) step of ALE adaptive meshing consists in fact of two steps:

- Remeshing: Sweeping iteratively over the mesh domain and moving nodes to smooth the mesh. Increasing the number of sweeps increases the intensity of adaptive meshing for each increment. The frequency of the adaptive meshing is the most influence parameters affecting the mesh quality and is user defined.
- Remmaping: Mapping solution variables from an old mesh to a new mesh by a process called advection sweep. Conservation of mass, momentum and energy.

The operator split approach helps solve complex problem, by braking them into much simpler ones. Illustrative description of the two steps in ALE formulation are described in the following figure.

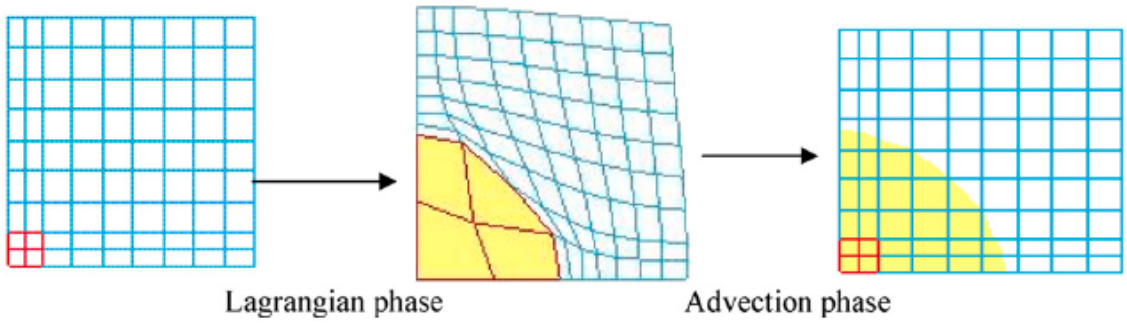

Figure 1.27: Lagrangian and Advection phases in ALE formulation [60]

Coupled Eulerian Lagrangian (CEL)

Although the ALE method is considered to be the best option for modelling powder compaction, some applications such as Fluid-structure interaction (FSI) problems are limited. The Coupled Eulerian–Lagrangian (CEL) method that attempts to capture the advantages both of the Lagrangian and the Eulerian methods. The FE mesh in CEL analysis usually constructed as a stationary rectangle through which the Eulerian material moves and impact the Lagrangian structure. In numerical analyses using this CEL method the Eulerian material is tracked as it flows through the mesh by computing its Eulerian volume fraction (EVF). Each Eulerian element is designated a percentage, which represents the portion of that element filled with a material. Contact between Eulerian materials and Lagrangian materials is enforced using a general contact that is based on a penalty contact method. A general contact algorithm does not enforce contact between the Lagrangian elements and the Eulerian elements. If the volume fraction is one, the element is completely filled with material, contrary to the completely void elements that take volume fractions equal to zero. The Lagrangian elements can move through the Eulerian mesh without resistance until they encounter an Eulerian element filled with material.

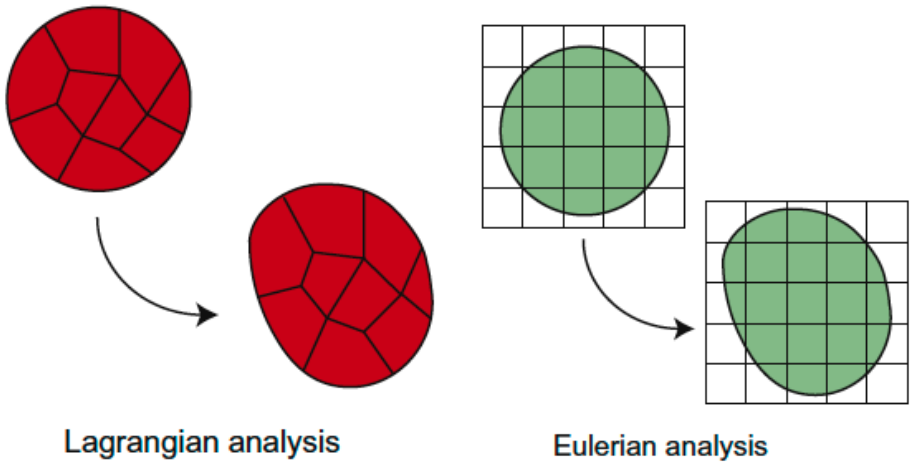

Figure 1.28: Coupled Eulerian–Lagrangian description

This page intentionally left blank.

Chapter 2

Materials and methods

Abstract

This chapter describes the materials and methods used for the development and investigation of the roll compaction process by a 3D FEM model. For this, it is necessary first to understand the different system designs and process parameters of the roll compactors used in this study. Then, the FE model and its implementation regarding the material behavior and process parameters is described in detail. In this work, the microcrystalline cellulose (MCC) powder is characterized by a density-dependent Drucker-Prager Cap constitutive model which is determined based on a standard experimentally calibration method. Additionally, the procedure to measure the density of produced roll compaction ribbons in order to validate the FEM models is described as well.

Resumé

Dans ce chapitre, sont décrits les matériaux et les méthodes utilisées pour le développement et l'investigation du procédé de compactage à rouleaux par la méthode des éléments finis en 3D. Dans un premier temps, les différents designs de presses à rouleaux étudiés dans ce travail sont présentés. Ensuite, le modèle éléments finis, les paramètres du procédé et le comportement du matériau en compression, basé sur la loi constitutive de Drucker-Prager Cap, sont décrits en détail. Dans ce travail, la poudre de cellulose microcristalline (MCC) est utilisée comme modèle de matériau. Les paramètres matériau du modèle sont déterminés expérimentalement en utilisant des essais mécaniques standard. De plus, la procédure de mesure de distribution de densité dans le compact, dont les résultats sont utilisés ultérieurement pour la validation de la modélisation éléments finis, est décrite.

2.1 Roll compaction design and process parameters

Two different roll compactors are used in this work. The Gerteis Mini-pactor® 250/25 (Gerteis Machinen + Processengineering AG, Jona, Switzerland) and Komarek® B050H laboratory press (K.R. Komarek Inc., Wood Dale, IL, USA).

The Gerteis Mini-pactor has two possible assemblies for side sealing: cheek plates or rimmed-roll as can be seen in Fig.2.1. The most commonly used sealing system is the cheek plates (i.e. fixed side seals), which are fixed and positioned in between the rolls. In order to avoid the problems caused by cheek plates, the Gerteis Mini-pactor also offers a rimmed-roll sealing system. The rimmed-roll is basically a ring, which is mounted on the bottom roll and acts as a sealing in the compaction region. The rolls are 250mm of diameter and 25mm of width, which are inclined and can be either with a fixed or varying gap (also called gap control)in between. The gap control uses an automatic feedback system which changes its values in order to reach a certain amount of compaction force for a given material feed.

The Komarek B050H laboratory press is constructed with a horizontal screw conveyor and two counter-rotating rolls with fixed side seals (i.e. cheek plates) in between. The rolls are 100mm of diameter and 38mm of width, which are vertically arranged and fixed with a specifically predefined gap in between the values of 1.5 to 6 mm.

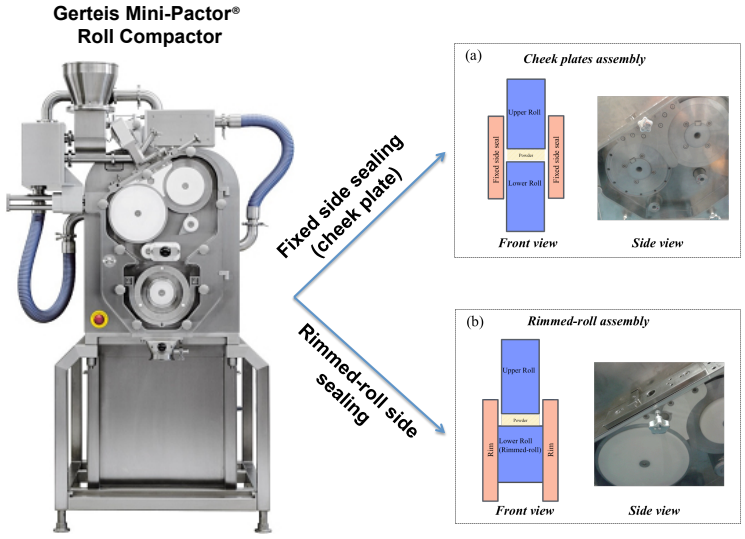

Figure 2.1: Gerteis Mini-pactor's two possible side seal assemblies a)cheek plates b)rimmed-roll.

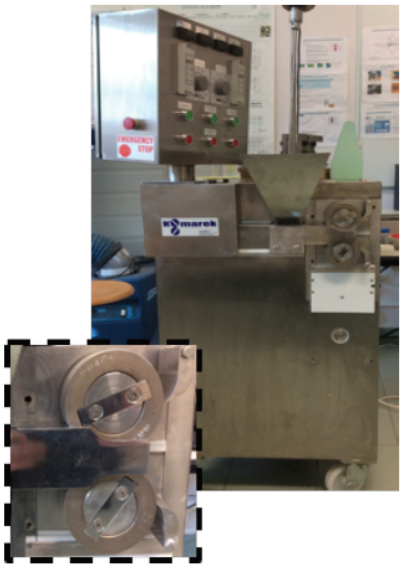

Figure 2.2: The Komarek B050H laboratory roll compactor

2.2 FEM Modeling

2.2.1 Overview

In this work, FEM is used to understand and predict the roll compaction process by obtaining the magnitudes and directions of stresses, strains and velocities. The FEM models were solved as a steady-sate problem using arbitrary Lagrangian-Eulerian (ALE) adaptive meshing in Abaqus/Explicit v6.14. The ALE adaptive mesh domain for steady-state problems is used to model material flowing through the mesh, consist of two Eulerian boundary regions (inflow and outflow), connected by Lagrangian or Sliding boundary regions[61]. An important aspect in solving steady-state problems is to follow the system and ensure reaching the steady-state condition. A history output for roll force and torque was obtained and plotted to validate the convergence. The density-dependent behavior described by the DPC model is implemented by an external user-defined VUSDFLD Fortran subroutine code. The inlet material density was set to be the tapped powder density as a result of the screw feeding. The Avicel PH 101 tapped density is about 0.47 g/cm^3 which corresponds to an initial relative density of 0.3.

First step in creating a Finite Elements (FE) model is to represent the geometry of the desired roll compactor. In the case of Komarek B050H roll compactor, the rolls diameter and width are 100 mm and 38 mm respectively and defined as analytic rigid surfaces. Once sketching the press dimensions, the region between the rolls is discretized and meshed using C3D8R three-dimensional continuum reduced integration elements. The smallest gap where the powder in contact under the rolls needs to be fixed and predefined, in the Komarek roll compactor, as 2 mm gap.

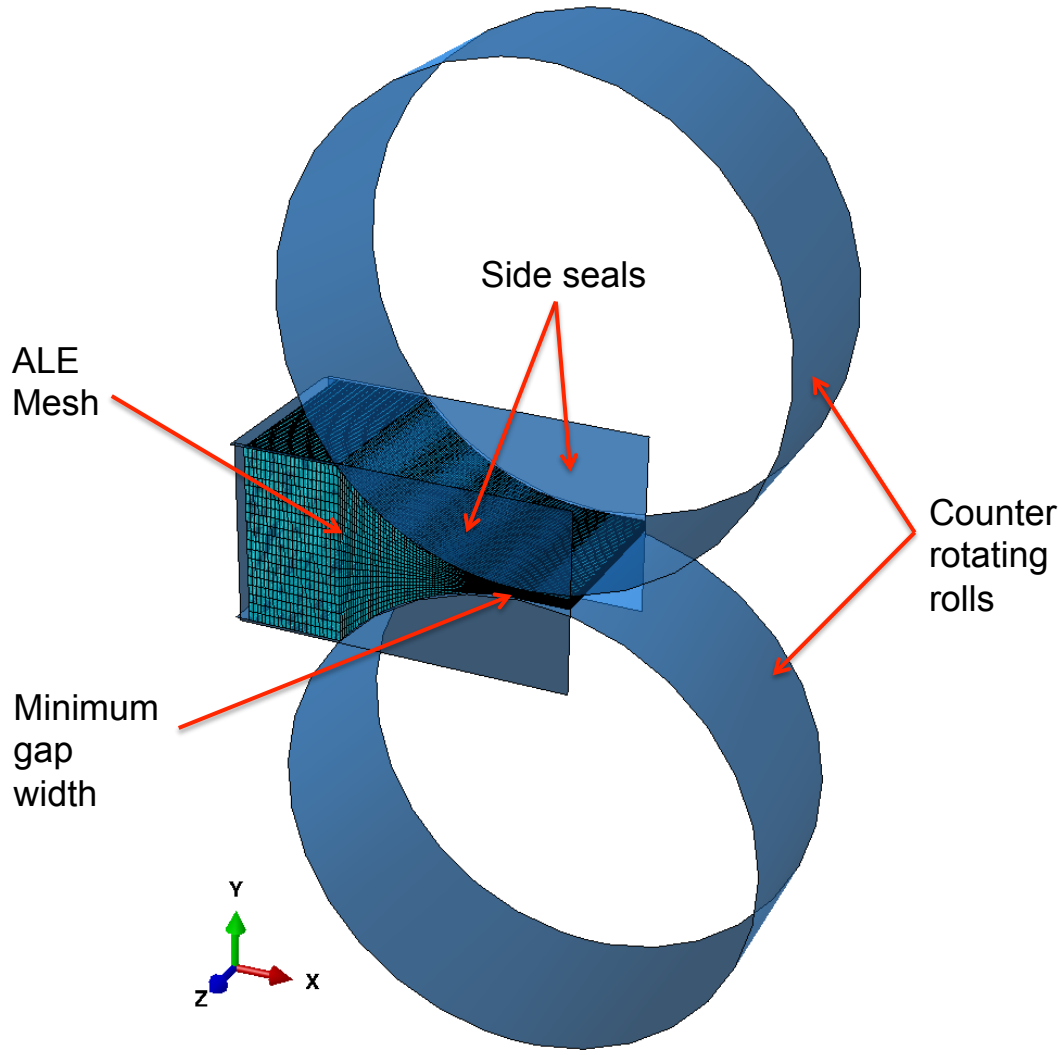

Figure 2.3: Schematic description of a typical FE model of roll compaction

2.2.2 Powder-tools interaction

The ALE method enables working both with the advantages of Lagrangian and Eulerian elements in the same part [62]. While the inlet and outlet surfaces are defined as Eulerian regions, the upper and lower surfaces that are in contact with the roll are defined as sliding surfaces. The contact between the rigid roll surface and the

sliding surface defined as surface-to-surface with a given coulomb coefficient of friction μ. For numerical reasons ,an ad hoc choice of constant friction coefficient was chosen. A value of μ=0.4 is the most representative single value obtained experimentally for a non lubricant case [4, 11]. The surfaces representing the boundary in the feeding region are defined as Eulerian regions with zero displacement boundary conditions in normal directions and spatial mesh constraint in all directions. These Eulerian boundary conditions represent a sealing system with zero friction and therefore no shear forces applied on the powder in the feeding region. The surfaces representing the contact between powder and side seals/rim rolls are defined as sliding region with spatial mesh constraint in the tangential directions. The contact between the outer surfaces representing the powder and the sealing system are defined as surface-to-surface with the same given coulomb coefficient of friction $\mu = 0.4$.

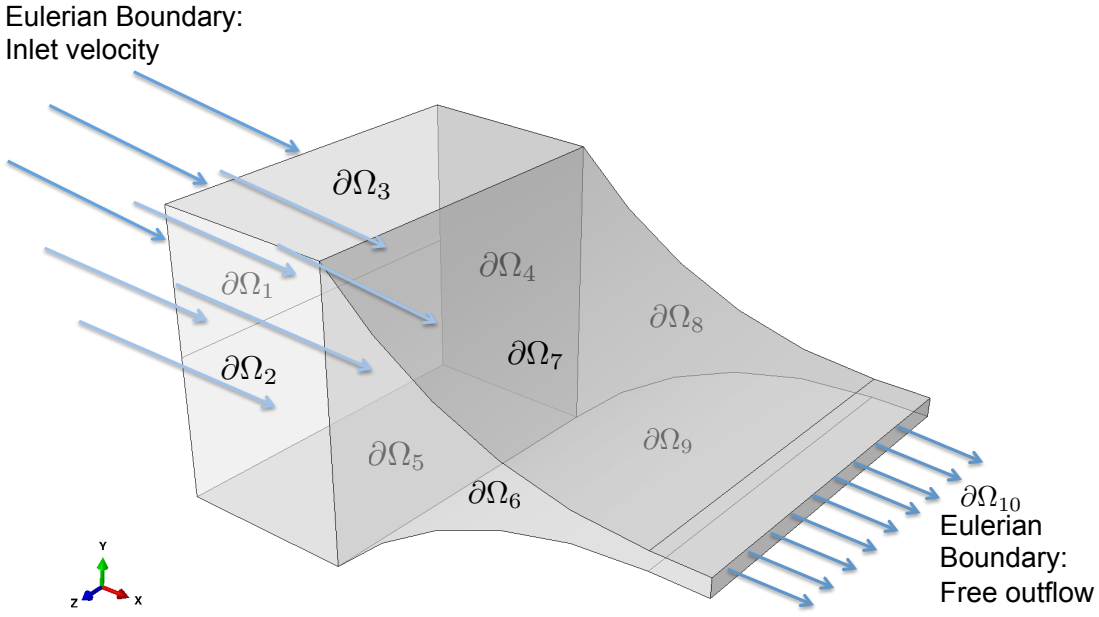

Figure 2.4: Boundary regions in the FE model

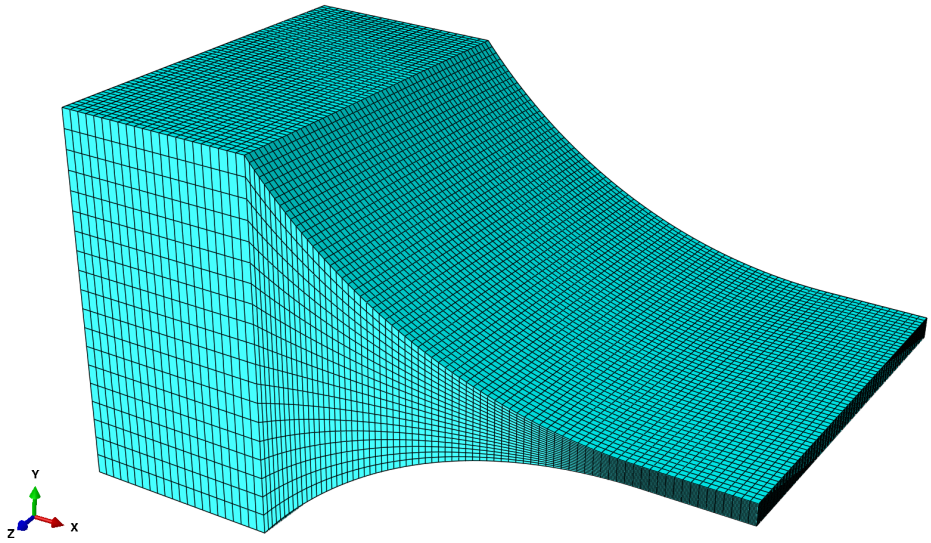

Figure 2.5: Discretized mesh of the powder region in the FE model

2.2.3 Boundary conditions

In the roll compaction process, the inlet stress is dependent both on the screw and press dimensions and process parameters. The inlet material is defined as simplified constant prescribed pressure or velocity. As the cross section area, shape and position of the inflow boundary are measured directly from the roll compactor and known in advance, both the material and mesh constraints must be applied. The inlet and outlet nodes were constraint in the normal direction to avoid translation in the stream wise direction and maintain a steady uniform flow. In order to improve convergence to the steady-state solution, a linear constraint equation was implemented both for the inlet and outlet nodes, constraining the material velocity to be uniform normal to the outflow. A roll rotational boundary condition about the z-axis was defined based on the roll rotating velocity in the experiment.

2.3 Powder

The powder used in this work is the microcrystalline cellulose (Avicel PH 101, FMC BioPolymer, Philadelphia, PA, USA). The MCC is one of the most important and widely used excipient in the pharmaceutical industry. It has excellent compressibility properties and used as diluent for drug formulations in the tableting process[63, 64]. Tablets with MCC show high strength and on the other hand disintegrate quickly. The true density of the powder blend was determined using a helium pycnometer (Accupyc 1330, Micromeritics Instrument Corp., Norcross, GA, USA) as ρ_{true}=1.56 g/cm^3. The bulk density was obtained from the manufacturer, having values of 0.32 g/cm^3 which corresponds to an initial relative density of 0.2. Magnesium stearate (MgSt) was used as lubricant in die compaction.

2.4 Drucker-Prager Cap Constitutive model

2.4.1 Overview

The behavior of the powder in FEM modelling, considered as porous compressible material, is described using the density-dependent Drucker-Prager Cap (DPC) model [65]. Assuming the material is isotropic, the model consists of three different parts: A shear failure surface representing shearing flow, a cap surface representing an inelastic hardening for plastic compaction and a transition zone between the two surfaces, providing smooth surface to avoid singularities in the modeling (Fig.2.6.). The cap surface serves two main purposes. It bounds the yield surface in pure hydrostatic compression and controls the volume dilatancy when the material yields in shear [66].

Experimental calibration of the DPC model for pharmaceutical [67, 68, 69, 70, 71, 72], metallic [73, 74] and ceramic [75] powders were extensively conducted in previous studies. The Drucker-Prager shear failure surface can be determined by two of the four experiments for measuring tablets strength: uniaxial tension, pure shear, diametrical compression and uniaxial compression tests. As the maximum

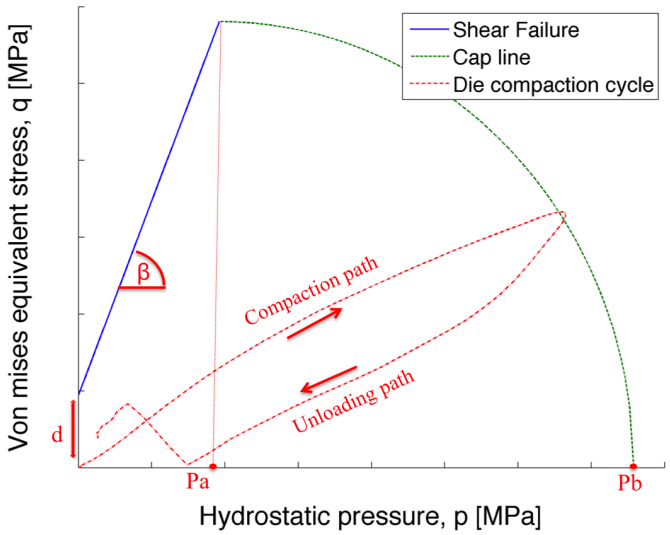

Figure 2.6: The Drucker-Prager Cap yield surface model in q-p plane.

loading values of each experiment are positioned on the shear failure line, by using two tests the shear failure line can be determined. The slope of the line represents the friction angle β, and the intersection with q axis represents the cohesion, d. The following equation represents the shear failure line, F_s:

$$F_s = q - d - p \tan \beta = 0 \tag{2.1}$$

Where the hydrostatic pressure (i.e. negative mean stress), p and the effective Von mises equivalent stress, q are obtained from the stress tensor, σ and defined as follows:

$$p = \frac{1}{3} tr\,(\sigma) \tag{2.2}$$

$$q = \sqrt{\frac{1}{2}\left[(\sigma_1 - \sigma_2)^2 + (\sigma_2 - \sigma_3)^2 (\sigma_3 - \sigma_1)^2\right]} \tag{2.3}$$

The cap yield surface is obtained by analyzing the stress state of the loading and unloading path in die compaction and written as:

$$F_c = \sqrt{(p - P_a)^2 + \left(\frac{Rq}{1 + \alpha - \alpha/\cos\beta}\right)^2} - R\,(d + P_a \tan\beta) \tag{2.4}$$

Where the density-dependent parameters R, d and β are the cap eccentricity, cohesive strength and internal friction angle, respectively. α is the smoothing transition constant that is used to define the smoothing transition between the shear failure surface and the cap. In this work, an arbitrary transition parameter of α=0.01 was chosen (typically 0.01< α <0.05) in order to ensure avoiding numerical singularities.

As mentioned previously, in order to obtain a smoothing transition between the shear failure surface and the cap yield surface, a transition surface F_t should be applied:

$$F_t = \sqrt{(p - P_a)^2 + \left[q - \left(1 - \frac{\alpha}{\cos\beta}\right)(d + P_a \tan\beta)\right]^2} - \alpha\,(d + P_a \tan\beta) \tag{2.5}$$

2.4.2 Determination of elastic properties

In this model, a simplified approach considering linear elasticity was implemented. This simplification is due to the difficulties extracting data from the non-linear behavior of the unloading in the experiment and mainly due to computational reasons, solving a linear elasticity. In fact, at low stresses and densities the elasticity is highly non-linear, whereas at high stresses and densities the elasticity shows higher linear behavior. Powder compaction can be adequately simulated by taking into account

only the linear elastic part. However, simulating the ejection and extraction out of the die (or rolls) requires the non-linear contribution of the elasticity as well.

From the generalized three-dimensional Hook's law stress-strain relationship, assuming linearly elastic isotropic materials and super-positioning the strain components in a cylindrical coordinates system (z,r,θ), the strain along each axis can be written as:

$$\varepsilon_{zz} = \frac{1}{E}\left[\sigma_{zz} - \nu\left(\sigma_{rr} + \sigma_{\theta\theta}\right)\right] \tag{2.6}$$

$$\varepsilon_{rr} = \frac{1}{E}\left[\sigma_{rr} - \nu\left(\sigma_{zz} + \sigma_{\theta\theta}\right)\right] \tag{2.7}$$

$$\varepsilon_{\theta\theta} = \frac{1}{E}\left[\sigma_{\theta\theta} - \nu\left(\sigma_{zz} + \sigma_{rr}\right)\right] \tag{2.8}$$

Considering the cylindrical die as rigid ($\varepsilon_{rr} = 0$) with axial symmetry conditions ($\varepsilon_{rr} = \varepsilon_{\theta\theta}$ and $\sigma_{rr} = \sigma_{\theta\theta}$) Eq.2.7. can be derived:

$$\Delta\varepsilon_{rr} = \frac{1}{E}\left[\Delta\sigma_{rr} - \nu\left(\Delta\sigma_{rr} + \Delta\sigma_{zz}\right)\right] = 0 \tag{2.9}$$

From Eq.2.9, Poisson's ratio ν can be expressed:

$$\nu = \frac{\Delta\sigma_{rr}}{\Delta\sigma_{rr} + \Delta\sigma_{zz}} = \frac{\frac{\Delta\sigma_{rr}}{\Delta\sigma_{zz}}}{\frac{\Delta\sigma_{rr}}{\Delta\sigma_{zz}} + 1} \tag{2.10}$$

In the same manner and by knowing the Poisson's ratio obtained in Eq.2.10, the

Young's modulus E can be expressed from Eq.2.6.:

$$\Delta\varepsilon_{zz} = \frac{1}{E}\left[\Delta\sigma_{zz} - \nu\left(\Delta\sigma_{rr} + \Delta\sigma_{rr}\right)\right] \tag{2.11}$$

$$E = \frac{\Delta\sigma_{zz}}{\Delta\varepsilon_{zz}}\frac{\left(1+\nu\right)\left(1-2\nu\right)}{\left(1-\nu\right)} \tag{2.12}$$

Therefore, it is needed to measure $\Delta\sigma_{rr}$ $\Delta\sigma_{zz}$ and $\Delta\varepsilon_{zz}$ in order to obtain the elastic properties from the unloading compaction curve (Eq.2.10. and Eq.2.12.).

2.4.3 Determination of shear failure

The shear failure line is constructed by knowing the cohesion d, which is the intersection with the q plane and the internal friction angle β which is the slope of the line. First the tensile and compressive strength of the compacted powder are determined using a diametrical compression test (Erweka TBH30, Erweka® Gmbh) and a unconfined uniaxial compression test. For diametrical compression, the failure strength σ_d and stress state (p-q) are defined as following:

$$\sigma_d = \frac{2F_d}{\pi D t} \tag{2.13}$$

$$p_d = \frac{2}{3}\sigma_d \qquad q_d = \sqrt{13}\sigma_d \tag{2.14}$$

Where F_d is the crushing force, D is the tablet diameter and t is the tablet

thickness. For the unconfined uniaxial compression test:

$$\sigma_c = \frac{4F_c}{\pi D^2} \tag{2.15}$$

$$p_c = \frac{1}{3}\sigma_c \qquad q_c = \sigma_c \tag{2.16}$$

Where σ_c is the axial compression failure strength and F_c is the axial compression force at the yield point. By knowing the stress state (p-q) of both test, the cohesion and internal friction angle can be calculated:

$$d = \frac{\sigma_c \sigma_d \left(\sqrt{13} - 2\right)}{\sigma_c - 2\sigma_d} \tag{2.17}$$

$$\beta = \tan^{-1}\left[\frac{3\left(\sigma_c - \sqrt{13}\sigma_d\right)}{\sigma_c - 2\sigma_d}\right] \tag{2.18}$$

2.4.4 Determination of cap surface

From the axial σ_{zz} and radial σ_{rr} pressure obtained in the instrumented die, considering cylindrical (r,θ,z)-coordinates with axisymmetry conditions ($\sigma_{rr} = \sigma_{\theta\theta}$), the mises-equivalent shear stress (Eq.2.3.), and the mean stress (Eq.2.2.), are simplified, respectively:

$$q = |\sigma_{zz} - \sigma_{rr}| \tag{2.19}$$

$$p = \frac{\sigma_{zz} + 2\sigma_{rr}}{3} \tag{2.20}$$

The evolution parameter P_a representing the hardening or softening driven by the volumetric plastic strain, the cap eccentricity R and the hydrostatic pressure P_b are obtained as follows:

$$P_a = \frac{-3q - 4d\tan\beta + \sqrt{9q^2 + 24dq\tan\beta + 24pq\tan\beta^2 + 16q^2\tan\beta^2}}{4\tan\beta^2} \tag{2.21}$$

$$R = \sqrt{\frac{2}{3q}(p - P_a)} \tag{2.22}$$

$$P_b = P_a + R(d + P_a\tan\beta) \tag{2.23}$$

The hydrostatic pressure yield surface P_b (Eq.2.23.) defines the position of the cap and dependent on the volumetric inelastic strain ε_{vol}^{in}. Eq.2.21. and Eq.2.22. are modified accordingly in order to introduce the smoothing transition parameter α [66].

$$P_b = P_b\left(\varepsilon_{vol}^{in}\right) \tag{2.24}$$

By measuring the bulk density ρ of the tablet after ejection and dividing it with the initial density ρ_0 of the powder when filling the die, the inelastic volumetric

strains ε_{vol}^{in} can be calculated:

$$\varepsilon_{vol}^{in} = ln\left(\frac{\rho}{\rho_0}\right) \tag{2.25}$$

2.4.5 Tablet compaction

Calibrating the DPC model requires the preparation of tables in different manners. For obtaining the elastic and the cap properties, a fully instrumented press is necessary. For the shear failure line, a simple compaction press can be used, however, certain important aspects must be kept. According to Doremus et al[76], for the diametrical compression test, it is important to ensure that failure arises from tensile fractures originating at the center of the specimen. To achieve this, the diametrical compression test must be carried out for tablets with aspect ratio $H/D \leq 0.25$, where H is the height and D is diameter of the specimen. For the axial compression test, in order to ensure the failure does not cross the two ends of the specimen, aspect ratio *(H/D)* of specimen must equal or larger than 2.0.

It is important to mention that the aspect ratios may vary for different materials and are only given as guidelines. Moreover, producing tablets with large heights may not sufficiently compact the powder to a solid dosage form, thus making it difficult to achieve large aspect ratios. Therefore, it is also necessary to observe and ensure that the desired failure path obtained.

2.4.6 Tablet compaction for elastic and cap properties

The die compaction cycles curves for different relative densities where obtained by a fully instrumented eccentric uniaxial press (Frogerais OA, France). The press is instrumented with five sensors that allow the measurement of the displacements of the upper and lower punches, the applied axial pressure σ_u, the transmitted axial pressure to the lower punch σ_l and the radial stress on the die wall σ_r. The die used was a fixed cylindrical die of 11.28 mm of diameter and 10 mm of height. First, the

upper punch is displaced downward, applying pressure on the powder and later the tablets are ejected out of the die by the lower punch. The tablets were prepared by automatically filling a powder mass of 0.305 ± 0.010 g into the die and compacting different predefined set of displacements (4.5 to 7.4 mm) which corresponds to a set of maximum pressures (6 to 180 MPa), obtaining a range of relative densities (0.38 to 0.91). During the compaction process, the pressures and displacements of the upper and lower punches as well as the radial stress on the die were recorded. For each displacement set, a total of ten tablets were produced, disregarding the first and last tablets data and storing the mean values of the other eight tablets.

2.4.7 Tablet compaction for shear failure properties

The shear failure line parameters of cohesion d and friction angle β were calibrated using diametric and unconfined uniaxial compression tests and utilizing Eq.2.17. and Eq.2.18. In order to minimize the density gradient, the specimens for diametrical compression and uniaxial compression test were prepared by lubricating the die tooling. For diametrical compression test, cylindrical flat tablets were prepared by filling a powder mass of 0.350 ± 0.005 g into the die and compacting at seven different pressures (from 10 to 120MPa), varying the compacted tablets thickness between 2.6 to 4.8 mm (resulting in relative densities of 0.46 to 0.85). Tablets for the compression test where produced using a cylindrical die of 11.28 mm of diameter and 90 mm of height. The aspect ratio *(H/D)* of 2.0 was obtained by compacting the tablet to a final height of 22 mm with varying the filling powder mass in order to obtain a range of 0.31 to 0.9 relative densities. For repeatability, in both cases, the mean of three measurements was used for each desired relative density.

2.4.8 Experimental calibration results

The Drucker-Prager Cap model parameters are plotted as a function of the relative density. The elastic properties obtained by analyzing the die compaction unloading curves using Eqs.2.12 and 2.10 are plotted in Fig.2.7. It can be seen the Young's Modulus is increasing exponentially from 0.8 to 7.4 GPa in the range between the

filling bulk density and a full dense material. The Poisson's ratio does not show a decisive exponential behavior, having scatter values from 0.1 to 0.24 for the same range of relative densities.

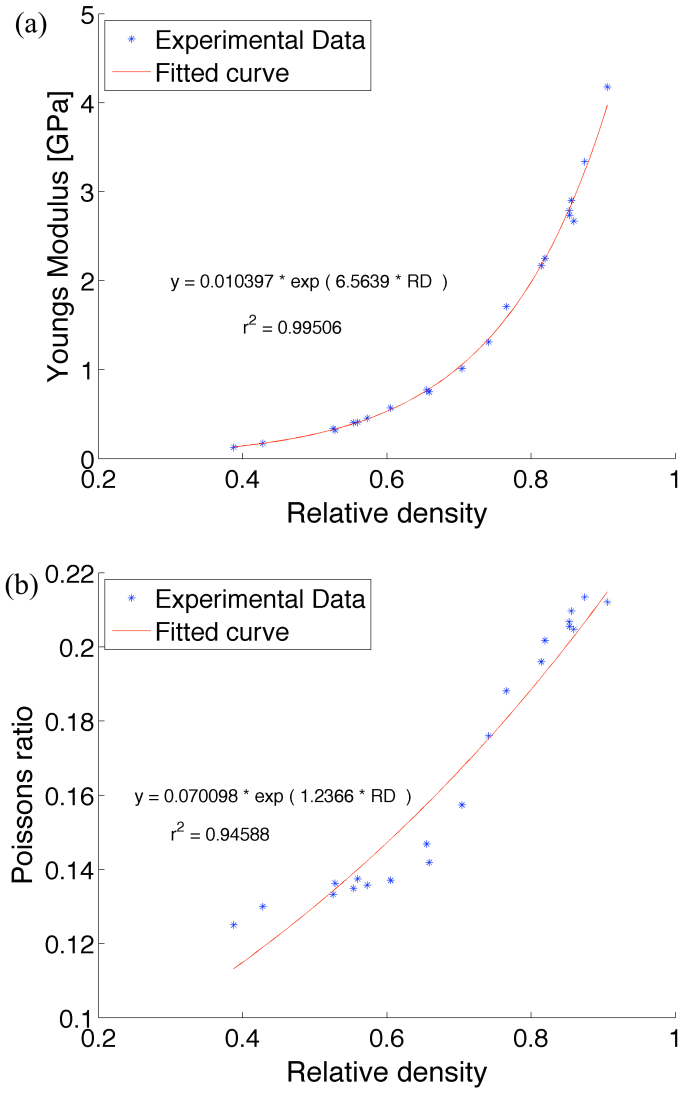

Figure 2.7: Elastic properties a)Young's Modulus, E and b)Poisson's ratio, ν

The cohesion and internal friction angle are obtained from nonlinear regression fittings of the diametrical and compressive tests and plotted for the desired relative

densities which the DPC model was calibrated(Fig.2.8.). As the Young's Modulus, the cohesion values increases exponentially with increasing relative density. The internal friction angle shows a nonlinear behavior, with a slight decrease for low relative densities and larger for high relative densities.

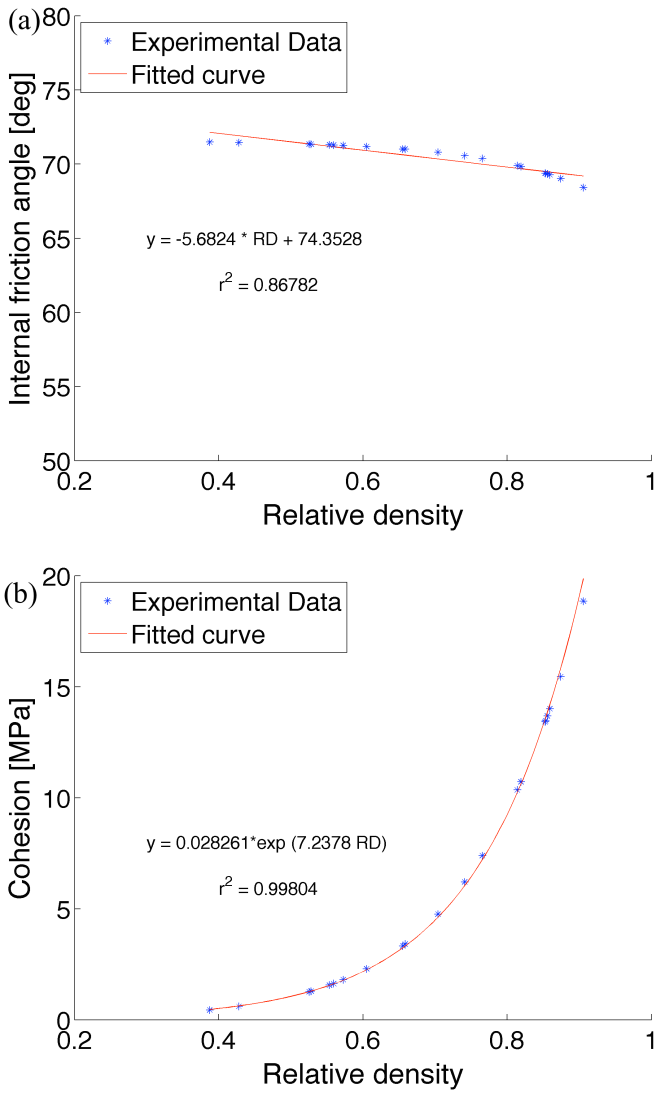

Figure 2.8: Shear failure parameters a)internal friction angle, β b) Cohesion, d.

The Cap line evolution parameter Pa, hydrostatic compressive stress Pb and the cap eccentricity R, which defines the shape of the cap are plotted against the relative densities (Figs.2.9&2.10.). The cap hardening is defined by 2.24, therefore, the hydrostatic compressive stress Pb is plotted as a function of the volumetric plastic strains as well(Fig.2.11.).

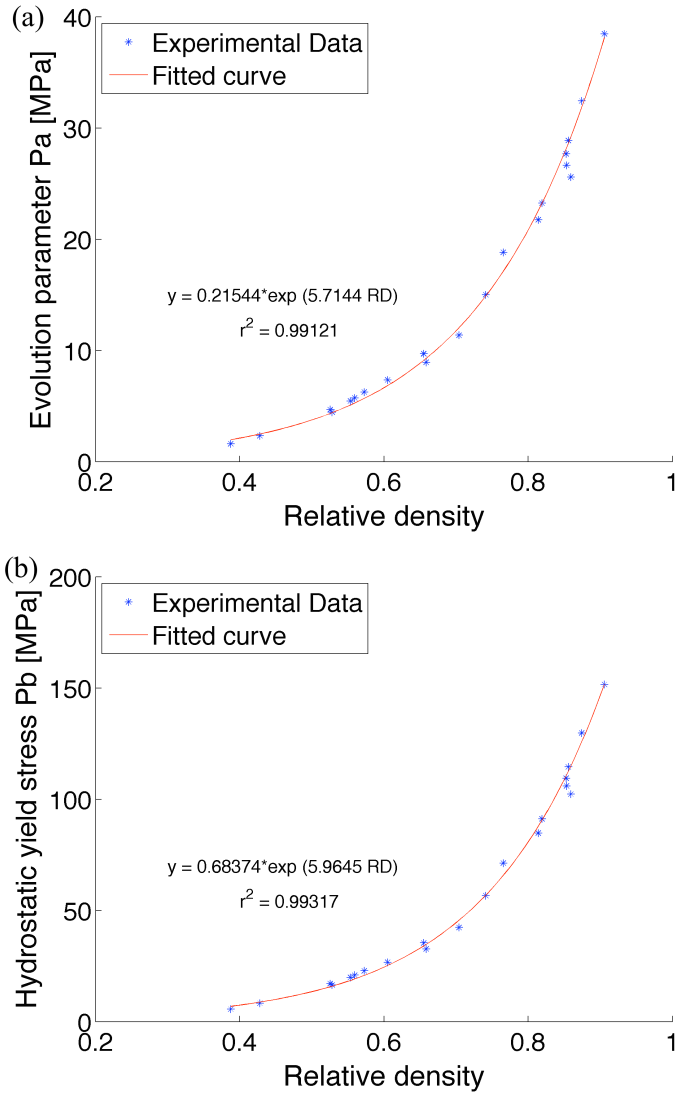

Figure 2.9: Cap parameters a)Pa and b)Pb as function of relative density.

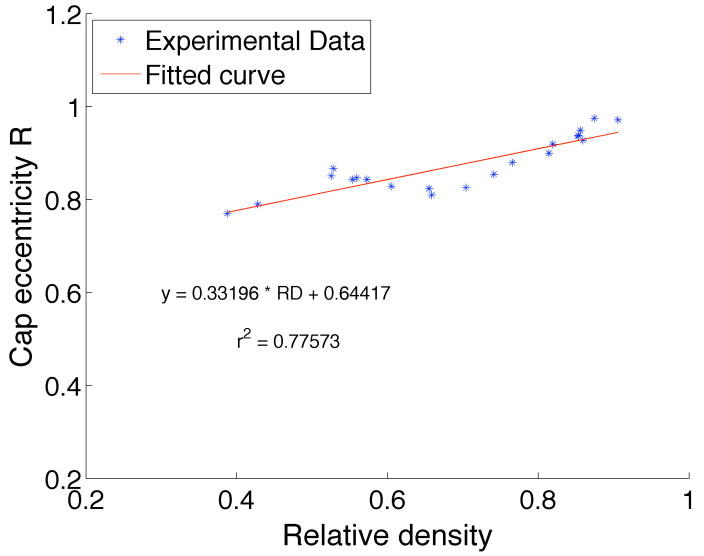

Figure 2.10: Cap eccentricity parameter R as function of relative density.

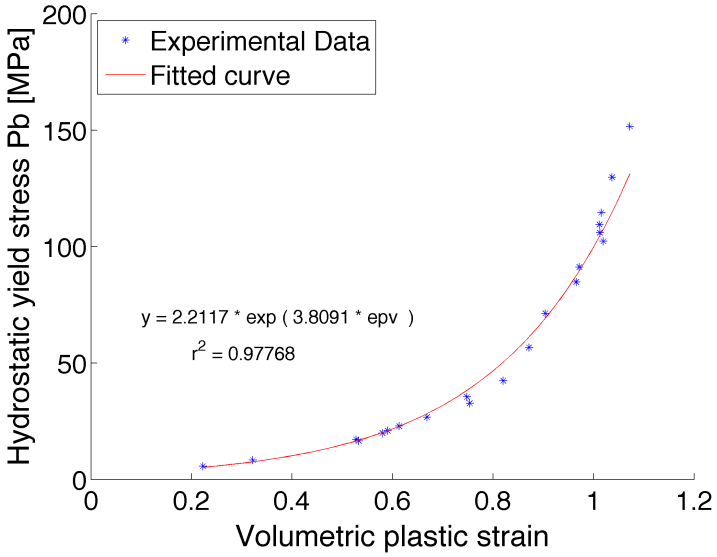

Figure 2.11: Hydrostatic compressive stress, Pb as a function of volumetric plastic strain

From the obtained results, the full DPC model is plotted with different isolines, representing each relative density(Fig.2.12). With the increasing relative density, the yield surface (or line in Fig.2.12) expands in stress space. It can be seen that each shear failure line has a different slope and intersection with the equivalent stress axis, which are represented by the density dependent internal friction angle and cohesion, respectively, plotted in Fig.2.8. The dotted lines are the die compaction curves in the p-q plane for different relative densities.

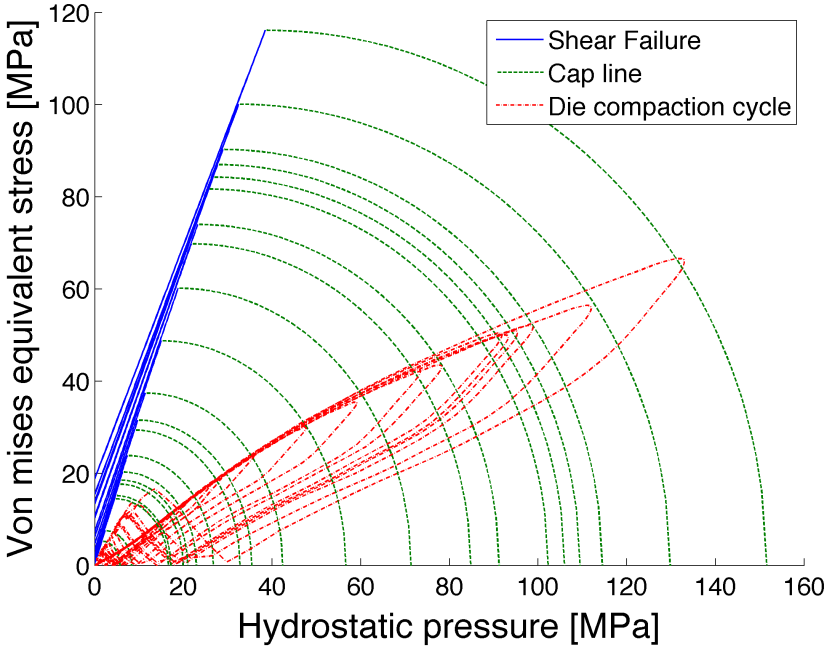

Figure 2.12: Experimental iso-density Drucker-Prager Cap

Most of the results show a clear and decisive exponential behavior which is used to extrapolate the DPC model for the low and high relative densities. However, some results such as the cohesion and the cap eccentricity did not show such behavior and may result in a non realistic extrapolated data. The results show a similar behavior as in the literature which is mostly done for MCC 102 with one exceptional study on MCC 101 [66].

2.5 Model validation: ribbon's envelope density measurement

Ribbon samples collected from the roll compaction were analyzed for relative density values. The 2.5 cm wide ribbons were sectioned into rectangular pieces of approximately 0.6 × 1 cm. The mass of each piece was determined with a high precision balance. The ribbon relative density (RD) requires both powder true density (ρ_{true}) and ribbon envelope density (ρ_e). The envelope density of the ribbons was determined using an envelope density analyzer (Geopyc 1360, Micromeritics Instrument Corp., Norcross, GA, USA). The internal diameter tube, consolidation force and conversion factor of 25.4 mm, 51 N and 0.5153 cm^3/mm, respectively were used. Once obtaining both the true and envelope density, the sample's porosity (P) and the relative density can be expressed as follows:

$$RD = 1 - P = \frac{\rho_e}{\rho_{true}} \tag{2.26}$$

Chapter 3

Finite Element Analysis of roll compaction process and press designs

Abstract

This chapter, which is divided into two main parts, aims to utilize the previously introduced three-dimensional FEM model to study the effect of the different process and simulation parameters, as well as sealing system designs, on the roll compaction process. Firstly, the effect of process and simulation parameters, including feed conditions, wall friction, roller speed and mass scaling factor, on the predicted results were studied and discussed based on the data from the literature. The second part of this chapter focuses on modelling the effect of different sealing system design (rimmed-roll and cheek plates) that equips the main industrial roller presses on the ribbon's density distributions. In both configurations, the predicted density distribution of the ribbons was validated experimentally. These obtained results demonstrate the capability of FEM modeling to provide insight and help to achieve a better understanding of the roll compaction process.

Resumé

Ce chapitre est divisé en deux parties. Son objectif est d'utiliser le modèle d'éléments finis 3D, précédemment introduit pour étudier l'effet des paramètres procédé et le design des conditions de confinement sur les résultats du compactage à rouleaux. Dans une première partie, l'impact des paramètres de simulation du procédé, en particulier les conditions d'alimentation, le coefficient de frottement poudre-rouleau, la vitesse du rouleau, sur les résultats sont étudiés et discutés à la lumière des résultats de la littérature. La seconde partie de ce chapitre est centrée sur l'étude du rôle du système de confinement dans la distribution de densité dans le compact. Deux configurations principalement présentes dans les presses industrielles, sont considérées. Dans les deux configurations, les prédictions numériques des distributions de densité dans le compact, ont été validées par des mesures. Ces résultats ont permit de démonter le potentiel de la méthode utilisée à mieux décrire le procédé de compactage à rouleaux.

3.1 Effect of process and simulation parameters

First thing when interpreting steady-state process simulations, is to ensure the convergence of the system and reaching the steady-state conditions. Therefore, the roll reaction force in y-direction at the reference node was recorded during the entire calculation period. As seen from Fig.3.1 the system reaches a steady state after 3 seconds, obtaining a total roll reaction force of 4 kN by a given inlet constant feeding pressure of 1 MPa.

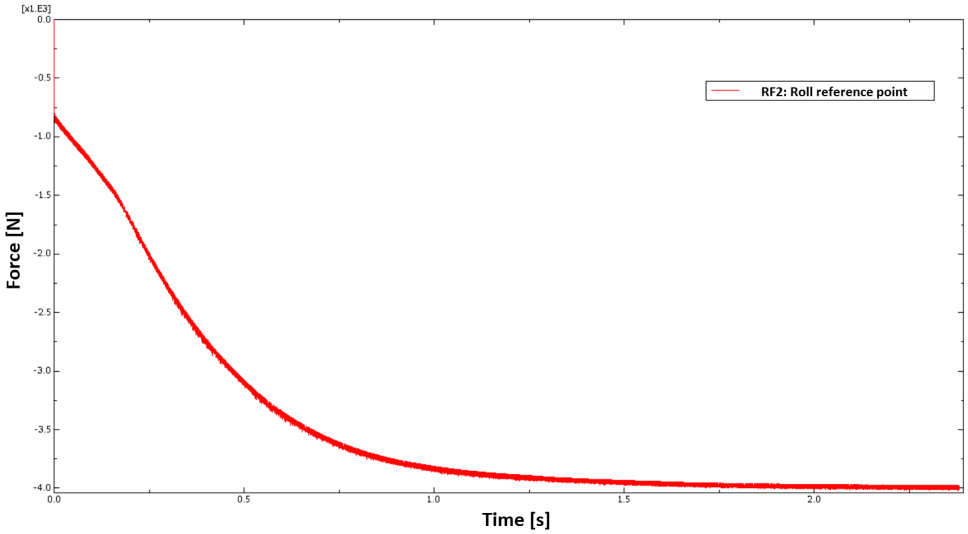

Figure 3.1: Reference FEM model steady-state condition

Once achieving the steady state, other results such as stresses, strains and velocities may be plotted. Another important aspect in FEM modelling using the Drucker-Prager Cap model is to plot the hydrostatic compression stress and the volumetric plastic strain to ensure the powder is under the correct stress state. The Final and most important validation of the model is to compare the obtained compacted powder density at the gap with the produced ribbon density.

The following figures visualizes the resulting density distribution (Fig.3.2), roll contact pressure (Fig.3.3) on the powder and vertical stress (Fig.3.4) (rolls do not appear for illustration reasons). As expected, due to the frictionless conditions from the sides, the results are uniform across the width. On the other hand, values of vertical stresses, roll pressure and relative density increases gradually from the feeding zone up to the smallest gap region in between rolls. The highest values obtained for the roll pressure and relative density are 33 MPa and 0.686, respectively.

This FEM model is used as a reference for further investigation of different simulation and process parameters, thus evaluating the model and investigating the roll compaction process based on result from the literature.

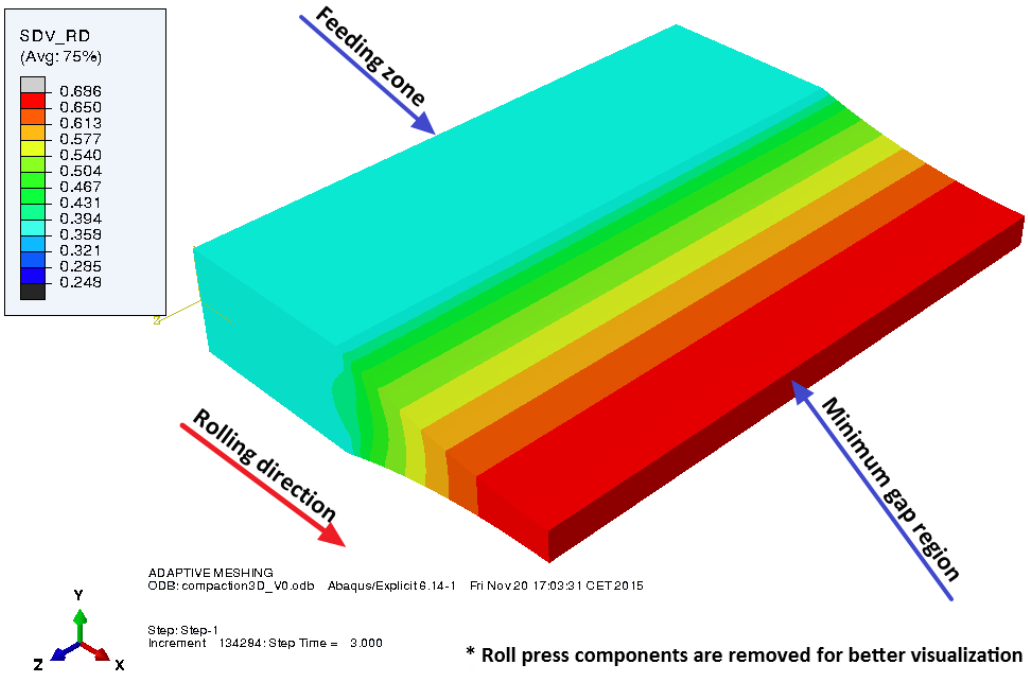

Figure 3.2: Reference FEM model results of relative density

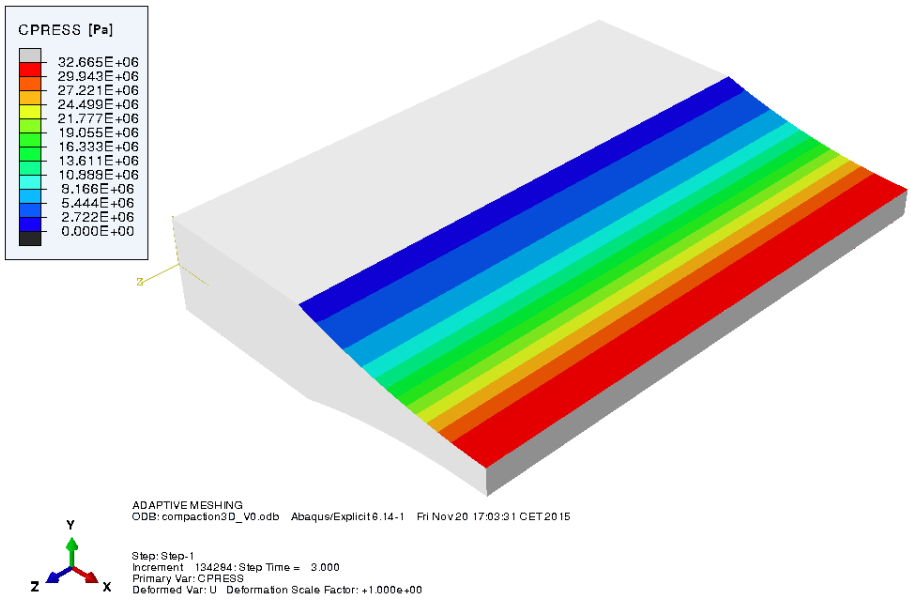

Figure 3.3: Reference FEM model results of roll contact pressure

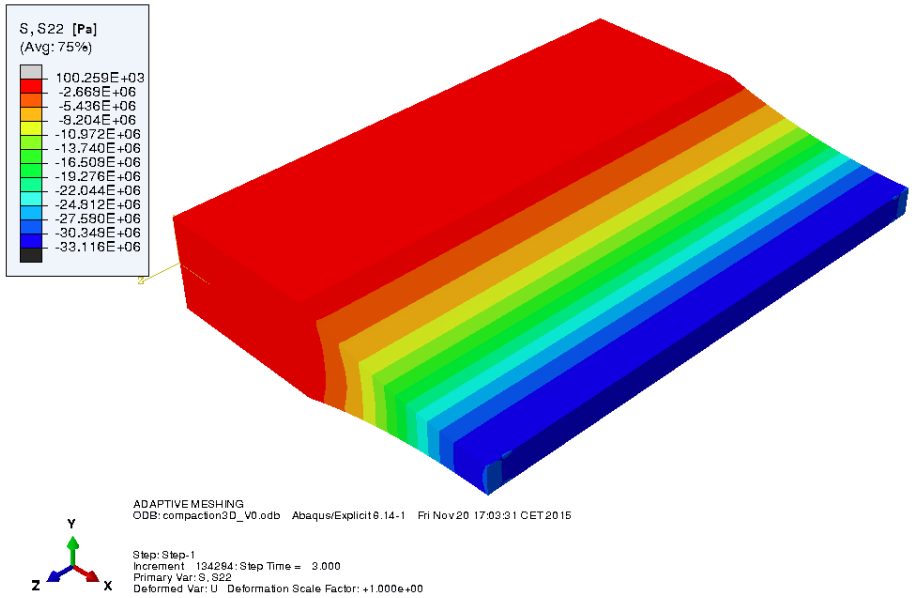

Figure 3.4: Reference FEM model results of vertical stress, σ_{22}

3.1.1 Effect of mass scaling

The advantage of mass scaling in increasing the computational speed of FEM modelling was introduced earlier in section 1.3.3. Therefore, a parametric study was done in order to investigate the maximum mass scaling factor that can be used in this model. In order to define the correct value, a series of different mass scaling factors between 500 to 1e6 are used and the FE models are simulated and compared.

The following figures visualizes the effect of mass scaling factor on the resultant roll pressure (Fig.3.5), shear stress (Fig.3.6) and ribbon's density (Fig.3.7).

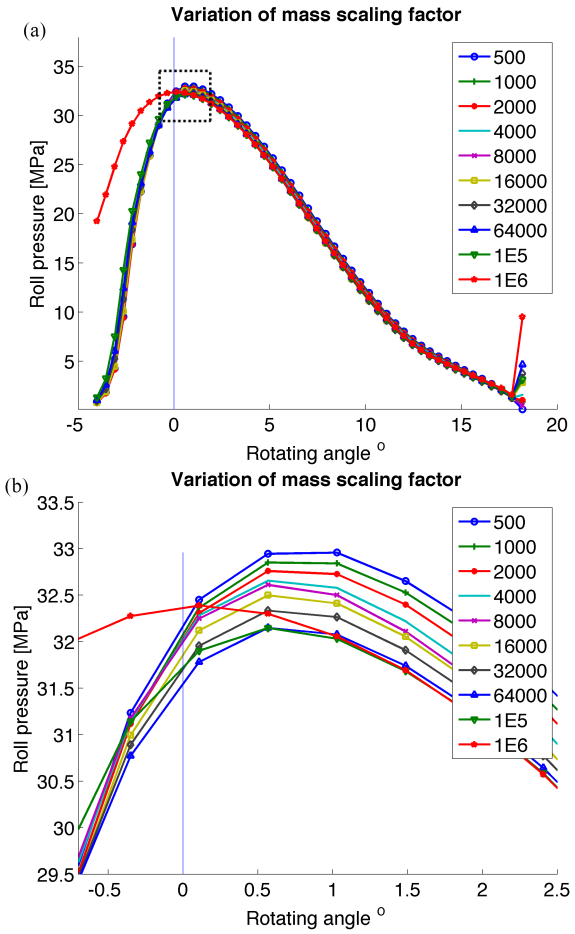

Figure 3.5: Effect of mass scaling on roll pressure along rolling direction

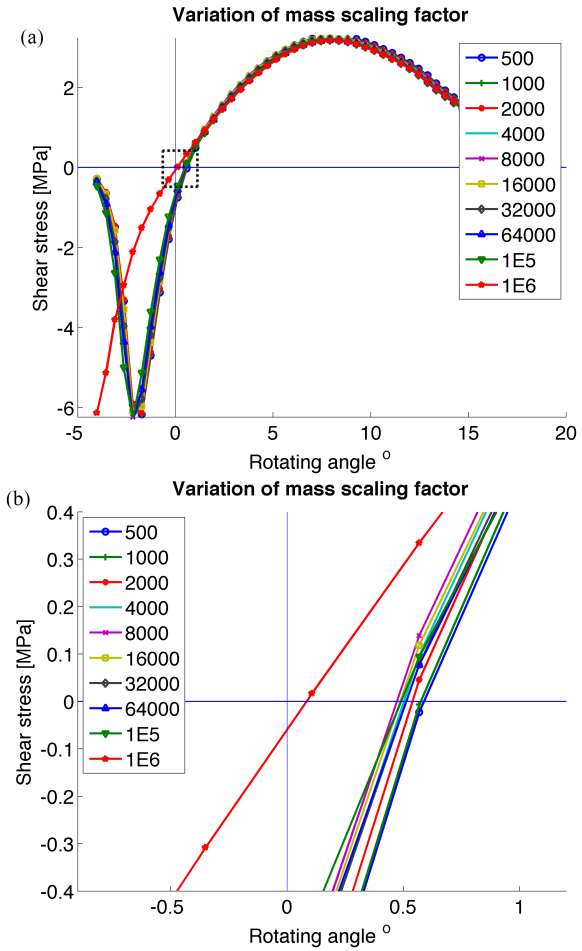

Figure 3.6: Effect of mass scaling on shear stress along rolling direction

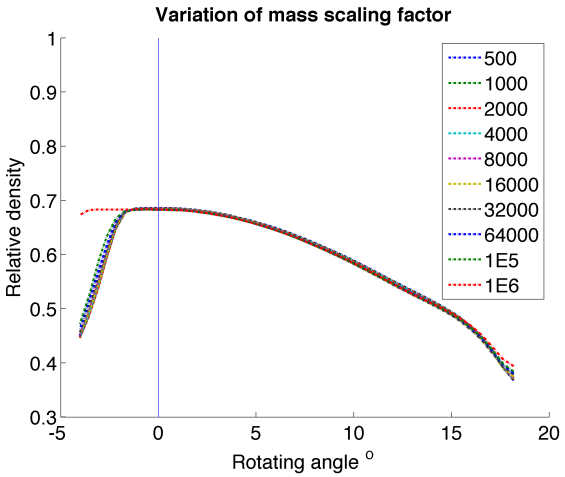

Figure 3.7: Effect of mass scaling on powder relative density along rolling direction

As can be seen in Figures 3.5-3.7, increasing the mass scale factor from 500 up to 1e5 has nearly shown any change in the results and considered to be identical. Using a mass scaling factor of 1e6 resulted in a large divergence from the previous results and is essentially meaningless. Therefore, in order to obtain the largest computational efficiency without altering the results, a mass scale of 1e5 was chosen for the following FEM simulations. Furthermore, a comparison of internal and kinetic energies was done. At low mass scaling values, the kinetic energy is only a small fraction of the internal energy over the majority of the roll compaction process history. At mass scaling of 1e6, the kinetic energy of the powder material is a significant fraction of its internal energy. By artificially increasing the stable time increment through mass scaling, we can now analyze the model in its natural time period. After choosing the maximum possible mass scaling, the FE model is simulated using a constant inlet feeding pressure of 1MPa.

3.1.2 Effect of inlet feed pressure

Analytical models of roll compaction, such as the Johanson model, introduces the feeding of material to the rolls by an inlet pressure. Based on this, most FEM models of roll compaction process were simulated with a given inlet feeding pressure as boundary condition. In order to investigate the validity of the current model with comparison to previous studies, the effect of inlet feed pressure on the roll compaction process was studied by varying the pressure in the range of 0.8 - 6 MPa.

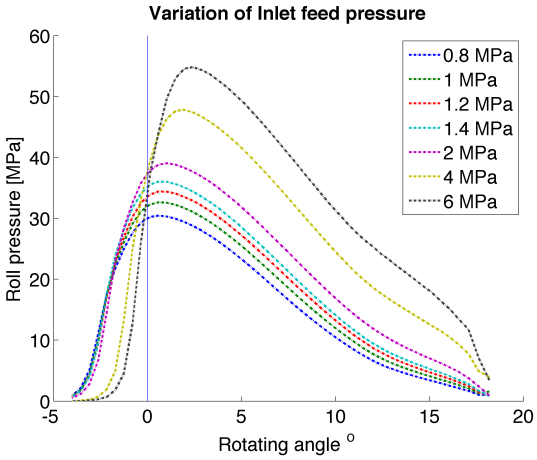

Figure 3.8: Effect of inlet feed pressure on the roll pressure

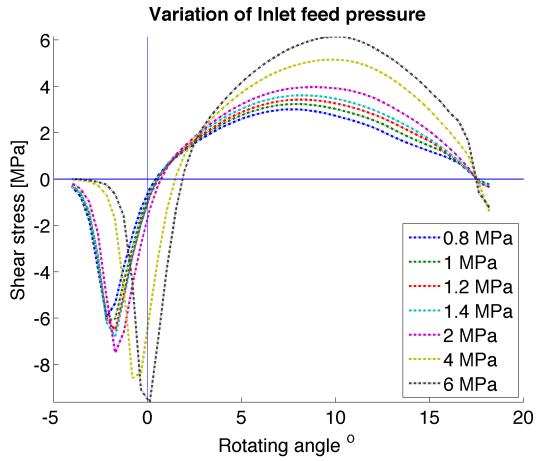

Figure 3.9: Effect of inlet feed pressure on the shear stress

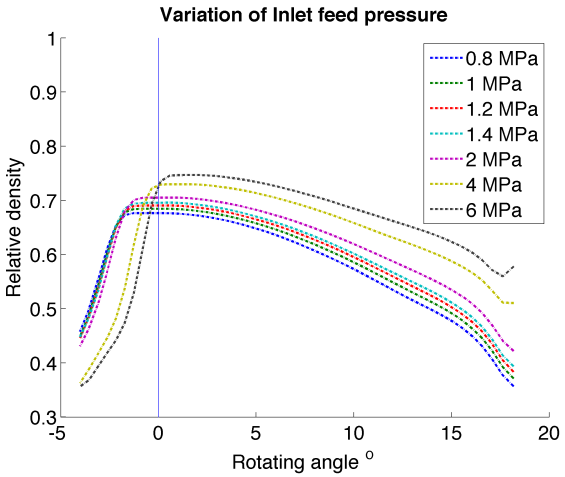

Figure 3.10: Effect of inlet feed pressure on the powder's relative density

As expected, an increase in the inlet feeding pressure results in an increase of the roll pressure(Fig.3.8), shear stress(Fig.3.9) and ribbon's density (Fig.3.10). Increasing the feed pressure from 0.8 to 2 MPa resulted in a small increase, whereas, for value of 4 and 6 MPa feeding pressure, the resultant roll pressure, shear stress and ribbon's density increased drastically. This result is in complete agreement with the Johanson analytical model and the previous FEM studies conducted for roll compaction process. Another interesting phenomenon that can be noticed is the shifting of the maximum roll pressure and the neutral axis (where the shear stress changes sign due to friction direction) towards the inlet region. This behavior suggests that the amount of powder provided by the screw feeder is too large and the system is over fed, thus blocking the machine.

3.1.3 Effect of inlet feed velocity

Using an inlet feed velocity to represent the screw feeding mass throughput in between the rolls is a more realistic way to simulate the roll compaction process. In this case, we vary the inlet feed velocity for the back nodes of the FE model from 0.01 to 0.03 m/s.

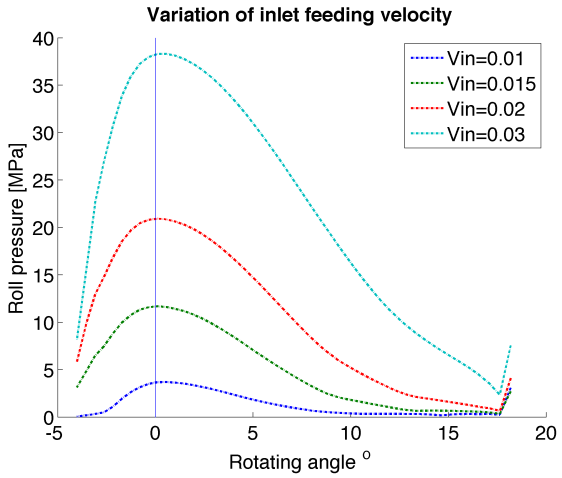

Figure 3.11: Effect of inlet feed velocity on the roll pressure

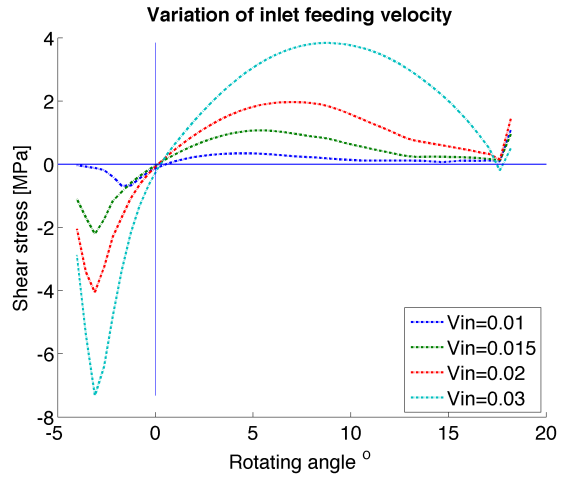

Figure 3.12: Effect of inlet feed velocity on the shear stress

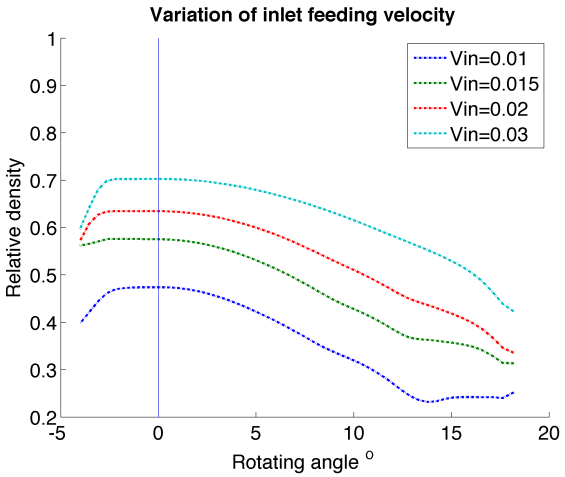

Figure 3.13: Effect of inlet feed velocity on the powder's relative density

The obtained results are similar to the previous ones using an inlet feeding pressure. An increase in the inlet feeding velocity results in an increase of the roll pressure, shear stress and ribbon's density. By comparing the results obtained by the two different inlet boundary conditions, it can be noted that a feeding pressure of 1.4 MPa was equivalent to an inlet feeding velocity of 0.03 m/s

3.1.4 Effect of friction coefficient

The formation of compacted ribbons in the roll compaction process are the result of the contact pressure, which exerts due to friction in between powder and rolls. Obviously, by increasing the friction coefficient between powder and rolls, the contact pressure will increase and consequently the compacted ribbon's relative density.

Figs.3.14-3.16 shows that indeed, an increase in the friction coefficient results in an increase of the roll pressure, shear stress and relative density. Moreover, it also causes the shifting of the maximum roll pressure and natural axis towards the minimum gap region.

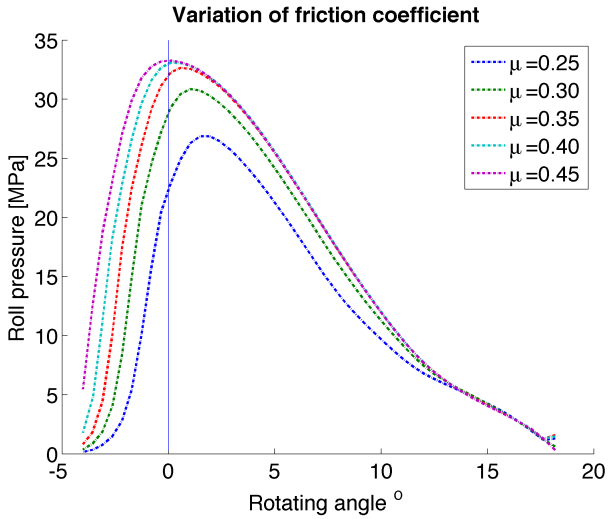

Figure 3.14: Effect of friction coefficient on the roll pressure

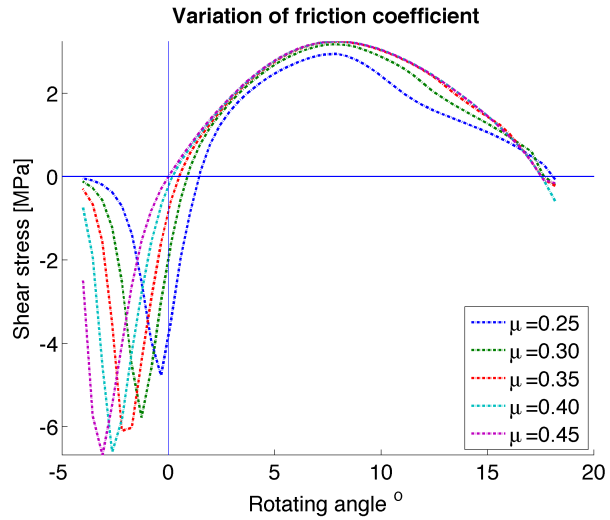

Figure 3.15: Effect of friction coefficient on the shear stress

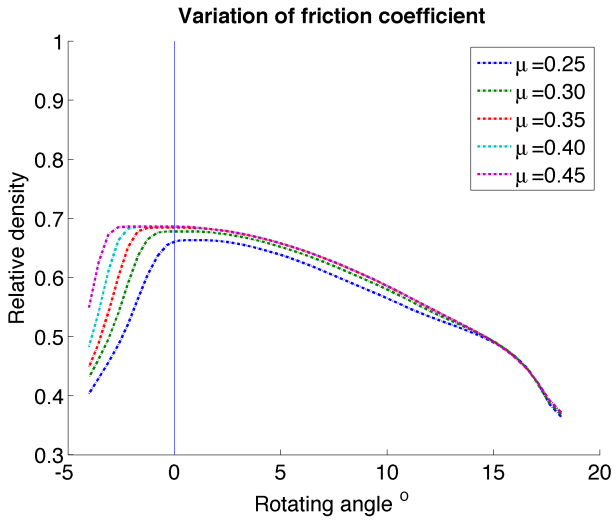

Figure 3.16: Effect of friction coefficient on the powder's relative density

3.1.5 Effect of roll speed (using inlet feed pressure)

As mentioned previously, one major limitation of the analytical models is that they do not represent the effect of roll speed. The following results show that in fact by introducing inlet feeding pressure, the roll speed does not have an effect on the roll compaction process and the resultant ribbons.

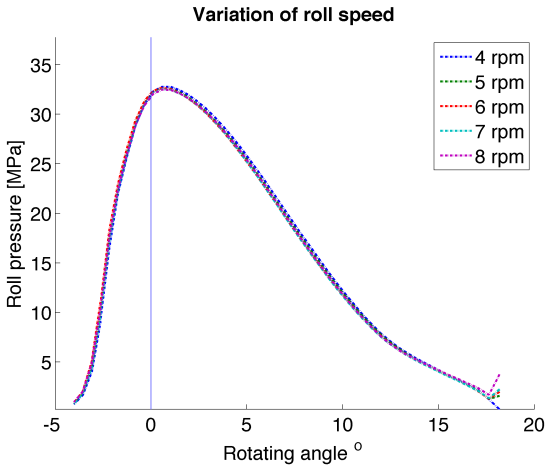

Figure 3.17: Effect of roll speed (using inlet feed pressure) on the roll pressure

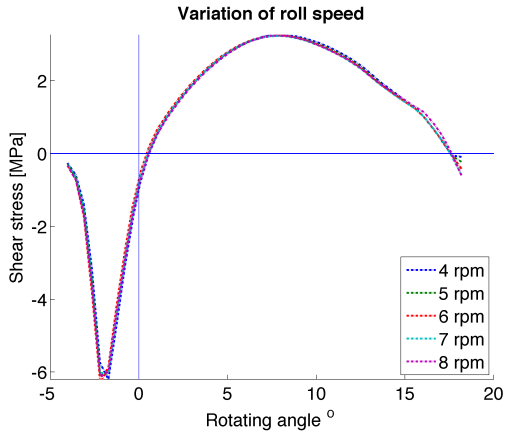

Figure 3.18: Effect of roll speed (using inlet feed pressure) on the shear stress

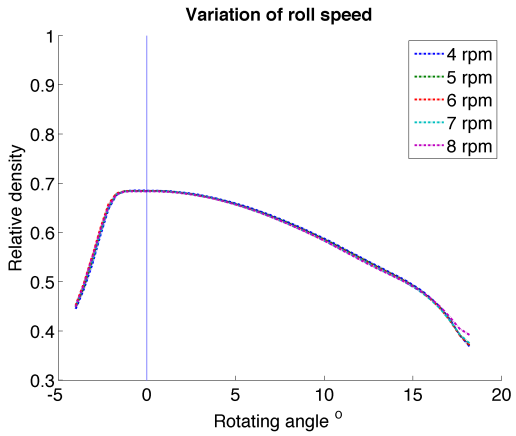

Figure 3.19: Effect of roll speed (using inlet feed pressure) on the relative density

Results show in Figs.3.17-3.19 are consistent with the assumption used in the Johanson model, which does not take into account the roll speed. In fact, the applied pressure is already a result of the inlet feeding powder material and its interaction with the rolls. In order to avoid the redundancy of the roll speed in numerical methods, it is recommended to use a far-field inlet pressure by extending the feeding zone and applying the inlet boundary conditions far from the rolls. However, this approach is less realistic as the distance between the last flight of the screw and the rolls is rather small

3.1.6 Effect of roll speed (using inlet feed velocity)

Based on previous results. A better way to represent the material throughput in the roll compaction process is to introduce an inlet feed velocity. By varying roll speed from 5rpm to 8rpm, using a constant inlet feeding velocity of 0.025 m/s.

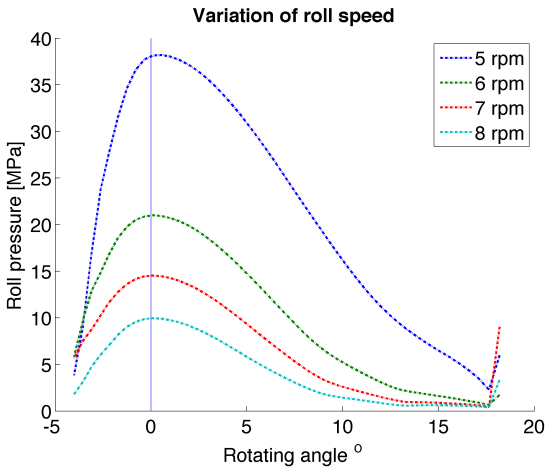

Figure 3.20: Effect of roll speed (using inlet feed velocity) on the roll pressure

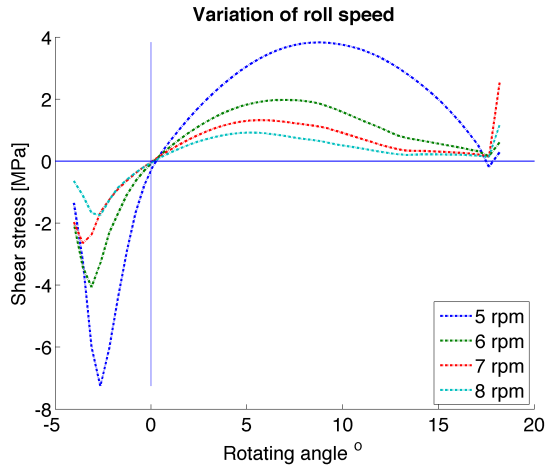

Figure 3.21: Effect of roll speed (using inlet feed velocity) on the shear stress

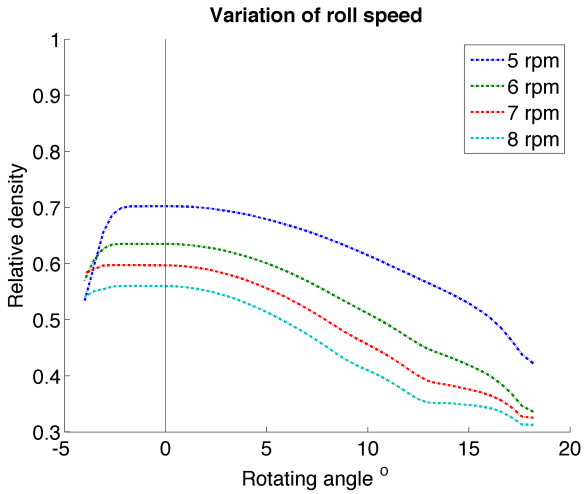

Figure 3.22: Effect of roll speed (using inlet feed velocity) on the roll powder's relative density

Results show the variation of roll pressure, shear stress and powder's relative density in between the rolls. Reducing the roll speed from 8rpm to 5rpm, increases the amount of powder in the system and as a consequent of larger mass content, the roll pressure (Fig.3.20) and relative density (Fig.3.22) increase. It has also shown the supirorty of using an inlet velocity boundary conditions, rather than a inlet pressure one.

3.2 Conclusions

The above simulation results of different process parameters clearly show the ability of FEM modelling to help better understand the roll compaction process. FEM results found to be comparable to previous experimental, analytical and numerical studies in the literature. These findings validate the capability of current modelling approach for further development and investigation of roll compaction based on FEM.

3.3 Effect of sealing system design*

As mentioned in section 1.2.4.2, roll compactors are constructed with a sealing system, limiting the loss of powder from the sides. However, the sealing system may result in unwanted non-uniform properties along the ribbon's width and may also exhibit fractured or incomplete compacted edges. Numerous experimental studies were conducted in order to evaluate the density distribution of roll compacted ribbons using destructive and non-destructive methods. Studies showed that using using roll compactors integrated with fixed side seals (cheek plates), results in non-uniformity along the ribbon's width with lower densification at the edges and higher at the middle of the produced ribbon. Moreover, cheek plates may also have a negative effect on the ribbon with fractured or incomplete compacted edges. For this, several roll compactors offers a rimmed-roll sealing system in order to reduce the cheek plates unwanted effects. This is only based on preliminary studies made by Funakoshi [45], which developed a roll compactor with concave-convex roll pair in order to avoid the loss of powder and to reduce the ribbon's heterogeneity.

The aim of this work is to investigate by FEM modeling the roll compaction process using both rimmed-roll and cheek plates sealing system design. More importantly, to provide a first insight on the roll compaction process using the rimmed-roll sealing system. Both designs are available in the Gerteis Minipactor and therefore was chosen for this study.

*This chapter has been publish in: Alon Mazor, Lucia Perez-Gandarillas, Alain de Ryck, Abderrahim Michrafy, Effect of roll compactor sealing system designs: A finite element analysis, Powder Technology, Volume 289, 2016, Pages 21-30, ISSN 0032-5910, http://dx.doi.org/10.1016/j.powtec.2015.11.039.

3.3.1 Finite Element (FE) model

Similarly to previous analyses, FEM models of the Gerteis Minipactor were solved as a steady-state problem using arbitrary Lagrangian-Eulerian (ALE) adaptive meshing in Abaqus/Explicit v6.14. The density-dependent behavior described by the calibrated DPC model (section 4.2.3.3) is implemented by an external user-defined VUSDFLD Fortran subroutine code. The inlet material density was set to be the tapped powder density as a result of the screw feeding. The Avicel PH 101 tapped density is about 0.47 g/cm^3 which corresponds to an initial relative density of 0.3.

First step in creating a Finite Elements (FE) model is to represent the geometry of the desired roll compactor. In the case of Gerteis Minipactor, the rolls diameter and width are 250 mm and 25 mm respectively and defined as analytic rigid surfaces. It is important to mention that the rolls here are smooth, rather than knurled in the experiment. Knurled rolls increases the complexity and the non-linearity of such simulations and are only represented by higher friction coefficient between the powder and the rolls. Once sketching the press dimensions, the region between the rolls is discretized and meshed using C3D8R three-dimensional continuum reduced integration elements. The smallest gap where the powder in contact under the rolls needs to be fixed and predefined as 1.5 mm gap. For the cheek plates case, two analytic rigid side surfaces bounding the mesh between the rolls. For the rimmed-roll case, the rim with diameter of 275 mm is integrated with the bottom roll and defined as analytic rigid surface as well. The FE models for both roll compactor sealing systems designs are visualized in Fig.3.23. It is important to mention that due to the unsymmetry of the rimmed-roll sealing system assembly, both FE model's geometry was constructed fully without taking into account symmetry conditions, which are usually applied to reduce computational costs.

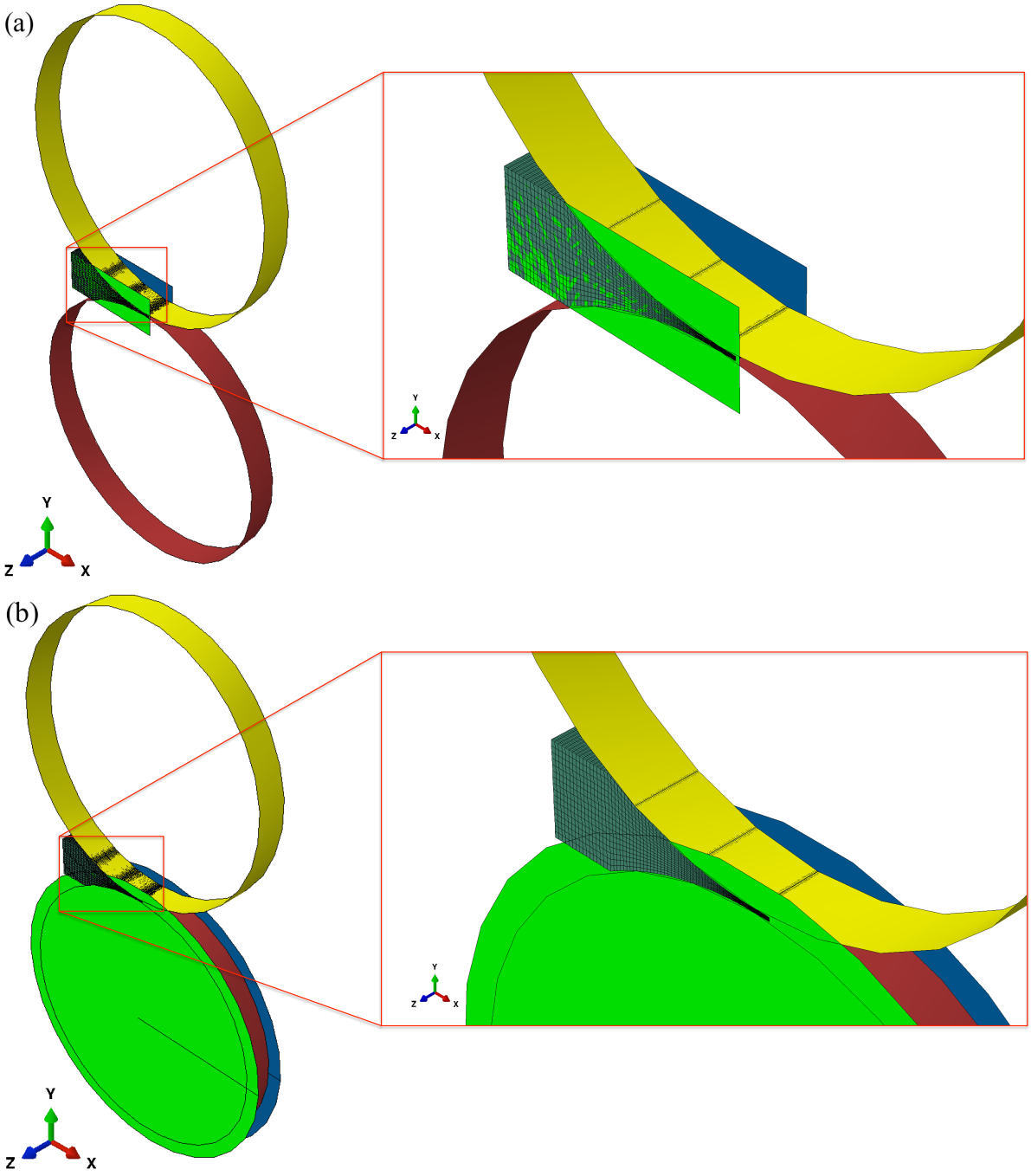

Figure 3.23: FE models of roll compactor with a)cheek plates and b)rimmed-roll

3.3.1.1 Boundary conditions

In this work the inlet was simplified and defined as a constant feeding pressure. First, two different inlet pressures cases, corresponding to a roll separation force of 6 and 8 kN/cm were investigated in order to validate the capability of the model. Then, a constant feeding pressure of 0.2 MPa in order to obtain the desired 4 kN/cm roll separation force (Fig.3.24). As the cross section area, shape and position of the inflow boundary are measured directly from the roll compactor and known in advance, both the material and mesh constraints must be applied. The inlet and outlet nodes were constraint in the normal direction to avoid translation in the stream wise direction and maintain a steady uniform flow. In order to improve convergence to the steady-state solution, a linear constraint equation was implemented both for the inlet and outlet nodes, constraining the material velocity to be uniform normal to the outflow. A rotational boundary condition in z-direction was defined based on the roll rotating velocity in the experiment, which was set to 2 rpm.

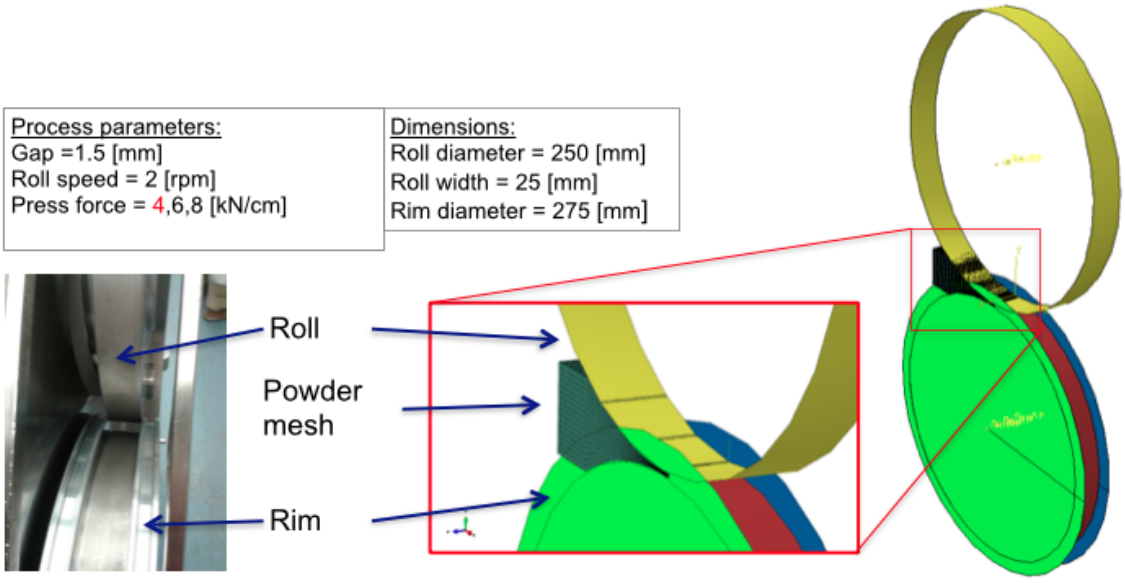

Figure 3.24: Detailed description of FE model using rimmed-roll sealing system

3.3.2 Simulation results

Once reaching a steady-state solution by obtaining a constant relative density and vertical reaction force on the roll pin, the FEM results were analyzed. A typical FEM modeling calculates stresses, strains and velocities. Due to numerical reasons, the results are obtained and plotted only for the material which is still in contact with the roll, up to the narrowest gap region. [11]. In addition, in this work, a user-defined subroutine was implemented using a state variable of the relative density, ($RD = RD_0 e^{-\varepsilon_v^p}$) which is calculate from the initial bulk density, RD_0 and the volumetric plastic strain, ε_v^p.

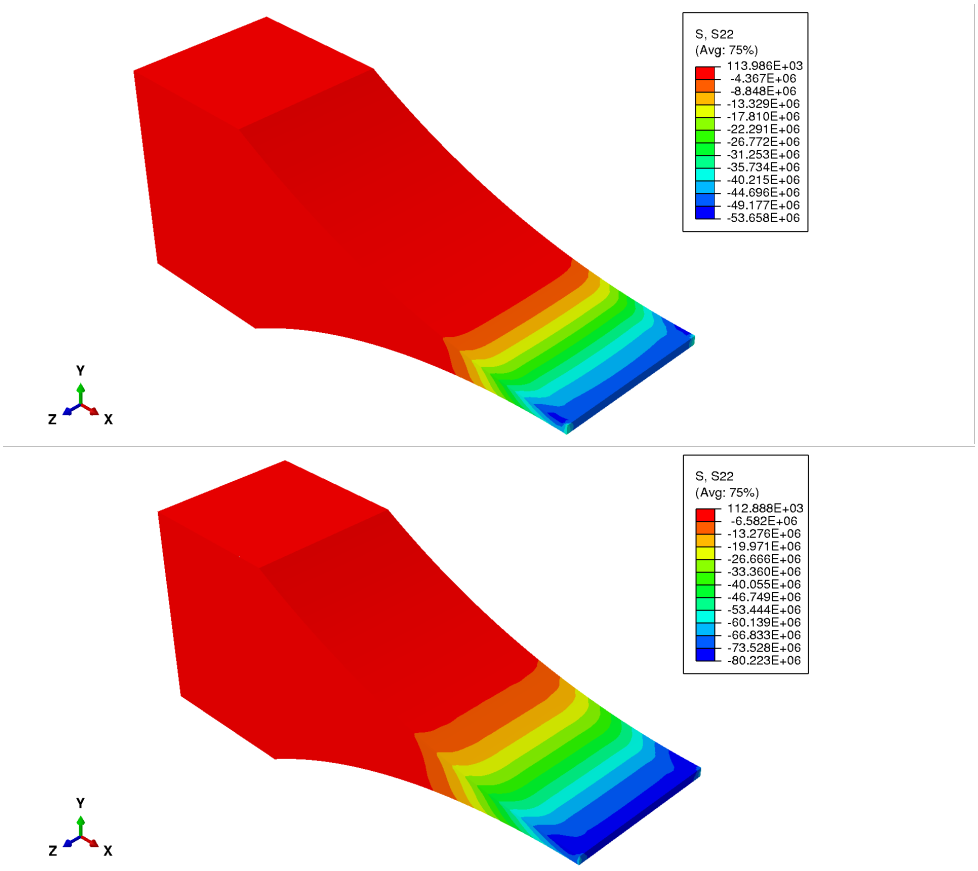

Figure 3.25: Resultant vertical stress, σ_{22} with a rimmed-roll for a)6 kN/cm and b)8 kN/cm roll separation force

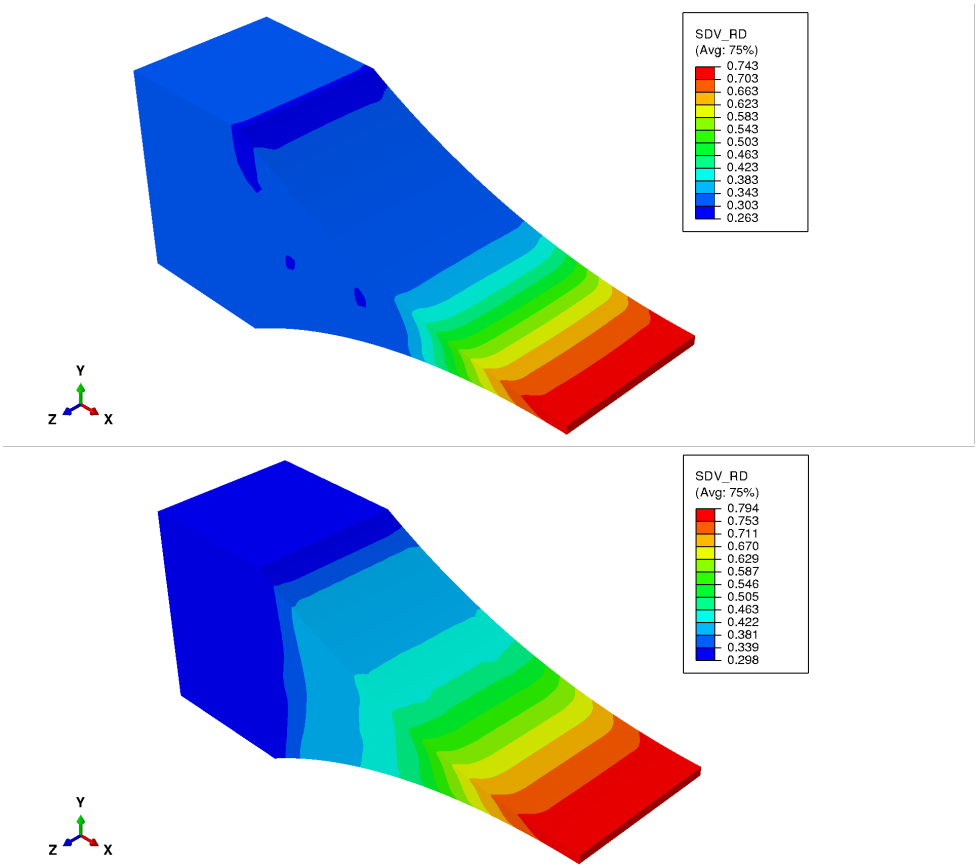

Figure 3.26: Resultant vertical stress, σ_{22} with a rimmed-roll for a)6 kN/cm and b)8 kN/cm roll separation force

Comparing both cases of cheek plates and rimmed-roll assemblies, the upper roll contact pressure distribution is visualized in Figs.3.27 & 3.28. First, it can be seen that for both sealing system designs, the contact pressure increases with the rolling direction until reaching a maximum value just before the narrowest gap. The contact pressure varies between 25 to 37 MPa and 29 to 33 MPa along the ribbon's width for the cheek-plates and rimmed-roll assemblies, respectively. The state variable relative density distribution of the powder between the rolls is visualized in Fig.3.29. The relative density varies between 0.59 to 0.64 and 0.60 to 0.62 along the ribbon's width for the cheek-plates and rimmed-roll assemblies, respectively.

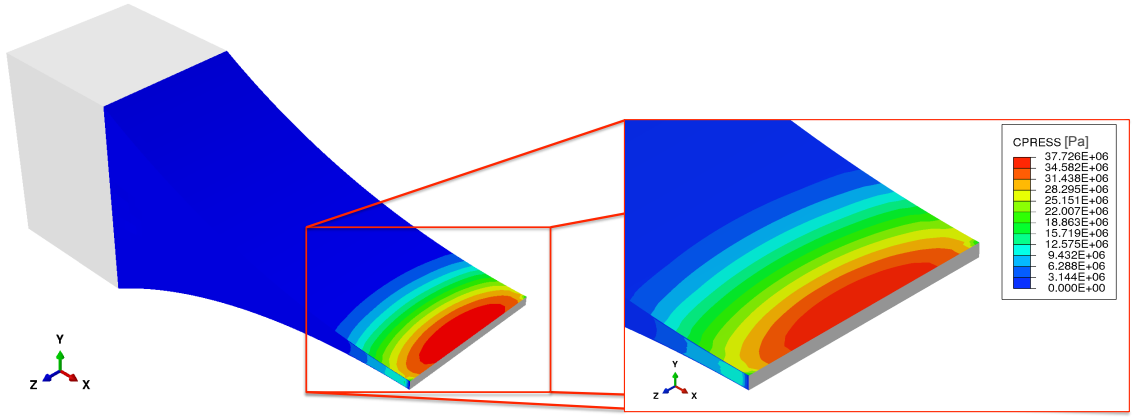

Figure 3.27: Contact pressure between powder and upper roll for cheek plates assembly

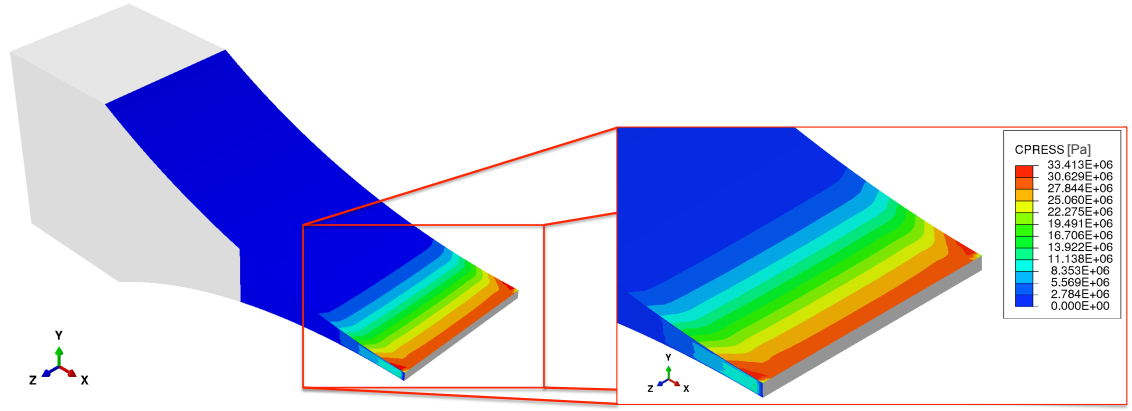

Figure 3.28: Contact pressure between powder and upper roll for rimmed-roll assembly

Results clearly show the effect of the cheek plates, causing a non-uniform roll pressure and density distribution with the highest values in the middle and the lowest in the edges. The powder was not adequately and uniformly delivered to the gripping and compaction zone. This occurred as the cheek plates preventing the powder flow and causes an uneven compaction across the ribbon's width, resulting in lower densification at the edges and higher at the middle of the produced ribbon.

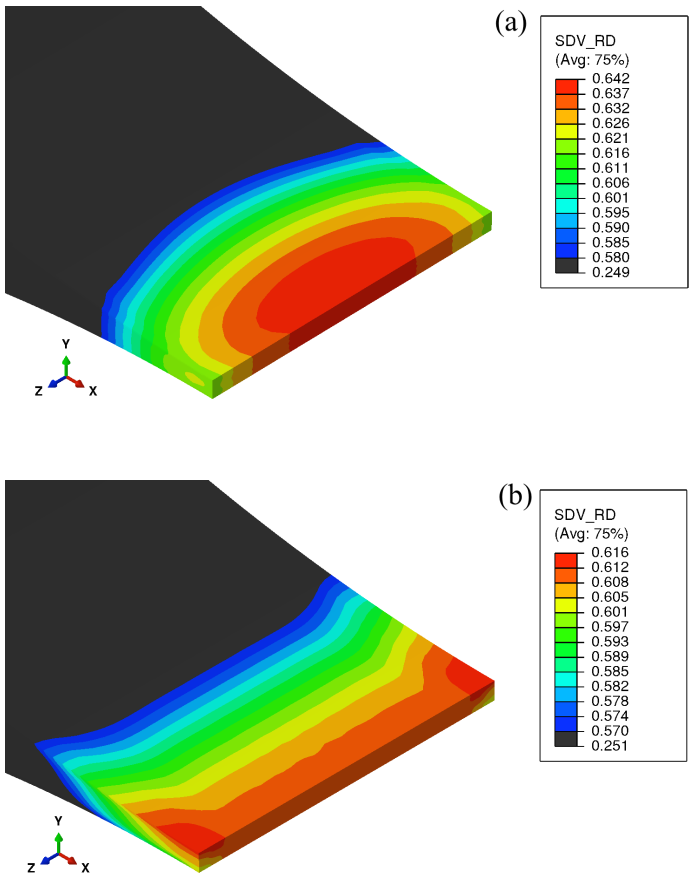

Figure 3.29: Relative density for the two sealing systems a)cheek plates and b)rimmed-roll

On the contrary to the cheek plates, the resultant pressure and density distribution with the rimmed-roll obtained higher values in the edges than in the middle and overall a more uniformly distributed. The rimmed-roll holds the powder mass and transporting it into the gripping zone between the rolls, protecting it from the adverse effect of the cheek plates. Additionally, the inner walls of the rims increase the contact area between the powder and the rolls, which increases the frictional drive in the edges.

3.3.3 Validation

To verify the results, the simulations are compared with experimentally measured values [77] and plotted in Fig.3.30. The results show overall the same tendency as the experimental measurements with an overestimation of ribbon density on the sides for cheek plates sealing system. On the other hand, for the cheek plates case, the results show agreement with the results obtained in the literature for different powder [11].

The difference between the FEM and experimental results for the cheek plates case may be explained by the non constant nature of friction coefficient which has a direct impact on the density gradient. However, for high contact forces and relative densities, the friction coefficient tends to asymptote to a constant value [78]. The difference in results may also be explained by the loss of powder occurs in the roll compaction process, whereas the FEM model considers mass conservation. The problem of leakage from the sides is especially significant for fine ($d_{50} = 50\mu m$) powders such as the MCC 101. Moreover, cheek plates may also have a negative effect on the ribbon with fractured or incomplete compacted edges. Therefore, it can be noted that the ribbon's non-uniformity properties for the cheek plates sealing system was mostly dominant by the loss of powder from the sides, rather than the effect of wall friction.

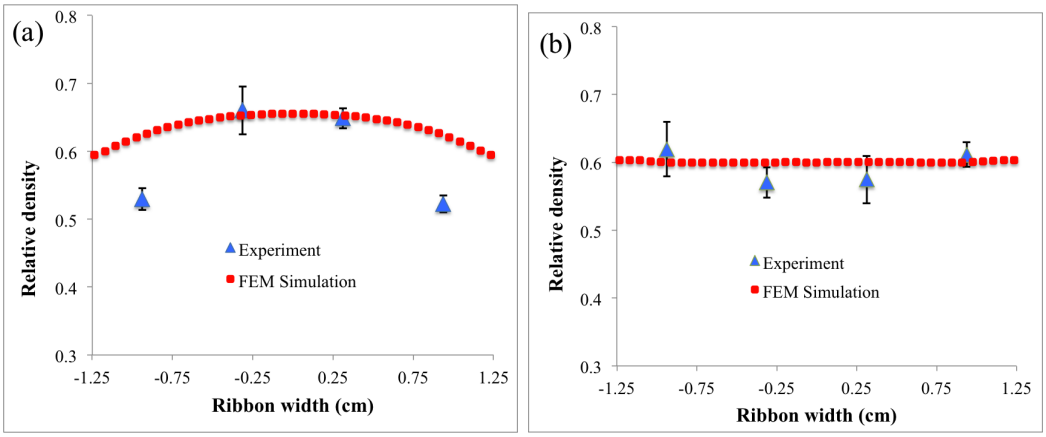

Figure 3.30: Ribbon's density distribution for a)cheek plates and b)rimmed-roll

This page intentionally left blank.

Chapter 4

A combined DEM-FEM approach to include the effect of feeding ⋆

Abstract

Previously, it was observed that although its conceptual simplicity, numerical modelling of the process is challenging due to the complexity involving two complementary mechanisms: feeding by the screw and powder compaction between the rolls. Indeed, the feeding conditions are determinant in the control of the process. Therefore, in order to better represent the behavior of the materials in both the feeding zone and the compaction zone, a three-dimensional simulation of the feed using the discrete element method (DEM) coupled with a finite element method (FEM) simulation of roll compaction, is developed in this chapter. The results obtained show a direct correlation between the speed of the particle driven by the screw and the compaction pressure applied by the roller, both oscillating with the same period. This resulted in a sinusoidal distribution of the density along the compact. This distribution corresponds to the signature of the screw. More precisely, the period of oscillation is equal to the duration of one revolution of the screw.

⋆This chapter has been publish in: Alon Mazor, Luca Orefice, Abderrahim Michrafy, Alain de Ryck, Johannes G. Khinast, A combined DEM & FEM approach for modelling roll compaction process, Powder Technology, 2017, ISSN 0032-5910, http://dx.doi.org/10.1016/j.powtec.2017.04.053.

Resumé

Il a été constaté auparavant que, malgré sa simplicité conceptuelle, la modélisation numérique du procédé est difficile en raison de la complexité impliquant deux mécanismes complémentaires: alimentation par vis et compactage de poudre entre les rouleaux. En effet, les conditions d'alimentation sont déterminantes dans le contrôle du procédé. Par conséquent, pour mieux représenter le comportement des matériaux à la fois dans la zone d'alimentation et dans la zone de compactage, une simulation tridimensionnelle de l'alimentation par la méthode des éléments discrets (DEM) couplée à une simulation par d'éléments finis (FEM) du compactage est développée dans ce chapitre. Les résultats obtenus montrent une corrélation directe entre la vitesse de la particule entraînée par la vis sans fin et la pression du compactage appliquée par le rouleau, tous deux oscillant avec la même période. Cela s'est traduit par une distribution sinusoïdale de densité le long du compact. Cette distribution correspond à la signature de la vis. Plus précisément, la période d'oscillation est égale à la durée d'un tour de la vis.

4.1 Introduction

Roll compaction is a process designed to compact fine powders to produce particulate granules, and it pertains to continuous manufacturing processes. During the process, powder is subjected to high pressure from the rolls, leading to the formation of compacted ribbons, which are later milled into granules. The ribbon's relative density largely influences the compactibility of granules and subsequently the final solid dosage form (i.e., compacted tablets) properties. Therefore, relative density is commonly used as a critical quality parameter of the roll compaction process. In order to ensure the consistency, repeatability and quality of the final dosage form, it is important to avoid heterogeneity of the produced ribbon.

A typical roll compactor consists of a single rotating screw, which feeds the material into a gap between two counter-rotating rolls and cheek plates on the sides to avoid leakage. The conveying of powder towards the rolls has a large influence on the roll compaction process. Experimental work showed that the delivery of powder by a screw feed is linearly related to the screw speed [46, 47]. An appropriate compaction is reached and maintained with a screw to roll speed ratio laying in a specific range. Simon and Guigon [47] also showed that by using a single feed screw, the compacted ribbon was neither homogeneous along the ribbon's width nor in time. Moreover, these fluctuations have the same period of the screw rotation. The impact of the screw motion on the compaction process is relevant for the ribbon properties, albeit not in a trivial way. Not only does the screw design affect particle flow [79] and mixing [80], but also powder properties play an important role [46, 81, 82]. In addition, the behaviour of simple screw feeders will differ as soon as they are coupled with other devices, which will alter the flow properties and the pressure distributions inside. A numerical example can be found in [83].

Numerous studies investigated analytically the roll compaction process. The most well-known analytical model is the Johanson model[6], which is able to determine the pressure along the roll surface, torque and separating force of the rolls, based on

the physical characteristics of the powder and dimensions of the press. The main limitation of the classical Johanson model is that it does not include the important process parameters of roll and screw speeds, which led to the extension of this model by Reynolds et al. [55]. However, these models are only one-dimensional and do not take into account the non-uniformity of the conveying of powder and as a result the non uniform roll pressure and ribbon's density distribution. Bi et al. [84] attempted to overcome this limitation by extending Johanson's model to account for a non-uniform powder velocity in the nip region. However, their result is of little experimental use because the model developed introduces a high variability in the predicted pressure peak, and because the estimation of a key parameter of the model cannot be measured experimentally.

To resolve this, Finite Elements Method (FEM) modelling was adopted to simulate the roll compaction process, starting with plane strain two-dimensional cases [2, 3, 4, 5], followed by the development of three-dimensional models to provide greater insight into the pressure and density distribution during the roll compaction processes [11, 85, 9, 10]. In these models, the effect of the screw feeder is approximately represented by a uniform or oscillatory inlet feeding pressure at the entry angle. Liu and Wassgren [86] implemented a mass-corrected version of Johanson's model analogous to [84] in a two-dimensional FEM model, yet based on two experimentally-determined fitting parameters. The results show a better agreement with the experimental pressure profile when compared to the original Johanson's model. However, the model still relies on experimental data, and only uses an arbitrary constant feed pressure, which does not account for the complex pressure pattern created by the screw conveyor. Michrafy et al. [9] investigated the effect of a constant inlet feeding velocity on the roll compaction process using cheek plates, which resulted in higher pressure and relative density in the middle of the ribbon compared to the edges. Cunningham et al. [10] compared a uniform inlet feeding velocity to a linearly decreasing velocity from the centre to the edges, where both cases have no friction between powder and cheek plates. In the case of uniform inlet feeding velocity, the maximum roll pressure and relative density were the same along

the ribbon's width. Using a non-uniform inlet feeding velocity, the powder is fed rather in the middle than at the edges, and consequently results in higher maximum roll pressure, shear stresses and relative density in the middle of the ribbon. These results are comparable with experiments only with the understanding that the conveying of powder in between rolls have a direct effect of the process. In conclusion, in all of the previous FEM models of roll compaction the inlet velocity or feed pressure values are chosen arbitrarily and do not represent the effect of screw feeding. Therefore, features associated to the periodic feeding, such as a non-uniform conveying in both space and time, are still unaccounted for.

The numerical modelling of the roll compaction process remains challenging due to the complexity involving two different mechanisms: the feeding by the screw conveyor and the powder compaction between the rolls. On one side, the incoming particle flow is a key parameter strongly influencing the compaction process, since it dictates the pace of the process and affects the homogeneity of the compacted ribbon. On the other hand, the material deformation under high stress, and the frictional conditions in the compaction region are the fundamental quantities needed to model the system.

In order to address these issues, we developed a combined three-dimensional Discrete Elements Method (DEM) and FEM methodology. DEM is naturally suited to model the conveying process and will be used to study the particle flow in the feeding zone. The results will be used as boundary inlet conditions for the FEM modelling of the compaction process, which is the best approach to study the compaction of porous materials under high pressure. In our work, the DEM and FEM are treated as complementary methods: combining them in the study of roll compaction enables us to take advantage of their strengths in the regions where they are respectively best suited. The aim of our study is therefore to improve the existing numerical models, leading to a more realistic description of the process which will head us to a better prediction of the final ribbon quality.

4.2 Materials and methods

4.2.1 Roll compaction design and process parameters

This work is based on the Komarek B050H Laboratory Press (K.R. Komarek Inc., Wood Dale, IL, USA). As described previously (Subsection) The Komarek roll compactor is constructed with a horizontal screw conveyor and two counter-rotating rolls with fixed side seals (i.e. cheek plates) in between. The process parameters of minimum gap width between rolls, rolls speed and screw speed were set to $\delta_{\min} = 0.2$cm, $\omega_R = 6$rpm and $\omega_S = 48$rpm, respectively. Further details about the roll press dimensions can be found in Table 4.1.

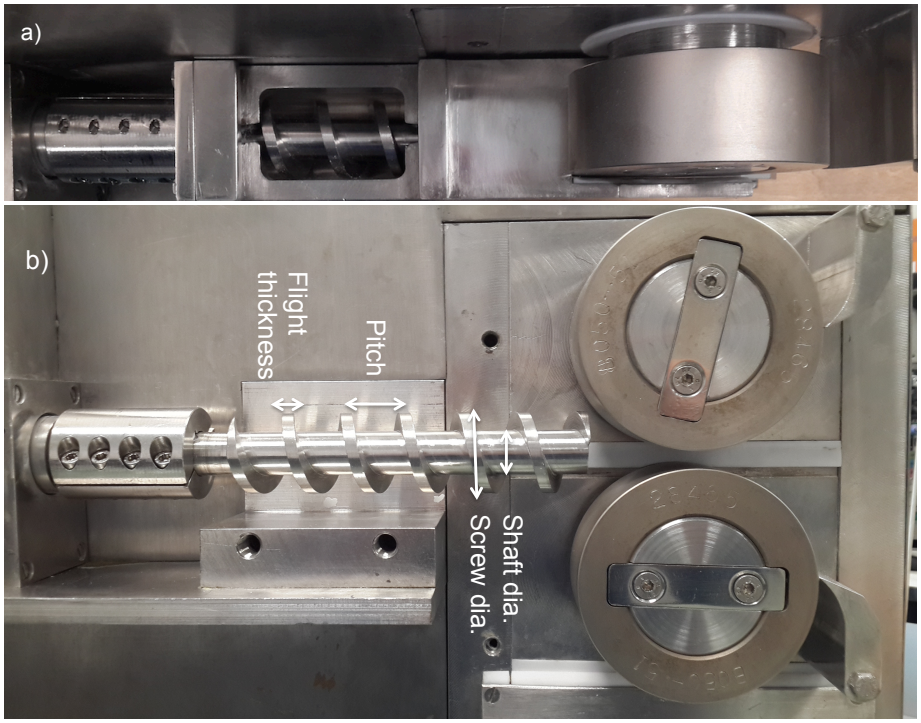

Figure 4.1: Komarek B050H roll compactor; a) Top view and b) Side view (w/o feed barrel and side seals)

Table 4.1: Komarek B050H roll compactor dimensions.

Part	Symbol	Size [cm]
Screw feeder		
Screw length	l_s	15
Pitch length	l_p	1.95
Flight thickness	t_{sf}	0.5
Flight diameter	d_{sf}	3.5
Shaft diameter	d_{ss}	1.9
Casing diameter	d_c	3.8
Roll press		
Rolls diameter	d_R	10
Rolls width	w_R	3.8
Minimum gap width	δ_{min}	0.2

4.2.2 Discrete Element Method (DEM)

In this work, the Discrete Element Method (DEM) modelling was part of a collaborative work and done by Mr. Luca Orefice at the Research Center Pharmaceutical Engineering GmbH (RCPE), Graz, Austria.

As already introduced, the Discrete Element (DE) numerical method ([87]) is highly suitable for studying the flow of solid particulate materials and obtaining the dynamic response of every single particle at any moment during the simulation. However, the results greatly depend on the interaction laws between the objects. Introducing particle deformation or breakage due to the high pressure still remains very challenging computational wise and gives unrealistic results. For this, the DE model is unsuitable for modelling the compaction of powder in between rolls and is only implemented in this work for conveying of powder by a screw feeder into the compaction region.

The particles used in this work are rigid, frictional non-deformable spheres of uniformly distributed poly-disperse radius in the range $r_P \pm 10\%$. The interaction between the particles is modeled according to the Hertzian spring-dashpot contact model [88, 89]. In our model, the particles were composed of *Micro-Crystalline Cellulose* (MCC) and the compactor's components material was steel. We recorded

Table 4.2: Parameters used in the DEM simulations.

Parameters and material properties	Symbol	Value
Particle mass density [g/cm^3]	ρ_P	1.56
Particle mean radius [cm]	r_P	0.09
Particle Young's modulus [Pa]	Y_P	1.0×10^{10}
Conveyor Young's modulus [Pa]	Y_C	1.8×10^{11}
Particle Poisson ratio [−]	ν_P	0.30
Conveyor Poisson ratio [−]	ν_C	0.30
Particle-particle restitution coeff. [−]	e_{PP}	0.83
Particle-conveyor restitution coeff. [−]	e_{PC}	0.80
Particle-particle sliding friction coeff. [−]	$\mu_{PP}^{\text{sliding}}$	0.53
Particle-conveyor sliding friction coeff. [−]	$\mu_{PC}^{\text{sliding}}$	0.20
Particle-particle rolling friction coeff. [−]	$\mu_{PP}^{\text{rolling}}$	0.25
Particle-conveyor rolling friction coeff. [−]	$\mu_{PC}^{\text{rolling}}$	0.10
Screw operational velocity [rpm]	ω_S	48
Rolls operational velocity [rpm]	ω_R	6
Gap width [cm]	δ	0.36
Time step [s]	δt	5.0×10^{-6}
Data output interval [s]	Δt	0.01

the DE simulation data every 2×10^3 time steps of length δt, resulting in a time interval of duration Δt between the monitored snapshots. The simulation parameters and the material properties are reported in Table 4.2. The DE simulations used for this study were performed using the *open source* DEM particle simulation code LIGGGHTS® [90].

A snapshot of the steady-state system is illustrated in Figure 4.2. As it can be seen, the axial velocity of the particles, which is almost uniform inside the screw barrel, quickly drops as soon as they approach the compaction region inlet, where they experience a considerable back-pressure due to a high density in this area. Regions of low velocity are located against the back wall of the compaction chamber. The particles' velocity rises as they approach the gap, where they are compacted (in reality) and are expelled. In this flowing regime, the data of interest were recorded along the inlet plane between the screw conveyor and the compaction region.

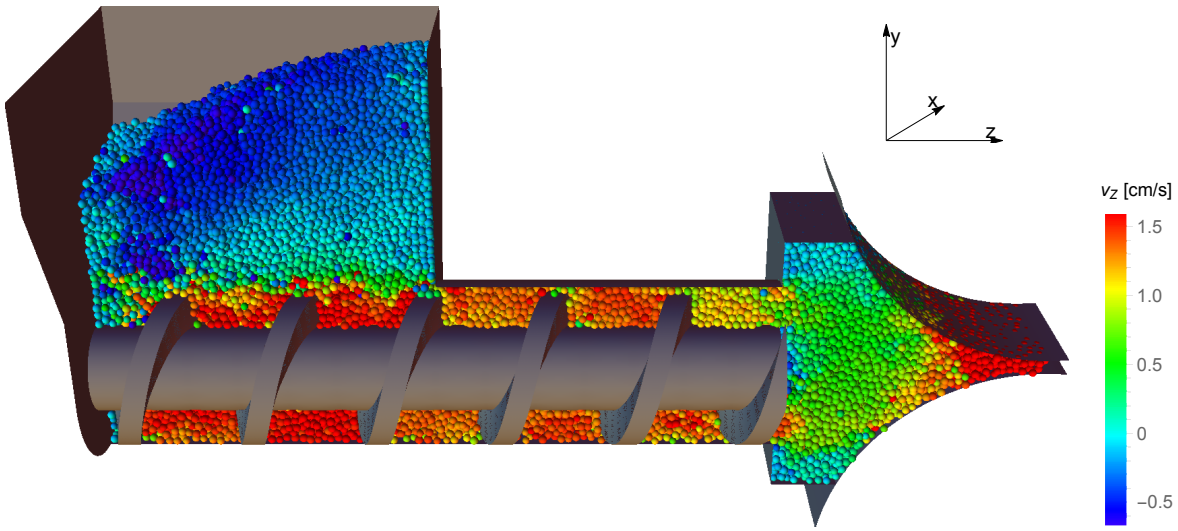

Figure 4.2: Vertical section of one snapshot of the system at steady-state, the particles are coloured according to their axial velocity v_z.

4.2.3 Finite Element Method (FEM)

In this work, FEM is used to investigate the effect of screw feeding velocity on the roll compaction process by obtaining the magnitudes and directions of stresses and strains. The FEM model was solved as a steady-sate problem using the Arbitrary Lagrangian-Eulerian (ALE) adaptive meshing in Abaqus/Explicit v6.14. The ALE adaptive mesh domain for steady-state problems is used to model material flowing through the mesh, and consist of two Eulerian boundary regions (inflow and outflow), connected by a Lagrangian or Sliding boundary region [61].

4.2.3.1 FE model

The Finite Element (FE) model is based on the geometry of the desired roll compactor. In the case of the Komarek press, the roll's diameter and width are $d_R = 10$cm and $w_R = 3.8$cm respectively, and defined as analytic rigid surfaces. The minimum gap width between the rolls remains fixed during FEM modelling, having a value of $\delta_{min} = 0.2$cm. Once sketching the press dimensions, the region between the rolls is

discretized and meshed by 80,000 C3D8R three-dimensional continuum reduced integration elements. The FE model of the roll compactor can be visualized in Fig.4.3. It is important to mention that due to the non symmetric feeding velocity, the FE model was constructed fully without taking into account symmetry conditions, which are usually applied to reduce computational costs.

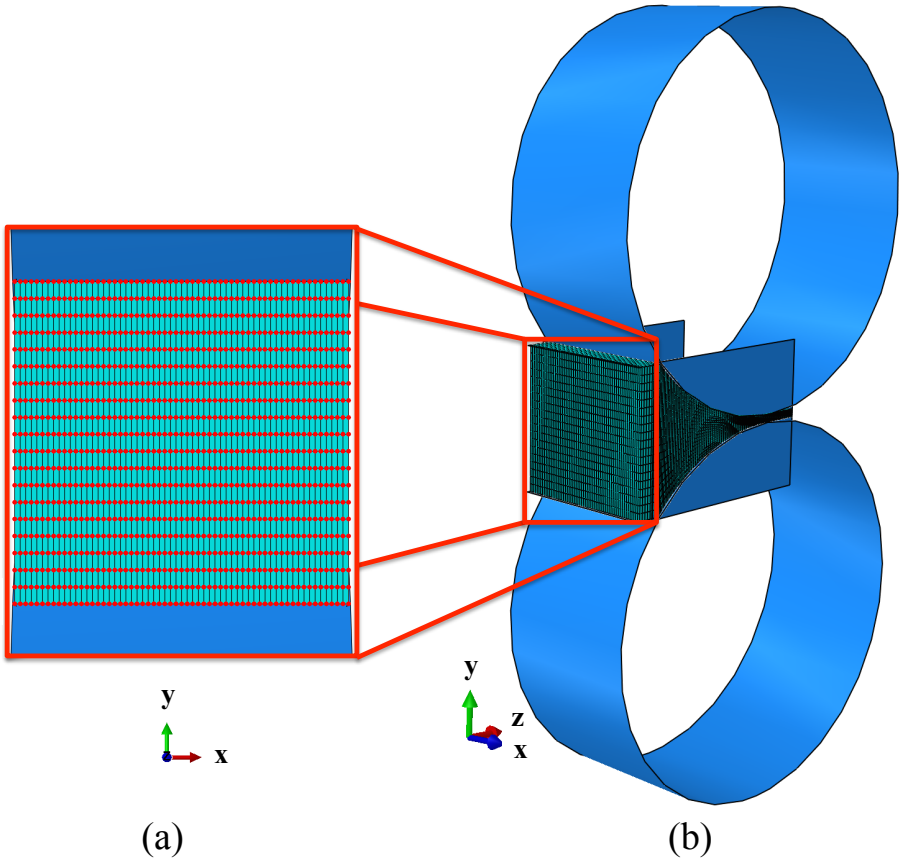

Figure 4.3: Visualization of the (a) Back inlet nodes and (b) Entire FEM model.

4.2.3.2 Boundary conditions

In FEM, introducing the powder into the roll compaction system is possible by two different boundary conditions: either pressure or velocity inlet. Applying a non-uniform pressure on each element face in an ALE adaptive mesh domain causes a

separate Lagrangian boundary region. Since Lagrangian corners are formed where Lagrangian edges meet, all nodes will follow the material in every direction, and each region becomes nonadaptive [61]. On the other hand, by assigning a non-uniform nodal velocity boundary condition to the inlet Eulerian region (Fig. 4.3), there is no alteration of the nodes to be nonadaptive and therefore was the approach chosen for this work. The inlet material density was set to be the tapped powder density as a result of the screw feeding. The MCC Avicel PH 101 tapped density ρ_{tapped} is about 0.47 g/cm^3, which corresponds to an initial relative density ρ_{rel} of 0.3. In addition, the rolls rotational boundary condition of $\pm$0.63rad/s about the x-axis was defined to represent ω_R.

As mentioned previously, the ALE method enables working both with the advantages of Lagrangian and Eulerian elements in the same part [62]. While the inlet and outlet surfaces are defined as Eulerian regions, the surfaces that are in contact with the rolls are defined as sliding surfaces. The contact between the powder mesh and the outer surfaces representing the sealing and rolls is defined as surface-to-surface with Coulomb friction coefficient for a non lubricant case of $\mu = 0.4$ [4, 11, 85].

4.2.3.3 Constitutive material model for continuum modelling

In this FEM modelling, the behavior of the powder, considered as a continuous porous compressible material, is described using the density-dependent Drucker-Prager Cap (DPC) model [65, 66] and implemented by an external user-defined VUSDFLD Fortran subroutine.

4.3 DEM results

For the purpose of our study, we computed the particle velocity field as a function of time via coarse graining of the DEM data that corresponds to the plane perpendicular to the screw axis located at the tip of the screw conveyor. In this area (Fig.4.4a), the particles flowed from a cylindrical casing of radius $R_C = 1.95$cm into the compaction region with a square section of width $w = 6$cm (Fig.4.4c).

The velocity field was evaluated along a planar grid composed of $N_X = 39$ and $N_Y = 25$ nodes along the x and y directions, respectively. For the coarse graining region we chose a square of side $l = 5$cm to obtain an inter-nodal distance of $dx = l/(N_X + 1) = 0.125$cm and $dy = l/(N_Y + 1) \simeq 0.192$cm in the two directions and set $\Delta = 2.5r_P = 0.225$. The chosen grid illustrated in Fig. 4.4b is superimposed on the DE data slice, where the red boundary outlines the region within which the particles contribute to the average over the selected grid. The resulting velocity field can be seen in Fig. 4.4c: after coarse graining, all information about the discrete components of the system is lost.

In our study we averaged in time over $N = 5$ screw turns. The final result was the particle flow during a single screw rotation split into $T_S/\Delta t - 1 = 124$ snapshots. Figure 4.5 shows the time-averaged Coarse Grained (CG) axial velocity component $\langle \bar{v_z}(\mathbf{r}; t^*) \rangle$ for three screw positions at inlet location z_1, where $t^* \in [0; T_S[$ is the absolute time of a screw rotation.

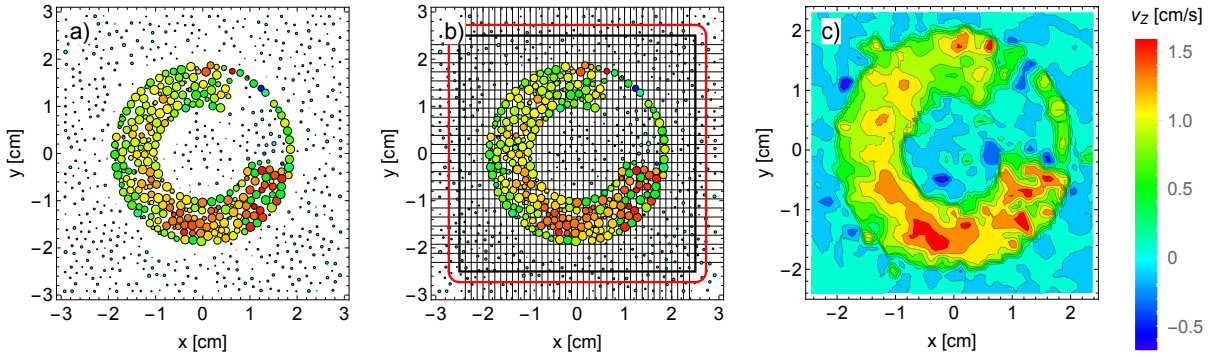

Figure 4.4: Schematic illustration of the coarse graining process (sub-figures left to right) along the x-y plane, with the particle direction of flow towards the reader and the screw rotating clockwise. The particles and field are coloured according to the axial component of the velocity v_z.

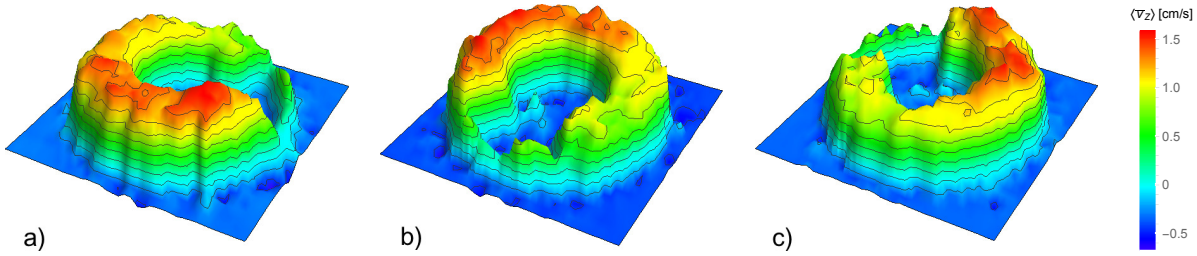

Figure 4.5: 3D plots of time-averaged CG axial velocity component computed for 3 screw positions. The absolute time corresponding to each snapshot is: a) $t^* = 0$, b) $t^* = T_S/3$ and c) $t^* = 2T_S/3$.

4.4 From CG to FEM

In order to implement DEM results into the Finite Element (FE) model, several steps are performed using MATLAB®. First, the function "ndgrid" is being called in order to define a new rectangular grid in x-y space, which represents the FE inlet mesh (Fig.4.3a). In the output $[x, y] = ndgrid\,(x_{min} : hx : x_{max}, y_{min} : hy : y_{max})$, the coordinate of the (i, j)-th grid is $(x_i, y_i) = (x_{min} + (i-1)\,hx, y_{min} + (j-1)\,hy)$.

Now that the new grid is formed in order to represent the FE mesh, DEM data are transferred. This is done by the "Interp2" function, which returns interpolated values of the DEM grid into the new FE grid using cubic interpolation. The interpolated value at a query point is based on a cubic interpolation of the values at neighboring grid points in each respective dimension.

For an equally spaced data, most interpolation functions are in the following form:

$$g(x) = \sum_{k=-1}^{N+1} c_k u(x - x_k) \tag{4.1}$$

Where the sampled data is described as $c_k = f(x_k)$ for a given sampled function f at an interpolation node x_k and u is the cubic interpolation kernel. For convenient reasons, the distance between the point to be interpolated and the grid point

being considered is defined as $s = (x - x_k)$. Moreover, a fundamental property of interpolation function is that they must coincide with the sampled data at the interpolation nodes (sample points). In other words, the corresponding interpolation function results in $g(x_k) = f(x_k)$.

The following cubic convolution interpolation kernel (Eq.4.2), proposed by R.Keys [91], is symmetric and defined by piecewise cubic polynomials in the intervals $|s| \leq 1$ and $1 < |s| \leq 2$. For $|s| > 2$, the kernel is zero. In its most general (symmetric) form, there are eight degrees of freedom and written as follows:

$$u(s) = \begin{cases} a_3|s|^3 + a_2|s|^2 + a_1|s| + a_0 & |s| \leq 1 \\ b_3|s|^3 + b_2|s|^2 + b_1|s| + b_0 & 1 < |s| \leq 2 \\ 0 & |s| > 2 \end{cases} \tag{4.2}$$

Simplifying the above equation is done by leaving one degree of freedom which can be identified with the slope of the kernel at $s = 1$, resulting in the following:

$$u(s) = \begin{cases} (a+2)|s|^3 - (a+3)|s|^2 + 1 & |s| \leq 1 \\ a|s|^3 - 5a|s|^2 + 8a|s| - 4a & 1 < |s| \leq 2 \\ 0 & |s| > 2 \end{cases} \tag{4.3}$$

Where a is the first derivative (or slope) of the kernel at $s = 1$ and controls the depth of the negative lobes of the interpolation function. For this work, a slope $a = -0.5$ was chosen, which offers a third-order convergence and guaranteed superiority to nearest-neighbor (first order) and linear interpolation (second order) [92].

$$u(s) = \begin{cases} \frac{3}{2}|s|^3 - \frac{5}{2}|s|^2 + 1 & |s| \leq 1 \\ -\frac{1}{2}|s|^3 + \frac{5}{2}|s|^2 - 4|s| + 2 & 1 < |s| \leq 2 \\ 0 & |s| > 2 \end{cases} \tag{4.4}$$

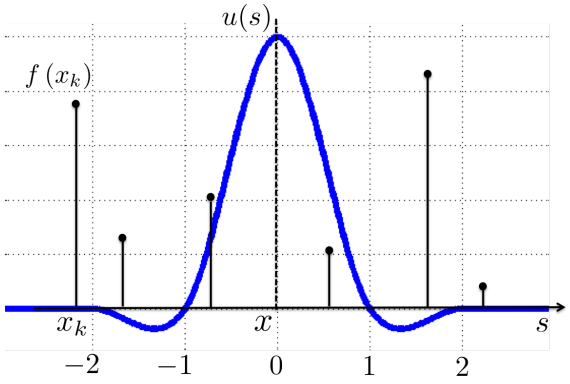

Figure 4.6: Interpolation kernel proposed by R.Keys [91]

Figure 4.6 illustrates the one-dimensional case, interpolating the value x from the discrete points $f(x_k)$ using the cubic kernel. The kernel function $u(s)$ is centered at point x, the location of the point to be interpolated. The interpolated value $g(x)$ is the weighted sum of the discrete neighboring points (2 to the left and 2 to the right) scaled by the value of interpolation function at those points.

When $x_k < x < x_{k+1}$, the cubic convolution interpolation function is:

$$\begin{aligned} g(x) = c_{k-1}\left(-s^3 + 2s^2 - 2\right)/2 + c_k\left(3s^3 - 5s^2 + 2\right)/2 \\ + c_{k+1}\left(-3s^3 + 4s^2 + s\right)/2 + c_{k+2}\left(s^3 - s^2\right)/2 \end{aligned} \tag{4.5}$$

Where $c_k = f(x_k)$ for $k = 0, 1, 2, ..., N; c_{-1} = 3f(x_0) - 3f(x_1) + f(x_2)$; and $c_{N+1} = 3f(x_n) - 3f(x_{N-1}) + f(x_{N-2})$.

For two-dimensional interpolation (i.e., Bicubic interpolation), the one-dimensional function is applied in both directions. It is a separable extension of the one-dimensional interpolation function. The Bicubic interpolation algorithms interpolate from the nearest sixteen mapped source pixels. Obtaining an interpolated value for a given point (yellow) is done in two steps. First (Fig.4.7b), an interpolation is done along the x-direction (red points) using the 16 grid samples (blue points). The following step (Fig.4.7c) is interpolating along the y-direction (red line) using the interpolated points from the previous step.

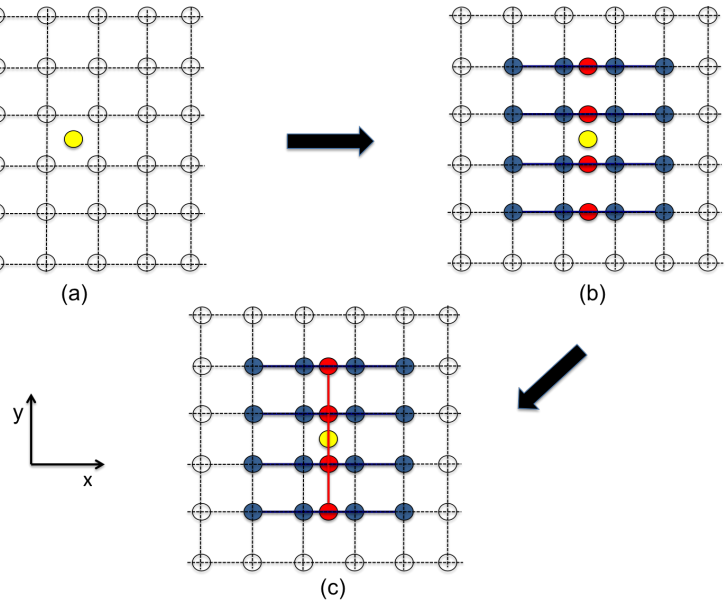

Figure 4.7: Schematic illustration of the Bicubic Convolution interpolation procedure. a) Initial point to be interpolated, b) First interpolation step along the x-direction. c) Final interpolation step along the y-direction

The above algorithm is applied to the DEM CG data at each time interval Δt during a screw period, resulting in a total of 124 matrices of 61x20 (i.e., 1220 elements) corresponding to the FE inlet nodes (Fig.4.3b). The velocity values for each absolute time t^* are then represented as an array in a separate file. Fig. 4.8 illustrates the previously described steps of constructing a new grid, which correlates to the FE mesh and interpolates the values from the DEM results.

The new interpolated data is then implemented as a FE nodal velocity boundary condition in Abaqus/Explicit using an external user-defined VDISP Fortran subroutine. At each absolute time t^*, the VDISP subroutine is being called and assigns the corresponding interpolated velocity values from the previously saved data file into the FE model in a chronological order to the predefined inlet nodes (Fig.4.9.).

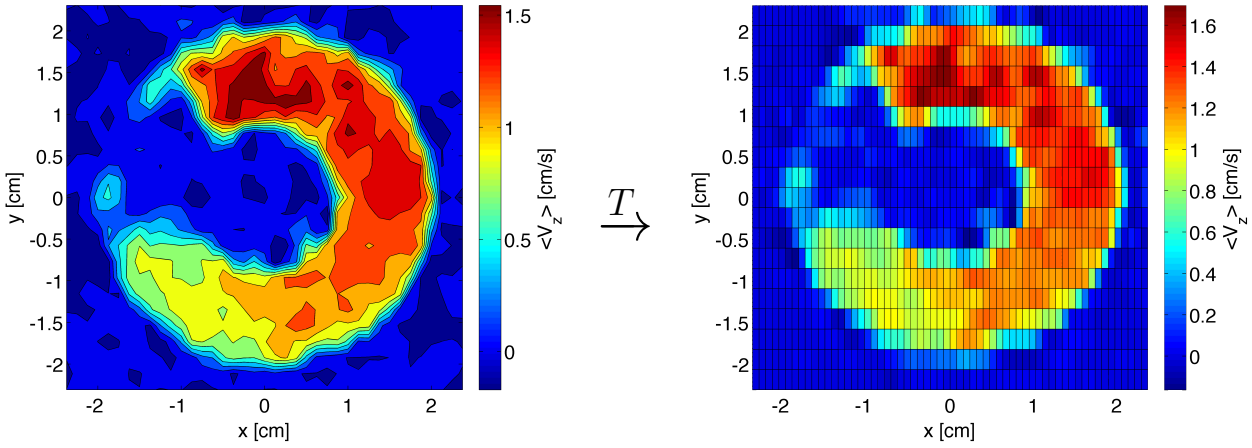

Figure 4.8: Plot of velocity field and the transition from CG result to FEM inlet boundary condition for $t^* = 0$. Axial velocity component $\bar{v_z}$ values for a) DEM coarse graining result and b) Corresponding FE inlet nodes.

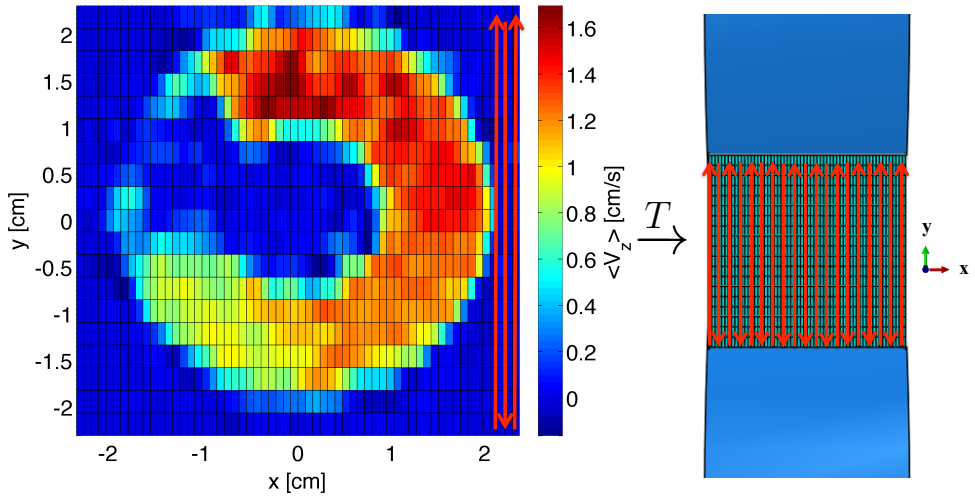

Figure 4.9: Schematic illustration of the procedure assigning axial inlet velocity interpolated values into the FE model. The red arrows shows the direction in which values are read in the data file and being assigned into the FE back nodes.

The flowchart in Fig.4.10 describes the entire procedure implemented in this work. The first part describes the numerical transition method used to bridge the gap between the DEM coarse grained results and the FE inlet nodes. The second step contains the FEM explicit simulation using the VDISP subroutine in order to implement the DEM data and solve the FE model for each time step.

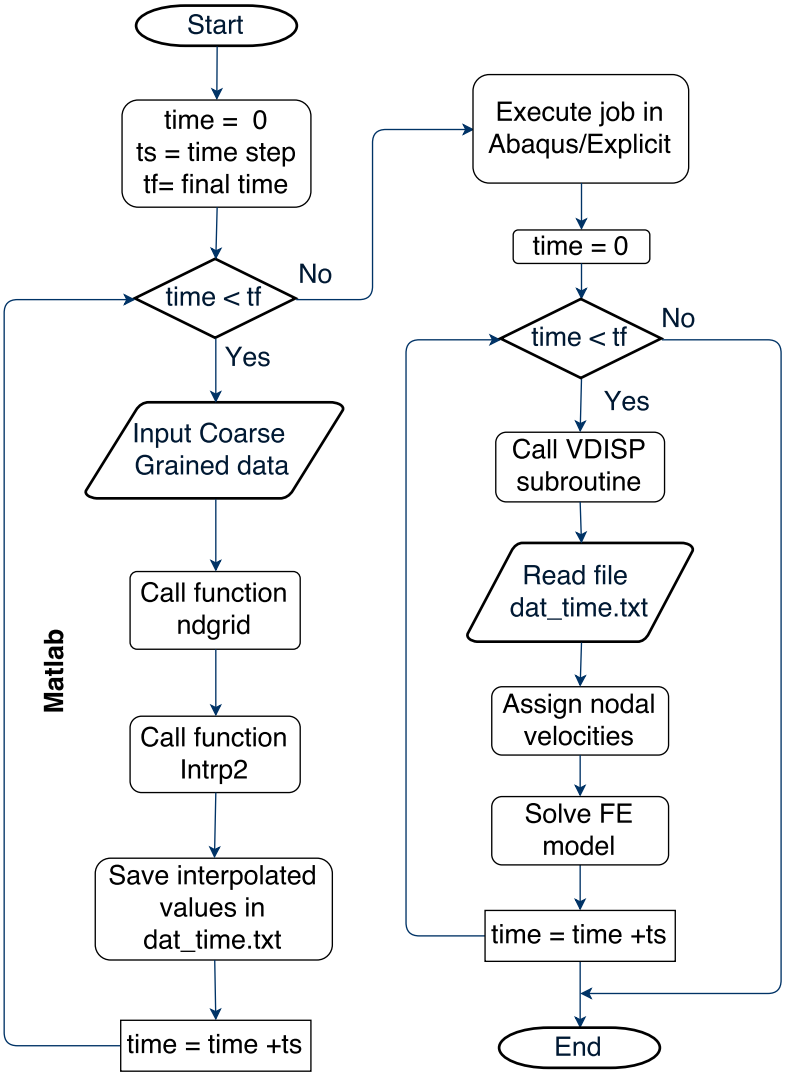

Figure 4.10: Flow chart block diagram describing the FEM simulation using CG results.

4.5 Results and discussion

Results obtained by DEM simulation (section 4.3), showed that the flow of powder being conveyed to the rolls, varies in velocity due to the rotation of the screw. This is in fact the main cause attributed to the inhomogeneity of the compacted ribbon, resulting in a "snake"-wise light transmission pattern [47]. Our results demonstrate the importance of combining DEM & FEM methods to obtain a more realistic model of the process.

4.5.1 Transition From DEM (CG) to FEM

In the previous section, the multi-scale approach was described in order to investigate the behaviour of granular material in roll compaction, by combining DEM at the micro scale into the FEM macro scale level.

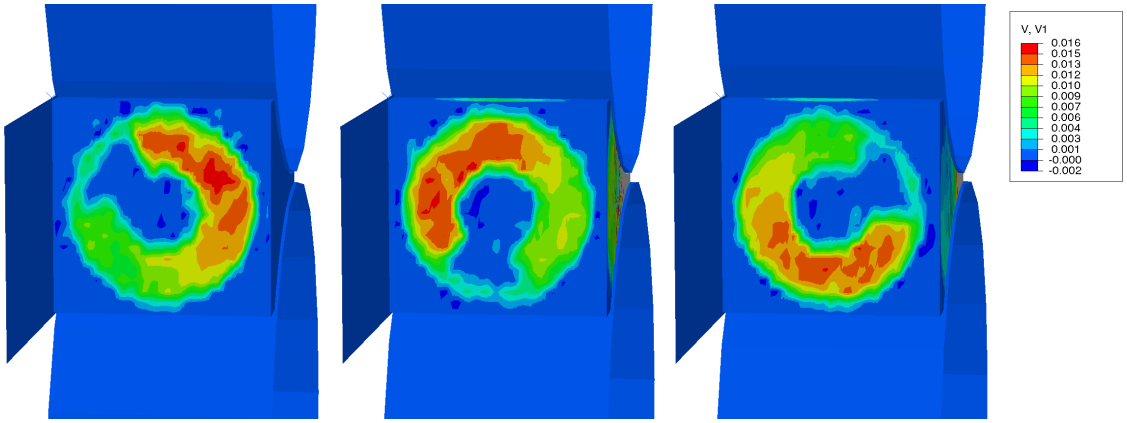

Figure 4.11: 3D plots of the axial velocity component $\bar{v_z}$ in the FE model (right seal removed for better visualisation) for 3 screw positions, with a counter-clockwise rotation. The absolute time corresponding to each snapshot is: a) $t^* = 0$, b) $t^* = T_S/3$ and c) $t^* = 2T_S/3$.

Figure 4.11 visualizes the result of the numerical transition method, which was used to gap between the different scales and used as input data in FEM modelling. By comparing the axial velocity component $\bar{v_z}$ in the FEM inlet nodes (figure 4.11) with the CG results (figure 4.5), it can be seen that feeding velocity field values and pattern are almost identical with some discrepancies due to the counter pressure from the rolls (except for $t^* = 0$ in figure 4.11a). Therefore, it is possible to successfully implement the DEM data into the FEM, and to represent the velocity of the powder entering the compaction region.

4.5.2 DEM & FEM combined simulation

By implementing the CG DEM results into the FEM, a numerical study on the effect of the screw blade position and the inhomogeneous inlet feeding velocity on the roll compaction process was conducted.

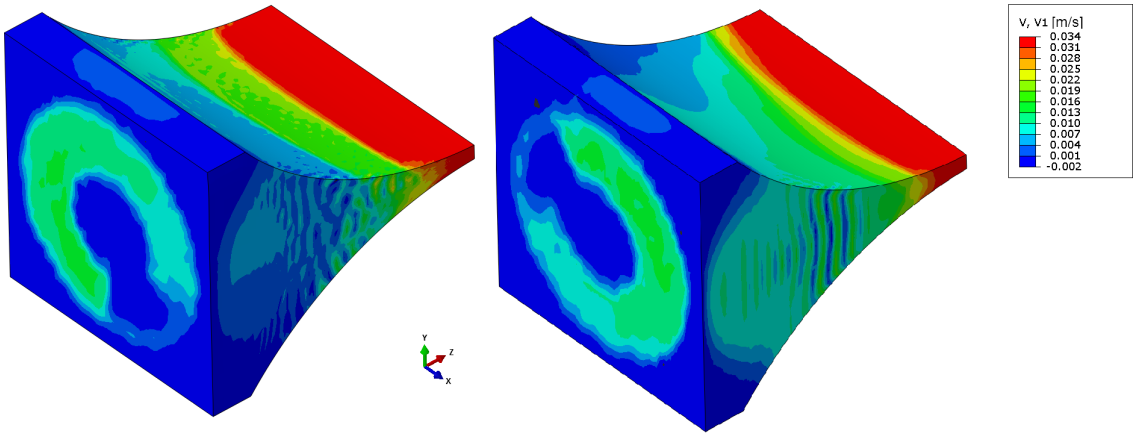

Figure 4.12: 3D FEM plots of powder axial velocity for 2 time steps: $t^* = 2.35s$ (left column) and $t^* = 2.9s$ (right column)

Figure 4.12 visualizes the 3D axial velocity of the powder during the simulation The implementation of the CG DEM results into the FE model is clearly noticeable, as well, as the distribution on the entire domain under the rolls.

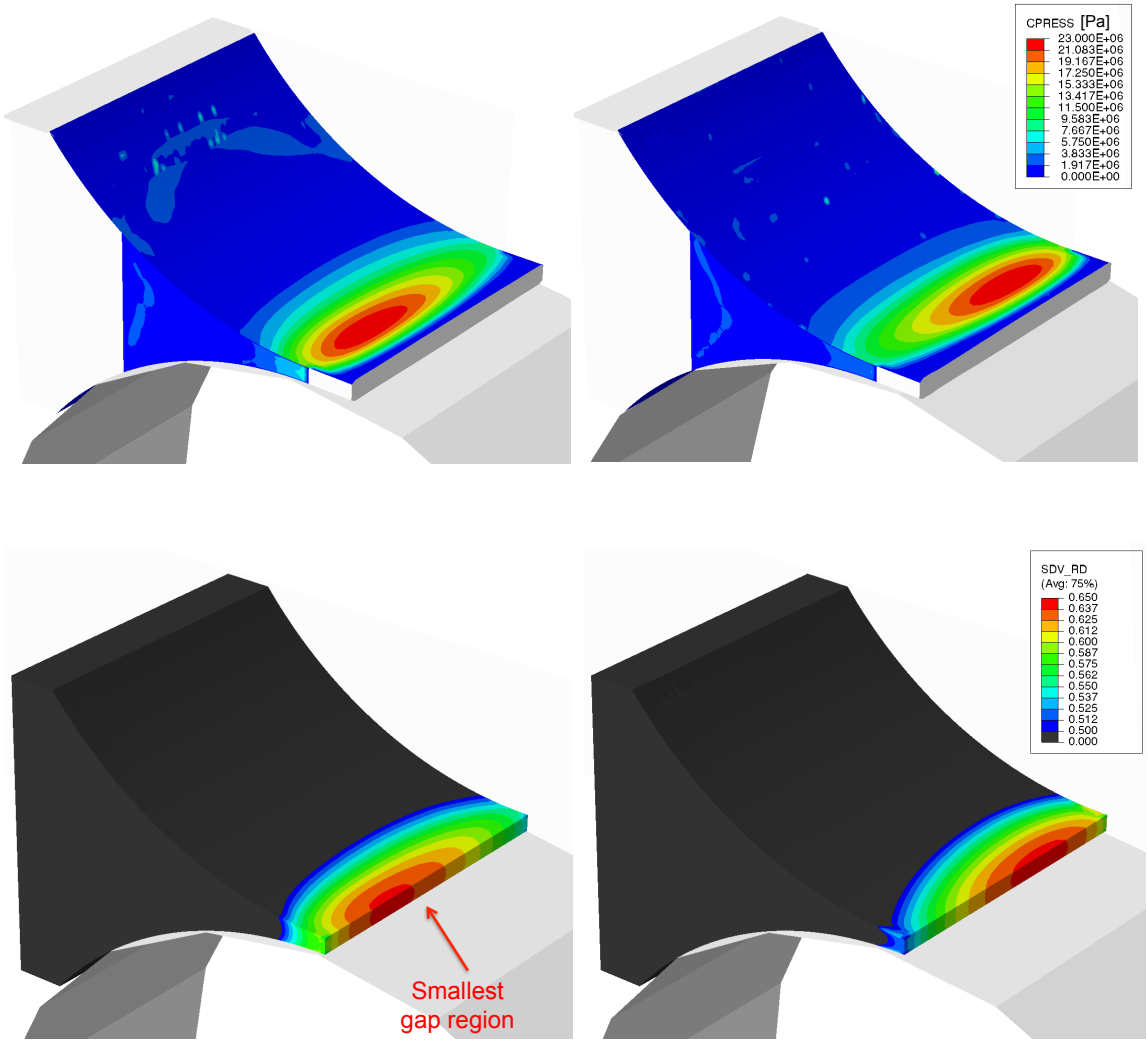

Figure 4.13: 3D FEM plots for 2 time steps: $t^* = 2.35s$ (left column) and $t^* = 2.9s$ (right column). The depicted values are: powder contact pressure (top row) and relative density (bottom row) at the outlet of the compaction region.

The resulting contact pressure and relative density (Fig. 4.13) are distributed non-homogeneously in the minimum gap region and vary with time as a result of the inlet feeding velocity. The maximum contact roll pressure and relative density positions in the minimum gap region vary with simulation time along the ribbon's width. It can be noted that the 3D axial velocity plot does not correspond to the pressure and density values at the minimum gap due to the fact that the influence of the inlet velocity takes effect only at a later stage. This means that, due to the distance between the inlet region and the minimum gap region, there is a certain phase shift between the sinusoidal pattern of the inlet velocity and the contact roll pressure and relative density.

In order to evaluate and quantify this variation during the process and consequently on a compacted ribbon, the values were monitored at two different positions with a distance of 5 mm from the left and right side seals (figure 4.14). Initially, the values of relative density and contact pressure are increasing gradually as powder is being delivered in between the rolls. At around $t^* = 3s$, the roll compaction reaches a steady-state condition, where the mean values of the relative density and of the roll pressure at the minimum gap region remain constant.

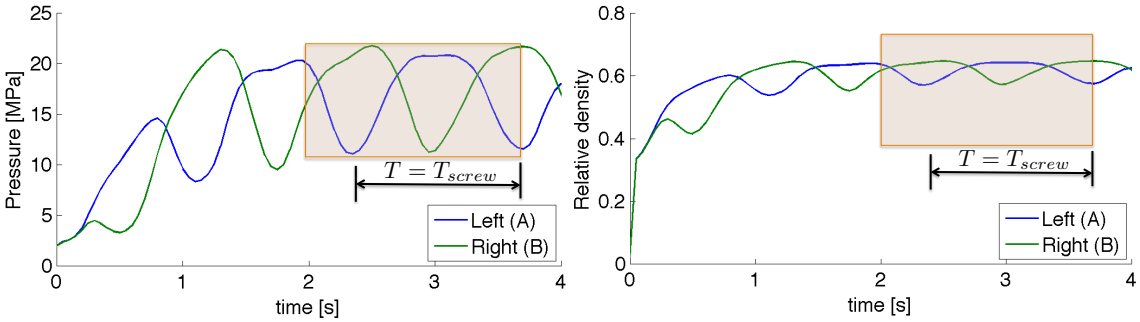

Figure 4.14: Plots of the a) roll contact pressure and b) relative density at two positions 5mm from both edges with respect of time. The highlighted region is the time domain used for plotting figure 4.15

Results obtained with our combined approach showed that the inlet feeding velocity has a direct effect on the resulting pressure and density distribution. Figure 4.14 clearly shows the variation of the value within simulation time. For a specific

time, the contact pressure and relative density values at one side of the ribbon are higher with respect to the other. Moreover, a sinusoidal pattern of the roll pressure and relative density during compaction is observed, having a period equal to the screw rotation period.

Due to numerical reasons, the results are obtained and plotted only for the material which is still in contact with the roll, up to the narrowest gap region [11]. Therefore, in order to illustrate the resultant roll compacted ribbon, multiple sliced snapshot at the gap region were taken at intervals of $\Delta t = 0.05s$ and assembled together. As can be seen clearly in figure 4.15, higher powder feeding rate in one side resulted in higher contact pressure and relative density on the same side under the rolls. This can be explain by transporting higher amount of mass into one side, thus increasing the nip angle which will ultimately result in higher compaction force and density.

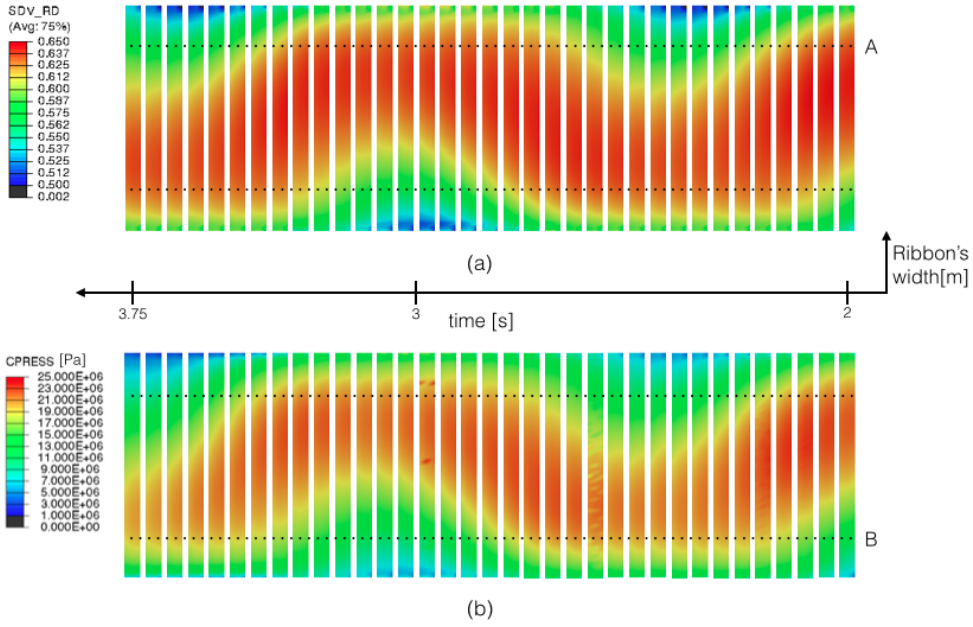

Figure 4.15: Multiple sliced snapshots of the a) relative density and b) contact pressure values obtained by the combined DEM-FEM simulations at the minimum gap region between $t = 2.00$s and $t = 3.75$s. The two highlighted positions A and B are the positions where the values of figure 4.14 are evaluated.

4.6 Conclusions

Roll compaction is a complex process involving two main parts, powder conveying using a screw feeder and compaction between two counter rotating rolls, where the powder undergoes large deformation. In this work, a combined DEM-FEM multi-scale approach was developed in order to investigate the behaviour of granular material in roll compaction.

DEM was used to model the flow of granular material through the screw conveyor into the compaction zone. The DEM simulation was successfully used to model the behaviour of particles in a screw feeder and to obtain the highly inhomogeneous (although periodic in time) velocity field at the interface between the screw feeder and the compaction region. Then, FEM was applied to simulate the powder compaction in between the rolls and to study the effect of the inhomogeneous inlet feeding velocity due to the screw feeder. The combined DEM-FEM methodology clearly shows the resultant inhomogeneous roll contact pressure and relative density over the rolls width, resulting in a "snake-wise" pattern over time. This behaviour is reflected in an inhomogeneously compacted ribbon. Moreover, the sinusoidal pattern of the roll pressure and relative density during roll compaction has a period equal to the screw rotation time.

Combining both DEM and FEM methods to model the roll compaction process allows us to take advantage of the strength of both methods in order to describe complex processes, and enables us to achieve a more realistic model of both the process itself and of the final product quality. The methodology proposed can be used to study how process parameters, such as screw and roll speeds, will likely affect the ribbon density and homogeneity. In addition, this coupled approach can be a useful tool to guide future design optimisations, with the aim to diminish the effect of the screw driven flow on the compaction final product.

Chapter 5

Floating roll using Coupled Eulerian Lagrangian formulation

Abstract

In roller presses, the gap between the rolls can fluctuate with the flow of incoming materials, which has not been possible to take into account in the previous simulations. This chapter presents a new Coupled Eulerian-Lagrangian (CEL) approach, attempting to take into account the fluctuation of the gap by allowing simulating the free flow of the material between and outside the rolls. The increase or the decrease of the gap is managed by a spring-stiffness with a given rigidity and miming the action of the hydrostatic pressure which controls the gap between the rollers. Preliminary results clearly show an increase in the gap between the rollers as a function of the stiffness of the spring and the force reaction of the roller. This work, still at the initial stage, constitutes a promising basis for further development of the model to simulate the actual operation of a roller press (adjustment of the gap as a function of the flow of material controlled by the feed screw).

Resumé

Dans les presses à rouleaux, l'entrefer peut fluctuer avec le débit de matière entrante, ce qui n'a pas été possible de prendre en compte dans les simulations précédentes. Ce chapitre présente des investigations par une nouvelle approche, pour tenter de prendre en compte les fluctuations de l'entrefer. Pour cela, une formulation couplée Euler-Lagrange, permettant de simuler l'écoulement libre de la matière entre et hors rouleaux, est mise en place. L'écartement ou le rapprochement des rouleaux est géré par une liaison de type ressort avec une rigidité donnée et mimant l'action de la pression hydrostatique qui pilote l'entrefer des rouleaux. Les premiers résultats montrent clairement une augmentation de l'écart entre les rouleaux et est fonction de la rigidité du ressort et la force de réaction du rouleau. Ce travail, encore à l'état préliminaire, constitue une base prometteuse de développement ultérieur du modèle pour simuler le fonctionnement réel d'une presse à rouleaux (ajustement de l'entrefer en fonction du débit de matière piloté par la vis d'alimentation).

5.1 Introduction

Previous work in this thesis has shown the complexity of the roll compaction process, involving different aspects of material behaviour, roll press designs and process parameters affecting the hydraulic pressure/compaction force and the final ribbons density. Nowadays, unlike the common laboratory roll compactors, most vendors offer more sophisticated automatic machines in order to achieve desired compression conditions and ribbon properties. These automated roller compactors are equipped with a programmable logic controller (PLC) to control process parameters using proportional–integral–derivative (PID) control strategy. PID controllers calculate the value of the manipulated variable based on the weighted sum of the error value (P), integral of the error (I), and the time derivative of the error (D) at the current moment. Theses weights including the proportional, K_p, the integral K_i and derivative, K_d gain constant values act as tuning parameters and are predefined. The PID attempts to correct the error between a measured process variable (output) and the desired set-value (input) by calculating and then providing a corrective signal that can adjust the process accordingly as shown in Figure 5.1. In many control systems, the D action is not necessary and is turned on only if the process dynamics are slow. The controllers in these systems are hence called PI controllers. Since the PID algorithm can control only one variable at a time based on only one measurement, multiple control loops are necessary for multi-variable processes.

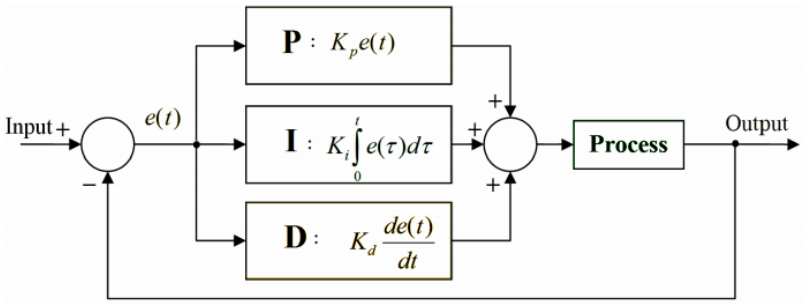

Figure 5.1: Closed-loop feedback single-output control using a PID controller [93].

For instance, the Gerteis Mini-Pactor offers different production modes options in order to control and maintain the desired process parameters and quality of produced ribbons. The ribbon density is controlled by a cascade control system involves two PI-controllers consisting of a master control loop for the hydraulic pressure and a slave control loop for the gap width [94]. This means that a master control loop is in charge of the hydraulic pressure to adapt the compaction force exerted on the slave (floating) roll, according to a given set value in the units of kN/cm. Whereas a slave control loop is in charge of the gap width in order to achieve a given set value by speed adjustment of the feeding screws via a PI control algorithm. Although a properly tuned multi-loop PID control system may have an adequate performance, it still relies on the user's expertise and based on online trial and error methods. This is based on the known fact that compaction force is the most important factor regarding the ribbon density and consequently the quality of granules. However, a feedback control loop detecting the density to adjust the compaction forces has not been developed yet. Nowadays there is an increase in interest of continuous manufacturing, which is based on online sensors, such as the real-time in-line near-infrared (NIR) monitoring, for the physical properties of the ribbons in order to automatic control the roll compactor and other pharmaceutical production processes.

To conclude, the automated roll press adjusts the screw speed in order to increase or decrease the amount of materials flowing in-between the rolls. The gap is then adjusted and kept in the desired value using the hydraulic pressure system in order to ensure the manufacturing of ribbons with the desired properties, set by the user. Simulating such an automated process is challenging with the current state of FEM models of roll compaction, which are not able to take into account the fluctuation of the gap according to the material flow arriving into the compaction zone. For this reason, a new FEM modelling approach is introduced, which may be used to represent a PID control system in order to understand the link between powder properties and process parameters on the compaction force, in a more cost-effective manner rather than intensive experimental work. In addition, the modelling approach mimics a continuous manufacturing process, monitoring the entire process starting from powder feeding up to the final ribbon properties.

5.2 Overview of numerical aspect

One of the limitation of FEM modelling of roll compaction using ALE formulation, is that the mesh and therefore the final shape, needs to be fixed prior the simulation. This is of course limiting the simulation as only the material inside the compactor ("in die") can be modeled without the extraction of ribbons. Moreover, this limitation also does not allow to model a floating roll, which means the roll is free to move vertically as a result of higher feeding rate of material. For this, we develop a Coupled Eulerian Lagrangian (CEL) formulation model in Abaqus/Explicit to allow material to flow in and out of the roll compactor freely without prior restrictions.

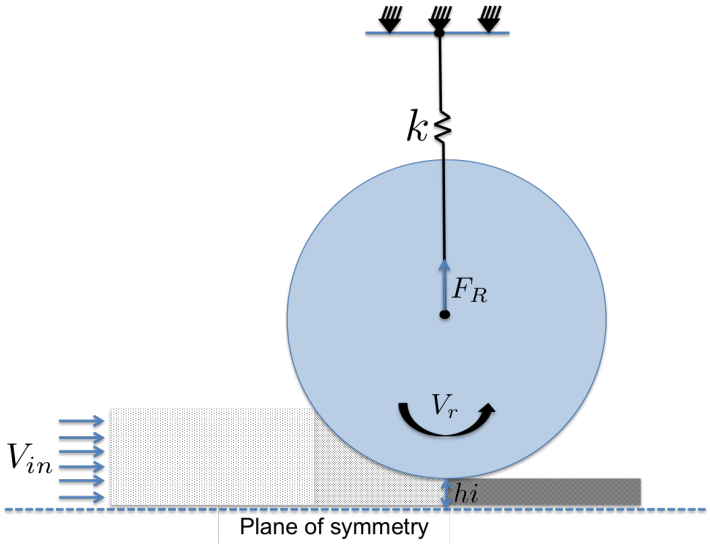

Figure 5.2: Scheme of floating roll

The FE mesh in CEL analyses usually represents a stationary rectangle through which the Eulerian material moves and impacts on the Lagrangian structure. Abaqus provides EC3D8R elements to model Eulerian problems, which may be completely or partially filled by the powder material, while the rest of the Eulerian grid is filled with void material. The material is tracked as it flows through the mesh by means of Eulerian volume fractions (EVF) which represent the ratios by which each Eulerian element is filled with material.

5.3 FE model

To reduce computational costs, the FE model is designed in a fourth-folded symmetry along the x-y and x-z planes. The model is composed of several parts including an Eulerian meshed region and Lagrangian roll, side seal and top plate rigid bodies. Infact, the top plate does not have any effect on the simulation and it is merely to represent the roll compaction hydraulic system design and its connection to the roll by a linear elastic spring connector.

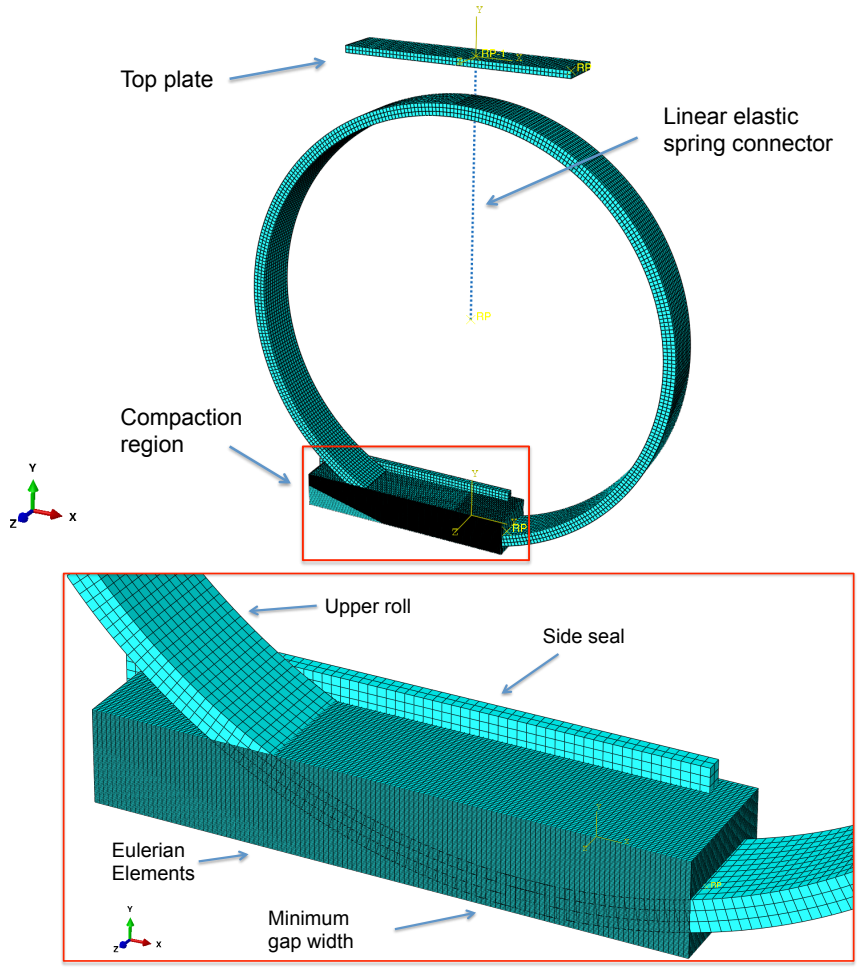

Figure 5.3: CEL Full FE model

The following keywords are added to the Abaqus input file to implement the above mentioned three-dimensional, 2-node spring element connector, with a given constant stiffness value of $9 \cdot 10^6$ N/mm.

```
*Element, type=CONN3D2, elset=Spring-Set-1
1, Roll-RF, 1
*Connector Elasticity, component=1
9e+6,
```

5.3.1 Boundary conditions

Unlike previous simulation using the ALE formulation, the interaction between the powder in the Eulerian mesh (Fig.5.4) and the rigid roll and side seal bodies is solved using a general contact algorithm, explicitly excluding the contact between the rigid bodies. In this work the inlet material throughput was simplified and defined as a constant feeding velocity of 0.01 m/s.

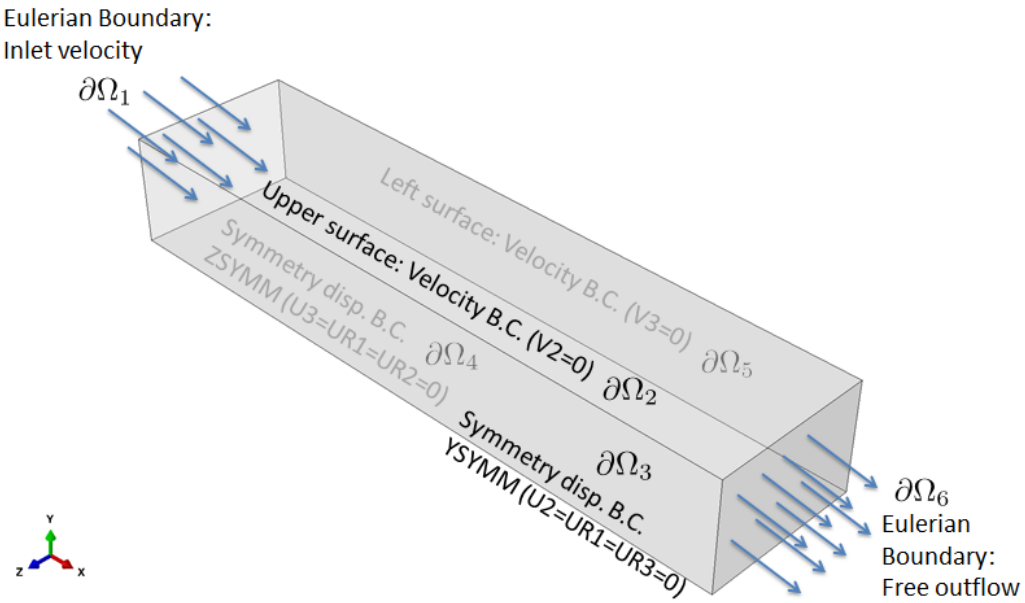

Figure 5.4: CEL Eulerian Block B.C.

5.4 Results

Similarly to the ALE solution, once reaching a steady-state solution by obtaining a constant relative density and vertical reaction force on the roll pin, the FEM results were analyzed. However, by solving using the CEL approach, the results are not restricted only to the material that is still in contact with the roll. This means that the material is free to expand elastically after the narrowest gap region, resulting in a final ribbon product (Fig.5.5).

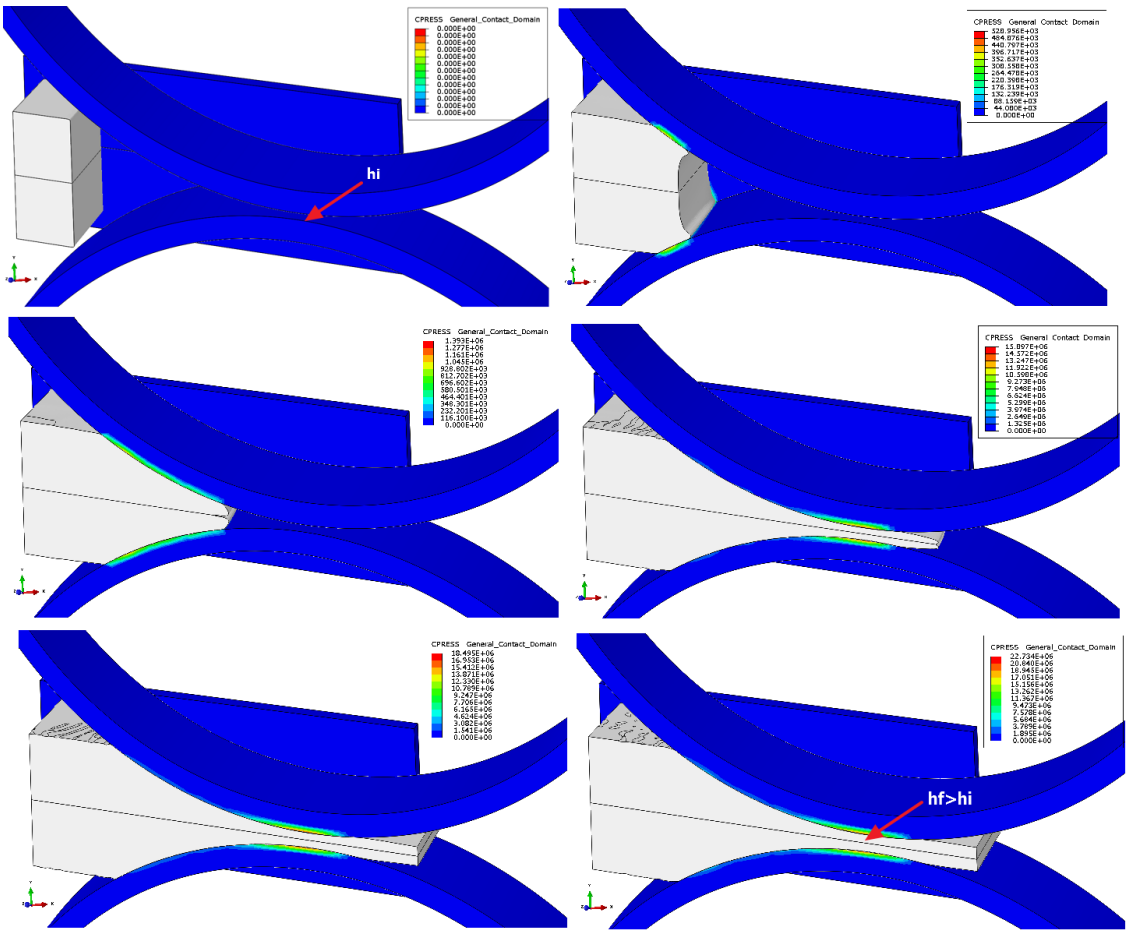

Figure 5.5: Powder flow and roll pressure during CEL modelling (Full model view by mirroring the symmetry planes).

Another interesting result is the increase of the gap between rolls from an initial height of h_i to a final height of h_f. This final roll position is a function of the spring's stiffness coefficient (i.e., hydraulic pressure) and the resultant roll reaction force. Therefore, the vertical displacement of the roll is linearly depedant on the resultant reaction force and increases gradually until reaches a steady-state condition.

Figure 5.6 visualizes the vertical stress (σ_{yy}) exerted on the powder material. It can be clearly noticed that the stresses varies both in the rolling direction and along the width, similarly to the previous obtained results using the ALE formulation (3.3). Focusing on the minimum gap region, the higher stresses are located in the middle of the ribbon (here right side as the model is quarter symmetric) whereas the lower value are at the edge closer to the side wall.

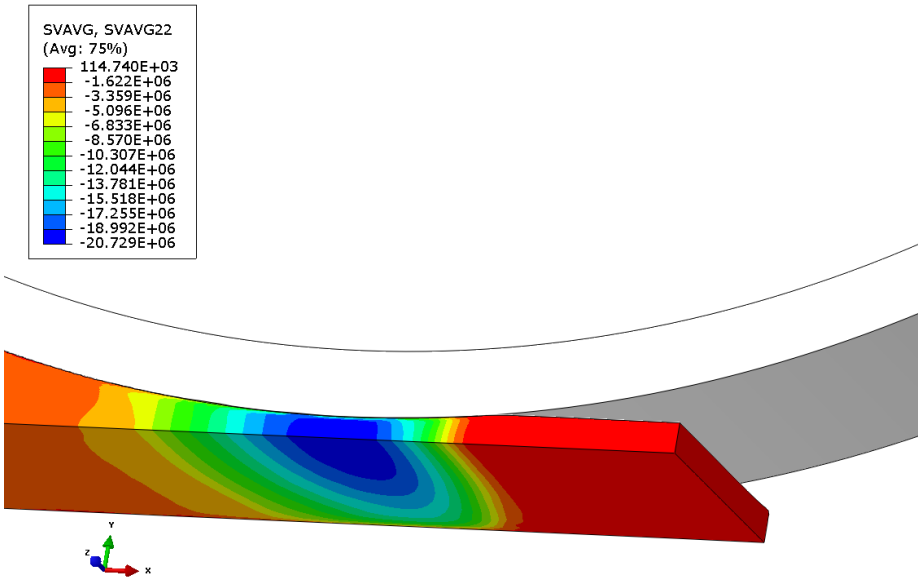

Figure 5.6: Vertial stresses, σ_{yy} on the fourth-folded symmetry model

In order to have a better understanding of the roll compaction process and the contact between powder and rolls, the contact pressure (Fig.5.7a) and shear stress (Fig.5.7b) on the roll are plotted.

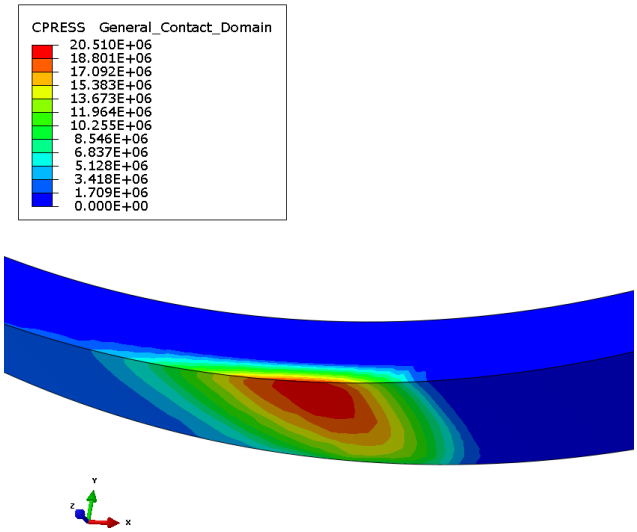

Figure 5.7: Resultant roll contact pressure in CEL FEM model

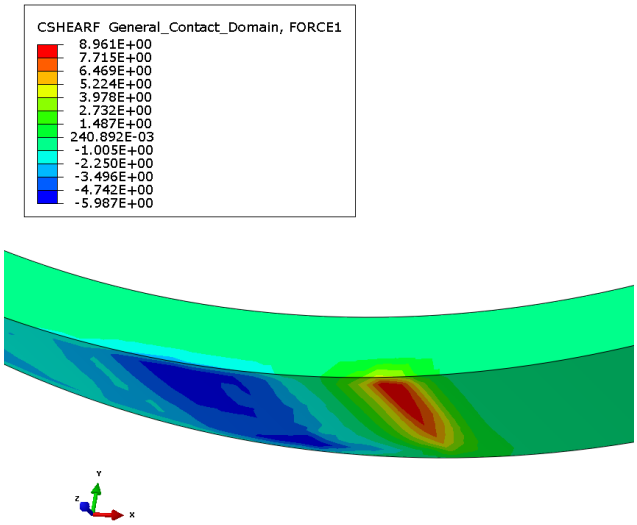

Figure 5.8: Resultant roll shear stress in CEL FEM model

Similarly to the previous results showed in Fig.5.6 ,the contact pressure (Fig.5.7) and shear stress (Fig.5.8) on the roll varies both in the rolling direction and along its width. The height value of contact stresses is located at the center of the roll (or here in the right edge due to symmetry) and slightly before the minimum gap region.

In a second step, a sensitivity study of the floating roll to the powder feeding throughput has been conducted using the developed CEL approach. Two models are simulated, one having a constant feeding velocity of 0.01 m/s and another with 0.015 m/s (See Appendix for additional figures).

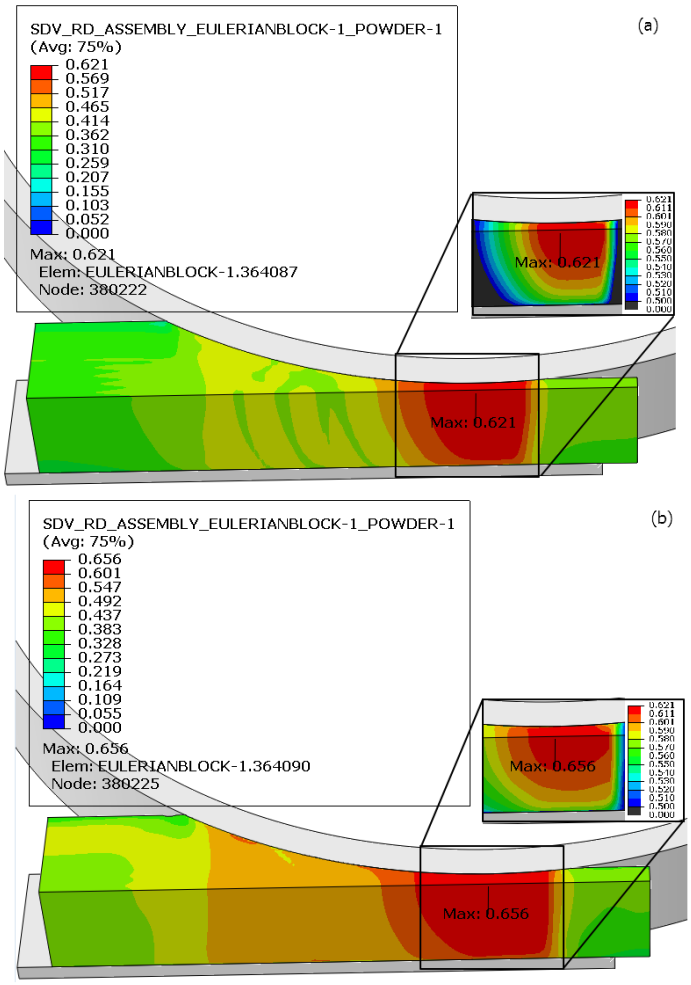

Figure 5.9: Resultant relative density for a given inlet velocity of a)0.01 and b) 0.015 m/s.

The relative density results clearly shows that with a higher amount of feeding material, the resultant powder density under the rolls is higher due to higher pressure from the roll (Fig.5.9). Moreover, for a constant spring's stiffness, the roll

displacement or in other words, the gap width increases with an increase in powder feed. These results emphasize the advantage of such modelling approach in order to simulate a more realistic and continuous manufacturing process.

It is important to mention that the current modelling approach is still limited, and as can be seen from Fig.5.9, the ribbon's density is unrealistic as the powder exhibits large dilation during the ejection from the rolls. Nonetheless, the elastic relaxation and expansion of the ribbon does seems realistic with reasonable values, which is obtained by the calibrated elastic parameters of E and ν.

5.5 Conclusions

The new developed CEL approach to model the roll compaction has proven itself comparable and in some cases, superior to the prior ALE method. Indeed, the powder is not restricted to a previously defined fixed mesh and is free to flow and contact different assembly components.

Moreover, results clearly show an increase of gap between rolls, which is a function of the spring's stiffness (i.e., hydraulic pressure) and the resultant roll reaction force. This lay foundation to a further development of the model by monitoring the roll reaction force and adjusting the feeding of powder and the hydraulic pressure in a continuous manner. Although this modelling approach is only at its initial stage, it is still very promising.

This page intentionally left blank.

General conclusions

The main objective of this work aimed to investigate by FEM modelling the roll compaction process and the effect of both the process parameters and the system design, such as sealing system and screw conveyor. More specifically, the planned and achieved objectives of this thesis include:

- ✓ Characterizing the microcrystalline cellulose (Avicel PH 101) powder in a continuous manner by the Drucker-Prager Cap constitutive model, with density-dependent properties.
- ✓ Study the effect of simulation and process parameters on current three-dimensional FEM modelling approach.
- ✓ Study the effect of sealing system design (Rimmed-roll or cheek-plates) based on current three-dimensional FEM modelling approach and validating the results experimentally.
- ✓ Develop a novel three dimensional modelling of the entire roll compaction process by including both the screw feeding and roll compaction unit in a combined DEM & FEM modelling approach.
- ✓ Introducing a newly developed Coupled-Eulerian Lagragian (CEL) approach for a more realistic roll compaction modelling. In this method, a floating roll and the ejection and production of final ribbon product can be modelled.

To start with, a fully experimentally calibrated density-dependent Drucker-Prager Cap (DPC) constitutive model to represent the behavior of the powder being compaction was performed. The obtained DPC model is then plotted having different isolines representing each relative density. The yield surface expands with an increase in the relative density, and therefore, alternates the DPC parameters of Pa, Pb, R, β and d, accordingly. Once obtaining the material behavior in a constitutive model, it is possible to implement it to an FEM model in Abaqus via a user-defined Fortran subroutine, named VUSDFLD.

The following step required is developing the FEM model. This is detailedly described in section 2.2 and generally applied to all models developed in this work. In this work, FEM is used to understand and predict the roll compaction process by obtaining the magnitudes and directions of stresses, strains and velocities. The FEM models were solved as a steady-sate problem using arbitrary Lagrangian-Eulerian (ALE) adaptive meshing in Abaqus/Explicit v6.14. First step in creating a Finite Elements (FE) model is to represent the geometry of the desired roll compactor. Once sketching the press dimensions, the region between the rolls is discretized and meshed using C3D8R three-dimensional continuum reduced integration elements. Using the ALE approach, which is common method being used to model roll compaction process using FEM, the smallest gap where the powder in contact under the rolls needs to be fixed and predefined prior to the simulation.

First FEM study conducted in this work aims to utilize the previously introduced three-dimensional FEM model to study the effect of the different process and simulation parameters on the B050H laboratory roll press. The obtained simulation results of different process parameters clearly show the ability of FEM modelling to help better understand the roll compaction process. Results found to be comparable to previous experimental, analytical and numerical studies in the literature. These findings validate the capability of current modelling approach for further development and investigation of roll compaction based on FEM.

Once the validity of the developed roll compaction FEM model has been established, further analyses are being made. This starts by investigation the effect of different sealing system designs (rimmed-roll and cheek plates) that equips the main industrial roller presses on the ribbon's density distributions. Results clearly show the effect of the cheek plates, causing a non-uniform roll pressure and density distribution with the highest values in the middle and the lowest in the edges. On the contrary to the cheek plates, the resultant pressure and density distribution with the rimmed-roll obtained higher values in the edges than in the middle and overall a more uniformly distributed.

This works begins with a general study of the effect FEM simulations result clearly show the effect of different process parameters on the developed roll pressure and density distribution in the compaction zone of powder between the rolls. Moreover, results show that using cheek-plates sealing system causes a nonuniform roll pressure and density distribution with the highest values in the middle and the lowest in the edges. On the other hand, the resultant pressure and density distribution with the rimmed-roll obtained higher values in the edges than in the middle and overall a more uniformly distributed. The combined DEM-FEM methodology clearly shows a direct correlation between the particle velocity driven by the screw conveyor to the feed zone and the roll pressure, both oscillating with the same period. This translates into an anisotropic ribbon with a density profile varying sinusoidally along its width. To validate the results, the simulations are compared with literature and experimentally measured values in order to investigate the ability of the model to predict the properties of the produced ribbons.

Last two chapters in this work introduces a newly developed FEM models in order to better represent the roll compaction process, taking into account the feeding of powder by a screw conveyor and the adjustment of gap between rolls by a continuous manufacturing approach. Therefore, to represent the materials' behavior both in the feeding zone and in the compaction area, a combined three-dimensional Discrete Element Method (DEM) and Finite Elements Method (FEM) is developed in this chapter. In the proposed approach, the DEM and FEM are treated as complementary methods, enabling us to take advantage of the strengths of both. Results show a direct correlation between the particle velocity driven by the screw conveyor and the roll pressure, both oscillating with the same period. This translates into an anisotropic ribbon with a density profile varying sinusoidally along its width, with a period equal to the duration of a screw turn.

Lastly, a new Coupled Eulerian-Lagrangian (CEL) approach, attempting to take into account the fluctuation of the gap by allowing simulating the free flow of the material between and outside the rolls is presented. The change in the gap between rolls is managed by a spring-stiffness with a given rigidity and miming the action of the hydrostatic pressure. First results clearly show an increase in the gap between the rollers as a function of the stiffness of the spring and the force reaction of the roller. This work, still in the preliminary state, constitutes a promising basis for further development of the model to simulate the actual operation of a roller press (adjustment of the gap as a function of the flow of material controlled by the feed screw).

To conclude, it is clearly shown, that theses obtained results demonstrate the ability of FEM modeling to provide insight and better understanding of the roll compaction process. FEM modeling may also be used in improving the quality of ribbons with new designs and process set-ups.

Perspectives

Results from this work have shown the importance and the adanvtages of simulating the roll compaction process by reducing expensive material usage and laboratory experiments in a trial and error approach. Based on this work, it is only needed to characterize the desired powder in order to study different material behaviour and their effect on the roll compaction process.

Moreover, this thesis work introduces new numerical approaches of simulating the roll compaction process in a more realistic manner, opening up new perspectives for future work.

- A combined DEM & FEM approach for modelling roll compaction process

  Conducting further investigations of the effect of screw feeder designs, orientations, and process parameters on the roll compaction process and the produced ribbons. More precisely, it is interesting to study different ratios of screw speed/roll speed on the ribbon nonuniformity. Furthermore, the distance between the last flight of the screw and the rolls has importance in the exerting counter pressure from the rolls and on the overall produced ribbons.

- A CEL formulation for modelling roll compaction process

  Continuation of the proposed CEL formulation approach by implementing a multi-loop PID controller, thus simulating an automatic roll press to achieve desired conditions. For instance, this can be achieved by implementing a VUAMP user-defined subroutine in Abaqus to perform an active control simulation based on PID controller. With this method, the magnitude of roll reaction force and gap width are monitored by sensors increment-by-increment as the simulation executes. Sensor values can be feedback into the model to produce actuation as an amplitude function. This can be used to adjust the inlet feeding boundary conditions and the roll's spring stiffness representing the hydraulic pressure via field variables.

Résumé en français

1. Introduction

Dans l'industrie pharmaceutique, le compactage à rouleaux est utilisé pour le processus de granulation sèche. Cela consiste à agglomérer des poudres fines ou des formulations en granules par densification mécanique sans l'ajout de liant liquide. Le but est d'améliorer la fluidité et l'homogénéité des formulations pour la compression directe. Ce qui minimise en particulier les problèmes de poudres fines [1]. Dans le compactage à rouleaux, la densification de la poudre est réalisée par la pression mécanique appliquée par deux rouleaux en contre-rotation, sur la poudre lorsque celle-ci passe dans l'entrefer. Le frottement entre la poudre poussée par la vis d'alimentation et la surface des rouleaux entraine progressivement la poudre dans l'espace étroit entre les rouleaux où la poudre est soumise à de fortes contraintes conduisant à la formation de compacts. Ces compacts sont ensuite fragmentés en granules à l'aide d'un système de broyage. Les propriétés des compacts et des granules en termes d'homogénéité et de résistance sont des attributs de la qualité du produit. Les premières études sur le processus de compactage à rouleaux ont montré que le comportement de la poudre sous les rouleaux peut être décrit par trois régions principales (Fig. 1):

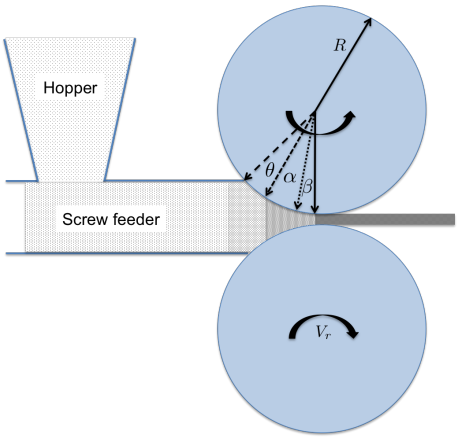

Figure 1: Représentation schématique du processus de compactage à rouleaux

Dans un premier temps, la poudre alimente les rouleaux à partir de l'angle d'entrée θ. Le processus d'entrainement de la poudre est basé sur le glissement relatif entre la poudre est les rouleaux en rotation avec une certaine vitesse. Ce processus est considéré responsable de l'entrainement de la poudre jusqu'à un angle α, appelé angle de pincement. La région [θ,α], est dénommée zone de remplissage par glissement. Dans cette zone, la pression appliquée par les rouleaux croît progressivement, mais reste modérée. De plus, grâce au glissement relatif entre la poudre et les rouleaux, la poudre avance avec une vitesse moins rapide que celle des rouleaux. Dans la région suivante définie par [α, 0], la poudre est considérée en contact permanent avec les rouleaux (zone de collage). C'est dans cette zone que la pression croît de manière importante en atteignant son maximum avant l'angle $\beta < 0$ (0 étant l'angle neutre) et entraine de grandes déformations dans la poudre. De plus, dans cette zone de collage, la matière et les rouleaux avancent macroscopiquement à la même vitesse. Enfin, le compact est éjectée de l'entrefer (zone [0,$\rightarrow$]). Dans cette phase de libération du compact, la pression décroit rapidement et, le compact est éjecté à une vitesse légèrement plus élevée que celle des rouleaux. La mise au point du procédé de compactage à rouleaux et son optimisation sont couramment basées sur des approches de type «essai-erreur». La densité du compact, c'est-à-dire la fraction solide, est l'un des paramètres de qualité critique du processus de compactage à rouleaux qui influence la compactibilité des granules.

L'effet des paramètres du procédé, des propriétés de la poudre, des systèmes de confinement des rouleaux et d'alimentation sur le processus de compactage à rouleaux a été étudié dans différents travaux expérimentaux [36, 37]. Il en résulte que l'impact le plus significatif sur la densité du compact est la pression du rouleau. La conception du système de confinement des rouleaux et, les conditions opératoires de fonctionnement ont un effet direct sur la qualité du compact produit. Afin d'assurer la consistance, la reproductibilité et la qualité de la forme posologique finale, il est important d'assurer l'homogénéité des propriétés des compacts. Mansa et al. [38] a constaté qu'une augmentation de l'angle de frottement effectif et de la cohésion de la poudre d'alimentation, entraînait une augmentation de l'angle de grippage α, tandis qu'une augmentation de la vitesse du rouleau entraînait une diminution de cet angle.

D'autres résultats importants ont été obtenus, tels que l'effet de la lubrification [40] qui résulte en une baisse de la pression maximale et de l'angle de grippage.

Non seulement les propriétés de la poudre et les paramètres du processus influencent le processus de compactage à rouleaux, mais aussi le système de confinement des rouleaux utilisé pour limiter la perte de poudre sur les côtés des rouleaux. En effet, il existe essentiellement deux systèmes de confinement : un confinement par des plaques métalliques fixées de part et d'autre des rouleaux et un autre système de confinement utilisant un rouleau surmonté d'une jante fixée sur le rouleau inférieur et qui limite la perte de matière lors du compactage. Il existe de rares études empiriques sur l'influence réelle du système de confinement sur les propriétés des compacts [40, 41, 42, 43, 44] .L'un des enjeux de cette thèse est d'étudier de manière approfondie (études expérimentale et modélisation numérique avec validation expérimentale) l'impact du système de confinement des presses à rouleaux sur les propriétés des compacts produits. D'autres problématiques liées au processus de compactage à rouleaux sont aussi d'intérêts fondamentales pour l'optimisation du procédé, mais qui, malheureusement, restent peu étudiés. Il s'agit entre autre de l'effet du système d'alimentation par vis et de l'air emprisonné dans la poudre sur le transport de poudres fines par exemple et sur le compactage entre les rouleaux (interaction entre l'air et le solide en compression). Les presses à rouleaux sont souvent équipées de système de pompes pour extraire l'excès d'air dans les poudres. Quelques études ont montré que l'alimentation et la présence de l'air ont une influence importante sur le processus de compactage à rouleaux [49, 50, 51, 54]. Ces aspects doivent être étudiées plus en profondeur pour mieux comprendre leur influence sur l'optimisation du procédé.

Beaucoup de résultats connus sont principalement obtenus par essais expérimentaux empiriques sur des poudres et des presses à rouleaux spécifiques (il en existe plusieurs types). Les résultats de ces essais sont souvent relatifs aux cas étudiés et ne permettent pas souvent de les généraliser. De plus, ces essais sont très coûteux en temps, en investissement matériel, capteurs et matière première quand l'étude concerne un principe actif par exemple. Pour cela, plusieurs modèles analytiques ont été développés pour permettre de mieux comprendre le processus. Cependant, malgré

leur pertinence, ces modèles analytiques sont encore limités. D'autres modélisations mathématiques plus complexes du processus sont nécessaires.

Au cours des deux dernières décennies, la modélisation par éléments finis (FEM) a été adoptée et développée pour simuler des processus de mise en forme de procédés pharmaceutiques. Les modèles FEM, appliquées au processus de compactage à rouleaux de poudre, ont commencé par considérer un cas bidimensionnel de déformation plane [2, 3, 4, 5]. Les résultats obtenus sont comparables et plus précis que ceux obtenus par les méthodes analytiques unidimensionnelle Johanson [6] et Slab [7, 8]. Avec l'augmentation de la puissance de calcul au cours des dernières années, le développement de modèles tridimensionnels a permis de mieux comprendre la distribution de la pression et de la densité durant le processus de compactage à rouleaux [9, 10, 11].

2. Objectifs

Le but de ce travail est d'étudier par modélisation numérique, le processus de compactage à rouleaux dans sa globalité en 3D (alimentation par vis et compactage entre les rouleaux). En particulier, l'effet des paramètres du procédé, l'impact du système de confinement des rouleaux (plaques fixes et rouleau avec jante de confinement) sur les propriétés des compacts ainsi que le système d'alimentation par vis et son effet sur les distribution de pression et des vitesses d'alimentation des rouleaux, sont analysés de manière approfondie. Compte tenu du large intervalle de variation de la densité de la poudre dans le procédé de compactage à rouleaux, deux méthodes numériques ont été mises en oeuvre pour modéliser le processus de compactage à rouleaux : l'écoulement de la poudre dans le système d'alimentation où la déformation de la matière est relativement petite, a été modélisé par la méthode des éléments discrets – DEM). Par ailleurs, le compactage entre les rouleaux a été modélisé par la méthode des éléments finis - FEM, mieux adaptée aux grandes déformations que subit la poudre dans cette zone. Une méthode d'interfaçage entre DEM et FEM a été proposée pour combiner les deux approches et simuler le procédé dans sa globalité. Enfin, le développement de nouvelles simulations numériques permettant de

prendre en compte le caractère variable de l'entrefer, du au débit de matière fluctuant, est aussi d'intérêt numérique important. Dans ce cadre, les premières bases du développement ont été initiées. L'effort devra être poursuivi pour répondre à cette problématique à la frontière entre la technologie du procédé et les outils mathématiques.

Plus spécifiquement, les objectifs de cette thèse comprennent:

- Caractérisation de la poudre de cellulose microcristalline (Avicel PH 101) de manière continue par le modèle de comportement Drucker-Prager Cap, avec des propriétés dépendant de la densité. Suivi par modélisation FEM tridimensionnelle pour étudier l'effet de différents paramètres de processus et valider les simulations à partir d'études antérieures dans la littérature.

- Etudier l'effet de la conception du système d'étanchéité (plaques fixes et rouleau surmonté de jante) en se basant sur l'approche FEM avec validation expérimentalement des prédictions.

- Développement de nouvelles approches de méthodes combinées DEM-FEM et couplage Lagrangien-Eulérien (CEL) afin d'étudier les effets l'alimentation à vis et du rouleau flottant pour simuler un gap variable. Ces approches peuvent être étendues à d'autres procédés continus où la porosité de la poudre varie subit de grandes variations.

3. Contenu des chapitres

Le chapitre 1 commence par un bref historique du processus de compactage à rouleaux et de son développement au cours des deux dernières décennies. L'utilisation des tests «essai et erreur» était couramment utilisée pour comprendre le processus de compactage des rouleaux et pour répondre à la qualité du produit par la conception dans le processus de fabrication. L'effet des paramètres du procédé, des propriétés de la poudre en vrac, des systèmes de confinement des rouleaux et le système d'alimentation sur le processus de compactage, étudiés dans la littérature, sont présentés dans ce chapitre. Néanmoins, la compréhension globale du processus de

compactage à rouleaux n'a pas encore été pleinement réalisée. La deuxième partie de ce chapitre décrit des modèles analytiques, suivis par des approches de modélisation numérique plus sophistiquées utilisant la méthode des éléments finis (MEF) pour une meilleure compréhension du processus de compactage à rouleaux. Enfin, le contexte théorique de cette approche de modélisation FEM est présenté et résumé.

Le chapitre 2 décrit les matériaux et les méthodes utilisés pour le développement et l'étude du processus de compactage des cylindres par un modèle FEM 3D. Pour cela, il faut d'abord comprendre les différentes conceptions de systèmes et les paramètres de processus des presses à rouleaux utilisées dans cette étude. Ensuite, le modèle EF et sa mise en œuvre concernant le comportement du matériau et les paramètres du processus sont décrits en détail. Dans ce travail, la poudre de cellulose microcristalline (MCC) est caractérisée par un modèle de comportement Drucker-Prager Cap dépendant de la densité qui est déterminé sur la base d'une méthode d'étalonnage expérimentale standard.

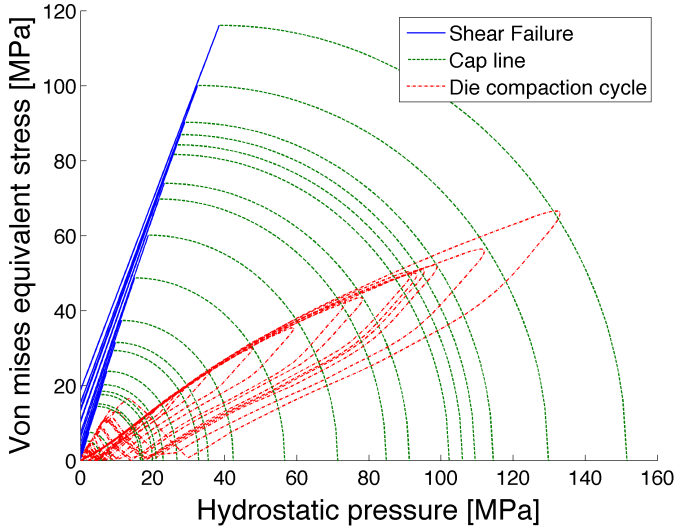

Figure 2: Calibration du modèle de Drucker-Prager Cap pour la cellulose microcristalline MCC101

Afin de valider les modèles FEM, une procédure de caractérisation des densités des compacts produits par compactage à rouleaux est décrite.

Le chapitre 3, divisé en deux parties principales, vise à utiliser le modèle FEM tridimensionnel précédemment introduit pour étudier l'effet des différents paramètres de processus et de simulation, ainsi que la conception des systèmes de confinement, sur le processus de compactage à rouleaux. Particulièrement, l'effet des paramètres du processus et de simulation, incluant les conditions d'alimentation, la friction aux parois, la vitesse du rouleau et le facteur d'échelle de masse, sur les résultats prédits ont été étudiés et discutés à partir des données de la littérature.

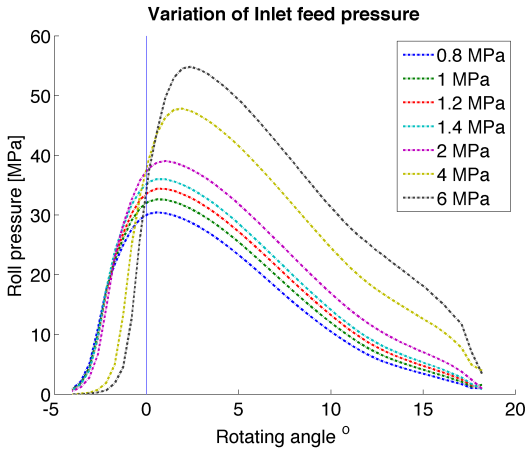

Figure 3: Effet de la pression d'alimentation sur la pression de compactage

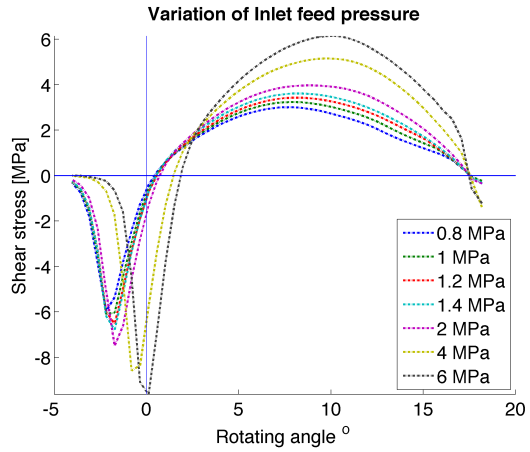

Figure 4: Effet de la pression d'alimentation sur la contrainte de cisaillement

Comme prévu, une augmentation de la pression d'alimentation d'entrée entraîne une augmentation de la pression du rouleau (Fig.3), de la contrainte de cisaillement (Fig.4) et de la densité du compact. Ce résultat est en accord complet avec le modèle analytique de Johanson et les études FEM précédentes menées pour le processus de compactage à rouleaux. Un autre phénomène intéressant qui peut-être remarqué est le déplacement de la pression maximale du rouleau et de l'axe neutre (axe où la contrainte de cisaillement change de signe en raison de la direction de frottement) vers la région d'entrée. Ce comportement pour une pression d'alimentation d'entrée élevée suggère que la quantité de poudre fournie par l'alimentation est trop grande, entrainant ainsi le blocage de la presse. Les résultats de la simulation de différents paramètres du processus montrent clairement la capacité de modélisation FEM pour aider à mieux comprendre le processus de compactage à rouleaux. Les résultats FEM ont été jugés comparables aux études expérimentales, analytiques et numériques précédentes dans la littérature. Ces résultats valident la capacité de l'approche de modélisation actuelle à poursuivre le développement et l'étude du compactage à rouleaux basée sur FEM.

La deuxième partie de ce chapitre se focalise sur l'étude par FEM de la modélisation de l'effet du système de confinement des rouleaux (plaques fixes longeant les rouleaux ou rouleau surmonté d'une jante) équipant les principales presses à rouleaux industrielles, sur les distributions de densité dans le compact. Il est important de mentionner ici que, cette étude est la première à analyser et valider le processus de compactage à rouleaux en 3D en utilisant le système de confinement à l'aide d'un rouleau surmonté d'une jante. La pertinence des résultats de ces développements est confrontée aux mesures réalisées sur une presse «Minipactor Gerteis» pouvant être équipée avec les deux systèmes de confinement. En comparant les deux systèmes de confinement des rouleaux, la distribution de pression de contact du rouleau est visualisée sur les figures 5 et 6. D'abord, on peut voir que pour les deux systèmes de confinement, la pression de contact augmente jusqu'à atteindre une valeur maximale juste avant l'entrefer. La pression de contact le long de la largeur du compact , varie entre 25 et 37 MPa pour le confinement fixe par deux plaques et entre 29 et 33 MPa pour le confinement utilisant une rouleau surmonté d'une jante.

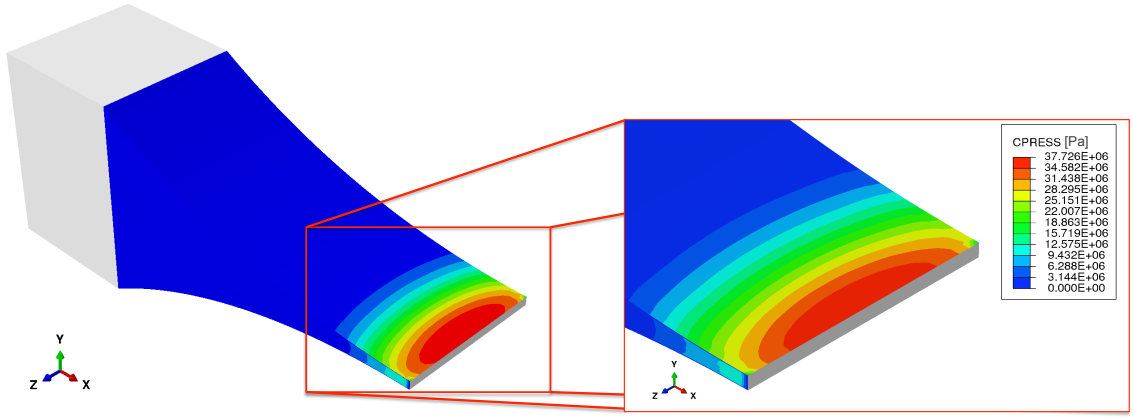

Figure 5: Distribution de pression de contact entre la poudre et le rouleau supérieur. Cas du système de confinement «plaques fixes».

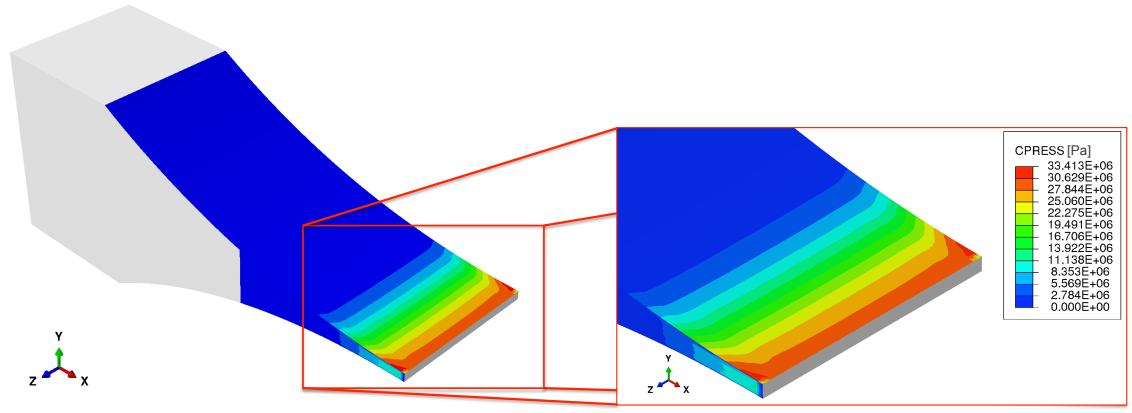

Figure 6: Distribution de pression de contact entre la poudre et le rouleau supérieur. Cas du système de confinement «rouleau surmonté d'une jante».

La distribution de densité relative de la poudre entre les rouleaux est visualisée sur la Fig.7. La densité relative le long de la largeur du compact, varie entre 0,59 et 0,64 dans le cas du système de confinement par plaques fixes, et entre 0,60 à 0,62 dans le cas d'un rouleau surmonté de jante.

Les résultats montrent clairement l'effet des plaques de confinement sur les propriétés du compact, provoquant une distribution de pression et de densité non uniforme dans la largeur avec des valeurs plus élevées au milieu et plus faibles sur les

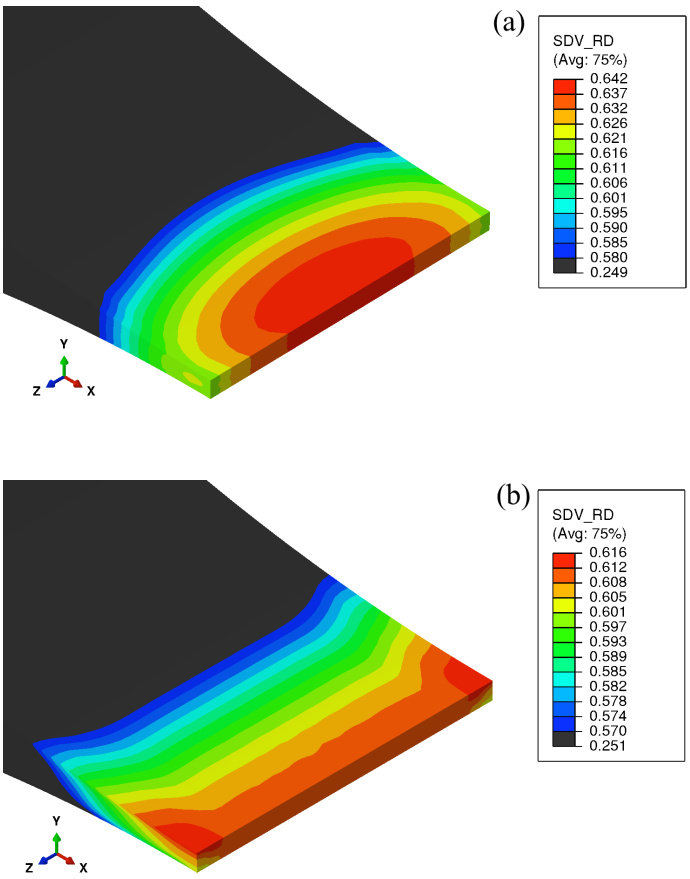

Figure 7: Distribution de la densité relative dans la largeur du compact. Cas plaques fixes (a) et rouleau avec jante (b).

bords. La poudre n'est pas délivrée de manière uniforme dans la zone de compactage. Cela étant dû aux plaques fixes de confinement qui empêchent l'écoulement uniforme de la poudre et provoquent ainsi un compactage irrégulier à travers la largeur du ruban, conduisant à une densification non homogène. Contrairement au système de confinement par les plaques fixes, la distribution de pression et de densité résultante du système de confinement utilisant une roue surmontée d'une jante, montrent des distributions globalement plus uniformes avec cependant une localisation plus élevée sur les bords que dans le centre. Cela est dû au frottement contre la jante du rouleau qui cumule la poudre en la transportant dans la zone de compactage.

Pour valider les résultats, les simulations sont comparées à des valeurs mesurées expérimentalement [77]. Les résultats montrent dans l'ensemble la même tendance que les mesures expérimentales avec une surestimation de la densité du compact sur les bords pour le système de confinement par plaques fixes. D'autre part, pour le cas de la roue avec une jante, les résultats montrent un accord avec les résultats obtenus dans la littérature pour différentes poudres [11].

Le chapitre 4 commence par une vue d'ensemble de la conception la presse à rouleaux, comportant généralement une seule vis rotative, qui alimente le matériau dans un espace entre deux rouleaux tournant en contre sens et possédant des plaques fixes de confinement sur les côtés des rouleaux pour éviter les pertes en poudre. Malgré la simplicité conceptuelle du compactage à rouleaux, la modélisation numérique du processus de compactage à rouleaux reste difficile en raison de la complexité impliquant deux mécanismes coopératifs: l'alimentation des rouleaux par une vis sans fin et le compactage de la poudre entre les rouleaux. Les mécanismes physiques et mécaniques dans chaque partie du procédé sont différents. De plus, la plage de variation de la porosité du matériau est grande. Dans la zone d'alimentation, le flux de particules entrant est un paramètre clé influençant fortement le processus de compactage, puisqu'il dicte la cadence du processus et affecte l'homogénéité du produit compacté. D'autre part, la déformation du matériau sous forte contrainte et les conditions de frottement dans la zone de compactage sont des ingrédients importants et nécessaires pour modéliser le système.

Par conséquent, afin de mieux représenter le comportement des matériaux dans la zone d'alimentation et dans la zone de compactage, une nouvelle simulation tridimensionnelle de l'alimentation utilisant la méthode des éléments discrets (DEM) couplée à une simulation par éléments finis (MEF) compactage, est développée dans ce chapitre. La DEM est naturellement adaptée pour modéliser le processus de transport et sera utilisée pour étudier le flux de particules dans la zone d'alimentation. Les résultats seront utilisés comme conditions aux limites d'entrée pour la modélisation FEM du processus de compactage, qui est l'approche la mieux adaptée pour prendre en compte la déformation du matériau. Dans notre travail, DEM et FEM sont traitées comme des méthodes complémentaires: leur combinaison dans l'étude

du compactage à rouleaux nous permet de tirer profit de leurs forces dans les régions où ils sont respectivement les mieux adaptées. Le but de notre étude est donc d'améliorer les modèles numériques existants, conduisant à une description plus réaliste du processus qui nous conduira à une meilleure prédiction de la qualité finale du compact.

Les résultats obtenus de la combinaison des méthodes DEM et FEM dans le procédé de compactage à rouleaux, montrent une corrélation directe entre la vitesse des particules entraînées par la vis (alimentation) et la pression de compactage appliquée par le rouleau, les deux oscillant avec la même période. Cela conduit à une distribution sinusoïdale de la densité le long du compact (figure 9). Cette répartition correspond à la signature de la vis. Plus précisément, la période d'oscillation est égale à la durée d'un tour de la vis.

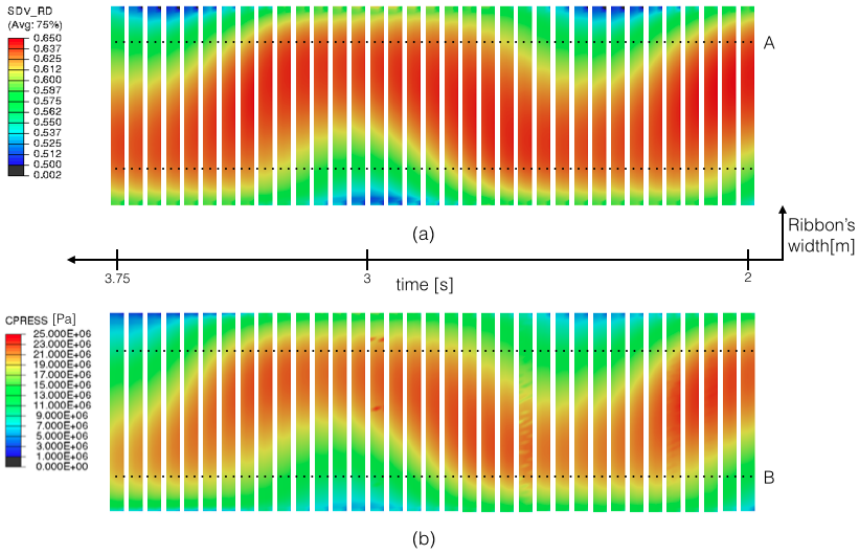

Figure 9: Densité relative (a) et pression de contact (b) au cours du procédé. Résultats de simulation obtenue par combinaison de méthodes DEM et FEM.

Dans le procédé de compactage à rouleaux, l'entrefer entre les rouleaux n'est pas fixe et peut varier pendant la production pour s'adapter à la variation de débit de matière tout en gardant une qualité de compact identique. Pour tenir compte de cette contrainte, le chapitre 5 décrit une nouvelle approche couplant une méthode

Lagrangienne et eulérienne (CEL) pour une modélisation plus réaliste du compactage à rouleaux.

De nos jours, la plupart des fournisseurs proposent des machines automatiques sophistiquées afin d'obtenir les conditions de compression et les propriétés de compact souhaitées. Ces presses à rouleaux automatisées sont équipées d'un automate programmable (PLC) pour contrôler les paramètres du procédé. Cet automate est basé sur une stratégie de commande dite «proportional–integral–derivative (PID)», permettant de prendre en compte la fluctuation de matière due à la nature de la poudre et l'alimentation par vis.

Dans les presses à rouleaux, l'entrefer peut fluctuer avec le flux de matière entrante. Ce mécanisme n'a pas été pris en compte dans les simulations précédentes. Ce chapitre présente une nouvelle simulation, tentant de prendre en compte la fluctuation de l'entrefer en permettant de simuler la libre circulation de la matière entre les rouleaux. L'augmentation ou la diminution de l'entrefer est gérée par une raideur de ressort avec une rigidité donnée et mimant l'action de la pression hydrostatique qui contrôle l'entrefer. Les résultats préliminaires montrent clairement une augmentation de l'écart entre les rouleaux en fonction de la rigidité du ressort et de la réaction en force du rouleau (figure 10). Ce travail, encore à l'étape initiale, constitue une base prometteuse pour la poursuite du développement du modèle afin de simuler le fonctionnement réel d'une presse à rouleaux (réglage de l'entrefer en fonction de l'écoulement du matériau contrôlé par la vis d'alimentation).

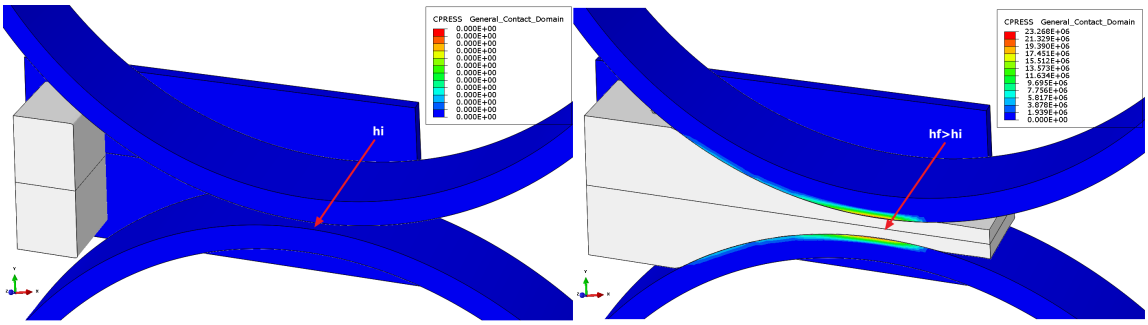

Figure 10: Ecoulement de la poudre et pression de compactage dans le cas de la méthode CEL

La nouvelle approche CEL développée pour modéliser le compactage à rouleaux s'est montrée prometteuse dans la prise en compte d'un entrefer variable. En effet, la poudre n'est pas limitée à une maille fixe comme dans l'approche ALE. La poudre s'écoule librement dans les mailles tout en développant le contact avec les différentes composantes de la presse. De plus, les résultats montrent clairement une augmentation de l'entrefer entre les rouleaux, qui est fonction de la rigidité du ressort (qui mime la pression hydraulique) et de la force de réaction résultante au niveau rouleau, considéré comme un outil rigide. Ces résultats préliminaires montrent que l'approche peut-être prometteuse pour modéliser finement le procédé en ajustant l'alimentation en fonction du pilotage de la pression hydraulique (raideur du ressort) et la force de réaction du rouleau.

4. Conclusion générale

L'objectif principal de ce travail était d'étudier par MEF la modélisation du processus de compactage à rouleaux, l'effet des paramètres du procédé et du système de confinement des rouleaux (plaquettes fixes ou rouleau avec jante) et l'alimentation par vis sans fin sur les propriétés du compact, en particulier la distribution des pressions et de la densité relative. Plus précisément, les objectifs atteints de cette thèse sont :

- Caractérisation de la poudre de cellulose microcristalline (Avicel PH 101) de manière continue par le modèle de comportement Drucker-Prager Cap, avec des propriétés dépendant de la densité. Dans ce cadre, les paramètres du modèle de Drucker-Prager / Cap, dépendant de la densité, ont été calibrés expérimentalement sur une poudre de Cellulose microcristalline. La méthode standard de calibration a été mise en œuvre.

- Développer une modélisation 3D du compactage à rouleaux (FEM - ALE) et étudier l'effet des paramètres de simulation et de procédé sur les propriétés du compact. Les résultats obtenus ont été jugés comparables aux études expérimentales, analytiques et numériques de la littérature. Ces résultats valident la

capacité de l'approche de modélisation actuelle à poursuivre le développement et l'étude du compactage à rouleaux basé sur l'approche FEM.

- Étudier l'effet du système de confinement de la poudre de part et d'autres du rouleau (plaques fixes et roue surmontée de jante) sur les propriétés d'homogénéité des compacts. Dans ce cadre, les prédictions des distributions de densité dans le compact et des pressions de compression ont montré que l'utilisation de plaques fixes de confinement sur les bords des rouleaux ne favorisait pas l'homogénéité des propriétés du compact. Cependant, l'utilisation du système de confinement avec une roue surmontée de jante apportait plus d'homogénéité des propriétés du compact. Ces prédictions en termes de distribution de densité ont été validées expérimentalement. Le modèle FEM, ALE 3D ainsi développé a montré sa capacité à mieux expliquer le rôle du système de confinement sur la qualité du produit (compact).

- Développer une nouvelle modélisation tridimensionnelle de l'ensemble du processus de compactage à rouleaux en incluant à la fois l'unité d'alimentation par vis et l'unité de compactage à rouleaux dans une approche combinée de modélisation DEM et FEM. La méthodologie suivie montre clairement une corrélation directe entre la vitesse des particules en sortie de la zone d'alimentation par vis sans fin, et la pression du rouleau. Ces deux variables oscillent avec la même période. Cela se traduit par un compact anisotrope avec un profil de densité variant sinusoïdalement le long de sa longueur, avec une période égale à la durée d'un tour de vis.

- Mise en place d'une nouvelle approche couplant l'approche lagrangienne et Eulérienne (CEL) est mise en place pour une modélisation plus réaliste du compactage à rouleau (prise en compte du caractère variable de l'entrefer). Dans ce cadre, la procédure choisie a montré sa capacité à prendre en compte le caractère variable de l'entrefer. Cette démarche mérite d'être plus développée et approfondie pour aller vers le contrôle de l'alimentation par vis en ayant une estimation numérique de la pression hydraulique et de la force de réaction du

rouleau.

L'ensemble des travaux de cette thèse a montré la complexité du procédé de compactage à rouleaux. Cette complexité est due au système d'alimentation par vis, à la variabilité de l'entrefer dépendant du débit irrégulier fournit par l'alimentation, à la grande plage de variation de la porosité du matériau particulaire en passant de l'état pulvérulent à l'état compact, au paramètres du procédé (vitesse du rouleau, système de confinement, inhomogénéité des pressions et des vitesses de la poudre à l'entrée du rouleau,..).

Des avancées notables ont été réalisées dans cette thèse en termes de modélisations numériques au service de la compréhension, prédictions et optimisation du procédé. Différentes techniques numériques ont été développées avec l'objectif principal de mieux représenter le procédé dans sa globalité. En particulier, la méthode DEM, FEM, CEL et la combinaison de la DEM et FEM pour mieux représenter les conditions d'entrée de la matière entre les rouleaux (conditions inconnues et non accessibles par la mesure), ont été proposées, mises en œuvre, testées et leurs prédictions ont été validées dans certains cas. Cependant, tout n'est pas résolu, ce qui laisse en perspective, une place à des extensions ou de nouveaux développements.

5. Perspectives

Ce travail de thèse introduit de nouvelles approches numériques pour simuler le processus de compactage à rouleaux de manière plus réaliste, ouvrant de nouvelles perspectives pour les travaux futurs.

- Mener des recherches plus poussées sur l'alimentation par vis sans fin et sur l'interaction entre la matière et les paramètres de la vis pour mieux prédire les vitesses et les pressions moyennes à la sortie de l'alimentation en présence des rouleaux. La combinaison ou le couplage de méthodes numériques avec chacune employée dans son domaine de validité physique est nécessaire. La DEM est une approche intéressante pour l'écoulement de la matière. Cependant, la considération de particules rigides limite son utilisation pour les applications de

matériau fortement déformable et compressible. La méthode des éléments finis (ALE) reste une approche bien adaptée à la simulation de la compression entre les rouleaux, mais ne permet pas de représenter l'écoulement dans la chambre d'alimentation par vis. Une combinaison entre CEL et FEM pourrait–être une alternative.

- L'autre perspective de ce travail, serait le développement de la méthode CEL pour le compactage à rouleaux pour tenir compte des spécificités du procédé (entrefer variable) et aller vers la mise en œuvre d'un contrôleur PID à plusieurs boucles, simulant ainsi une presse à rouleaux automatique pour atteindre les conditions souhaitées.

Publications issues de ce travail

- A. Mazor, L. Orefice, A. Michrafy, A. de Ryck, J. G. Khinast, A combined DEM & FEM approach for modelling roll compaction process, Powder Technology (In press).
- A. Mazor, L. Perez-Gandarillas, A. de Ryck, A. Michrafy, Effect of roll compactor sealing system designs: A finite element analysis, Powder Technology, 289 (2016) 21-30.

Conferences Internationales

- A combined DEM & FEM modelling of powder flow and compaction during roll pressing, PARTEC: International Congress on Particle Technology, April 2016.
- Effect of roll compactor sealing system designs: A finite element analysis, PARTEC: International Congress on Particle Technology, April 2016.

Prix

The 2nd best poster award – 'Most pharmaceutical relevant poster' , 7th international granulation workshop, Sheffield, UK 2015.

References

[1] P. Kleinebudde, Roll compaction/dry granulation: Pharmaceutical applications, European Journal of Pharmaceutics and Biopharmaceutics 58 (2004) 317–326. doi:10.1016/j.ejpb.2004.04.014.

[2] R. T. Dec, A. Zavaliangos, J. C. Cunningham, Comparison of various modeling methods for analysis of powder compaction in roller press, Powder Technology 130 (2003) 265–271. doi:10.1016/S0032-5910(02)00203-6.

[3] J. C. Cunningham, Experimental studies and modeling of the roller compaction of pharmaceutical powders, Strain (July) (2005) 267.

[4] A. Michrafy, H. Diarra, J. A. Dodds, M. Michrafy, L. Penazzi, Analysis of strain stress state in roller compaction process, Powder Technology 208 (2011) 417–422. doi:10.1016/j.powtec.2010.08.037.

[5] A. R. Muliadi, J. D. Litster, C. R. Wassgren, Modeling the powder roll compaction process: Comparison of 2-D finite element method and the rolling theory for granular solids (Johanson's model), Powder Technology 221 (2012) 90–100. doi:10.1016/j.powtec.2011.12.001.

[6] J. R. Johanson, A Rolling Theory for Granular Solids, J. Appl. Mech 32(4) (1965) 842–848. doi:10.1115/1.3627325.

[7] T. V. Karman, Contribution to the Theory of Rolling, Math. Mech. 5(2) (1925) 139–141.

[8] V. P. Katashinskii, Analytical determination of specific pressure during the rolling of metal powders (In Russian), Soviet Powder Metal Ceram. 10(6) (1986) 765–772.

[9] A. Michrafy, H. Diarra, J. A. Dodds, M. Michrafy, Experimental and numerical analyses of homogeneity over strip width in roll compaction, Powder Technology 206 (1-2) (2011) 154–160. doi:10.1016/j.powtec.2010.04.030.

[10] J. C. Cunningham, D. Winstead, A. Zavaliangos, Understanding variation in roller compaction through finite element-based process modeling, Computers and Chemical Engineering 34 (7) (2010) 1058–1071. doi:10.1016/j.compchemeng.2010.04.008.

[11] A. R. Muliadi, J. D. Litster, C. R. Wassgren, Validation of 3-D finite element analysis for predicting the density distribution of roll compacted pharmaceutical powder, Powder Technology 237 (2013) 386–399. doi:10.1016/j.powtec.2012.12.023.

[12] R. K. Dube, Metal strip via roll compaction and related powder metallurgy routes, International Materials Reviews 35 (1) (1990) 253–292. doi:10.1179/095066090790323993.

[13] E. Von Siemens, Rolling strips from metal powder, German patent 154,998 (1904).

[14] C. Hardy, Rolling strips from metal powder, US Patent 21,314,366 (1938).

[15] J. Marvin, Method and apparatus for briquetting of powdered metal, US Patent 2,341,732 (Feb. 15 1944).

[16] G. Naeser, F. Zirm, Walzen von bändern aus eisenpulver, Stahl und Eisen 22 (70) (1950) 995—-1004.

[17] G. I. Aksenov, G. A. Vinogradov, Theory and practice of rolling cermet powder in the Soviet Union (11) (1967) 861–868.

[18] J. H. Tundermann, A. R. E. Singer, Deformation and Densification During the Rolling of Metal Powders, Powder Metallurgy 12 (23) (1969) 219–242. doi:10.1179/pom.1969.12.23.011.

[19] T. Kimura, Study on Continuous Rolling Fabrication, in: Iron Powder Metallurgy, 1968, pp. 161–183.

[20] V. G. Sander, V. D. Henk, Roll compaction of Anhydrous Lactose and Blends of Anhydrous Lactose with MCC, Pharmaceutical Technology 1 (2009).

[21] R. W. Miller, Roller Compaction Technology, in: Handbook of Pharmaceutical Granulation Technology, Taylor and Francis Group, 2005, pp. 159–190. doi:10.1201/9780849354953.ch17.

[22] H. Rumpf, The Strength of Granules and Agglomerates, in: Agglomeration, John Wiley and Sons, 1962, pp. 379–418.

[23] C. Nyström, G. Alderborn, M. Duberg, P.-G. Karehill, Bonding surface area and bonding mechanism-two important factors fir the understanding of powder comparability, Drug Development and Industrial Pharmacy 19 (17-18) (1993) 2143–2196. doi:10.3109/03639049309047189.

[24] P. J. James, Particle deformation during cold isostatic pressing of metal powders., Powder Metall. 20 (1977) 199–204.

[25] C. Fuhrer, Substance behaviour in direct compression, Labo-Pharma Probl. Tech. 25 (1977) 759–762.

[26] T. M. Jones, The influence of physical characteristics of excipients on the design and preparation of tablets and capsules., Pharm. Ind. 39 (1977) 469–476.

[27] K. K. Roberts R. J., Rowe R. C., Brittle-ductile transitions in die-compaction of sodium chloride., Chem.Eng. Sci. 44 (1989) 1647–1651.

[28] W. L. W., N. Pilpel, The effect of particle shape on the mechanical properties of powders., Int. J. Pharm. 59 (1990) 145–154.

[29] A. C. Sebhatu T., A. G., The effect of moisture content on the compression and bond-formation properties of amorphous lactose particles., Int. J. Pharm. 146 (1997) 101–114.

[30] L. E. Holman, H. Leuenberger, The relationship between solid fraction and mechanical properties of compacts - the percolation theory model approach., Int. J. Pharm. 46 (1988) 35–44.

[31] K. K. Roberts R. J., Rowe R. C., The effect of punch velocity on the compaction of a variety of materials., Pharm.Pharmacol. 37 (1985) 377–384.

[32] M. J. Nyström C., S. J., Studies on direct compression of tablets II.The influence of the particle size of a dry binder on the mechanical strength of tablets., Int. J. Pharm. 10 (1982) 209–218.

[33] P. E. Evans, G. C. Smith, The compaction of metal powders by rolling. II. – An examination of the compaction process, Powder Metallurgy 2 (3) (1959) 26–44. doi:10.1179/pom.1959.2.3.002.

[34] G. a. Chekmarov, A. P. ;Vinogradov, Investigation of specific pressure, specific friction, and the coefficient of friction during metal powder rolling, Soviet Powder Metallurgy and Metal Ceramics 2 (14) (1963) 26–30.

[35] A. D. R Cohn, H Heilig, Critical evaluation of the compactor, J. Pharm. Sci. 55 (1966) 328—331.

[36] F. Jaminet, H. Hess, Studies on compacting and dry granulation (in German).

[37] S. Inghelbrecht, J. P. Remon, Roller compaction and tableting of microcrystalline cellulose/drug mixtures, International Journal of Pharmaceutics 161 (2) (1998) 215 – 224. doi:http://dx.doi.org/10.1016/S0378-5173(97)00356-6.

[38] R. Mansa, Roller compaction of pharmaceutical excipients and predictiopn using intelligent software.

[39] G. Bindhumadhavan, J. P. K. Seville, M. J. Adams, R. W. Greenwood, S. Fitzpatrick, Roll compaction of a pharmaceutical excipient: Experimental validation of rolling theory for granular solids, Chemical Engineering Science 60 (2005) 3891–3897. doi:10.1016/j.ces.2005.02.022.

[40] A. M. Miguélez-Morán, C. Y. Wu, H. Dong, J. P. K. Seville, Characterisation of density distributions in roller-compacted ribbons using micro-indentation and X-ray micro-computed tomography, European Journal of Pharmaceutics and Biopharmaceutics 72 (1) (2009) 173–182. doi:10.1016/j.ejpb.2008.12.005.

[41] I. Akseli, S. Iyer, H. P. Lee, A. M. Cuitiño, A Quantitative Correlation of the Effect of Density Distributions in Roller-Compacted Ribbons on the Mechanical Properties of Tablets Using Ultrasonics and X-ray Tomography., AAPS PharmSciTech 12 (3) (2011) 834–853. doi:10.1208/s12249-011-9640-z.

[42] H. Lim, V. S. Dave, L. Kidder, E. Neil Lewis, R. Fahmy, S. W. Hoag, Assessment of the critical factors affecting the porosity of roller compacted ribbons and the feasibility of using NIR chemical imaging to evaluate the porosity distribution, International Journal of Pharmaceutics 410 (1-2) (2011) 1–8. doi:10.1016/j.ijpharm.2011.02.028.

[43] M. Khorasani, J. Amigo, J. Sonnergaard, P. Olsen, P. Bertelsen, J. Rantanen, Visualization and prediction of porosity in roller compacted ribbons with near-infrared chemical imaging (NIR-CI), Journal of Pharmaceutical and Biomedical Analysis 109 (2015) 11–17. doi:10.1016/j.jpba.2015.02.008.

[44] N. Souihi, G. Reynolds, P. Tajarobi, H. k. Wikström, G. Haeffler, M. Josefson, J. Trygg, Roll compaction process modeling: transfer between equipment and impact of process parameters, International Journal of Pharmaceutics 484 (2015) 192–206. doi:10.1016/j.ijpharm.2015.02.042.

[45] S. E. Funakoshi Y., Asogawa T., Use of a novel roller compactor with a concavo-convex roller pair to obtain uniform compaction pressure, Drug Dev. Ind. Pharm. 3(6) (1977) 555–573.

[46] O. Simon, P. Guigon, Correlation between powder-packing properties and roll press compact heterogeneity, Powder Technology 130 (2003) 257–264. doi:10.1016/S0032-5910(02)00202-4.

[47] P. Guigon, O. Simon, Roll press design - Influence of force feed systems on compaction, Powder Technology 130 (2003) 41–48. doi:10.1016/S0032-5910(02)00223-1.

[48] T. Lecompte, P. Doremus, G. Thomas, L. Perier-Camby, J. C. Le Thiesse, J. C. Masteau, L. Debove, Dry granulation of organic powders - Dependence of pressure 2D-distribution on different process parameters, Chemical Engineering Science 60 (2005) 3933–3940. doi:10.1016/j.ces.2005.02.026.

[49] M. Fayed, L. Otten, Size enlargement by agglomeration, in: Handbook of powder science and technology, Van Nostrand Reinhold Co., 1984, Ch. 6, pp. 354–363.

[50] D. Worn, R. Perks, Numerical simulation of roll compaction of aerated powders, Powder Met. 3 (1959) 45–71.

[51] G. Vinogradov, I. Fedorchenko, Numerical simulation of roll compaction of aerated powders, Poroshkovaya Met. 3 (1969) 61–64.

[52] J. H. Tundermann, A. R. E. Singer, The Flow of Iron Powder During Roll Compaction, Powder Metallurgy 11 (22) (1968) 261–294. doi:10.1179/pom.1968.11.22.004.

[53] C. B. Johanson J.R., Fluid entrainment effects in roll press compaction, Powder Handl. Process. 1 (2).

[54] V. Esnault, D. Heitzmann, M. Michrafy, D. Oulahna, a. Michrafy, Numerical simulation of roll compaction of aerated powders, Chemical Engineering Science 104 (2013) 717–726. doi:10.1016/j.ces.2013.09.031.

[55] G. Reynolds, R. Ingale, R. Roberts, S. Kothari, B. Gururajan, Practical application of roller compaction process modeling, Computers and Chemical Engineering 34 (7) (2010) 1049–1057. doi:10.1016/j.compchemeng.2010.03.004.

[56] G. Y. Gun, S. A. Stebunov, D. Y. Ganelin, A. A. Frolov, Computer modeling and investigation of the process of rolling or porous materials, Soviet Powder Metallurgy and Metal Ceramics 11 (251) (1983) 21–26.

[57] G. Y. Gun, S. A. Stebunov, V. P. Katashinskii, Computer modeling and investigation of the metal powder rolling process, Soviet Powder Metallurgy and Metal Ceramics 1 (277) (1986) 10–14.

[58] A. Ibrahimbegovic, Nonlinear Solid Mechanics : Theoretical Formulations and Finite Element Solution Methods, 2009.

[59] O. Pantalé, J.-L. Bacaria, O. Dalverny, R. Rakotomalala, S. Caperaa, 2D and 3D numerical models of metal cutting with damage effects, Computer Methods in Applied Mechanics and Engineering 193 (2004) 4383–4399. doi:10.1016/j.cma.2003.12.062.

[60] M. Souli, F. Erchiqui, Experimental and numerical investigation of instructions for hyperelastic membrane inflation using fluid structure coupling, Computer Modeling in Engineering & Sciences 77 (3) (2011) 183–200. doi:10.3970/cmes.2011.077.183.

[61] P. U. Dassault Systems, ABAQUS Documentation.

[62] D. J. Benson, S. Okazawa, Contact in a multi-material Eulerian finite element formulation, Computer Methods in Applied Mechanics and Engineering 193 (2004) 4277–4298. doi:10.1016/j.cma.2003.12.061.

[63] J.-h. Yoon, S. H. Jeong, Material Properties and Compressibility Using Heckel and Kawakita Equation with Commonly Used Pharmaceutical Excipients, Journal of Pharmaceutical Investigation 40 (4) (2010) 237–244.

[64] H. Hiestand, D. Smith, Indices of tableting performance, Powder Technology 38 (2) (1984) 145–159. doi:10.1016/0032-5910(84)80043-1.

[65] S. Helwany, Applied Soil Mechanics with ABAQUS, 2007.

[66] L. H. Han, J. a. Elliott, a. C. Bentham, a. Mills, G. E. Amidon, B. C. Hancock, A modified Drucker-Prager Cap model for die compaction simulation of pharmaceutical powders, International Journal of Solids and Structures 45 (2008) 3088–3106. doi:10.1016/j.ijsolstr.2008.01.024.

[67] C.-Y. Wu, O. Ruddy, A. Bentham, B. Hancock, S. Best, J. Elliott, Modelling the mechanical behaviour of pharmaceutical powders during compaction, Powder Technology 152 (1) (2005) 107 – 117. doi:https://doi.org/10.1016/j.powtec.2005.01.010.

[68] A. Michrafy, D. Ringenbacher, P. Tchoreloff, Modelling the compaction behaviour of powders: Application to pharmaceutical powders, Powder Technology 127 (2002) 257–266. doi:10.1016/S0032-5910(02)00119-5.

[69] I. Sinka, J. Cunningham, a. Zavaliangos, The effect of wall friction in the compaction of pharmaceutical tablets with curved faces: a validation study of the Drucker–Prager Cap model, Powder Technology 133 (1-3) (2003) 33–43. doi:10.1016/S0032-5910(03)00094-9.

[70] J. C. Cunningham, I. C. Sinka, a. Zavaliangos, Analysis of tablet compaction. I. Characterization of mechanical behavior of powder and powder/tooling friction, Journal of Pharmaceutical Sciences 93 (8) (2004) 2022–2039. doi:10.1002/jps.20110.

[71] K. Lamarche, D. Buckley, R. Hartley, F. Qian, S. Badawy, Assessing materials ' tablet compaction properties using the Drucker – Prager Cap model, Powder Technology 267 (2014) 208–220. doi:10.1016/j.powtec.2014.06.050.

[72] A. Krok, M. Peciar, R. Fekete, Numerical investigation into the influence of the punch shape on the mechanical behavior of pharmaceutical powders during compaction, Particuologydoi:10.1016/j.partic.2013.12.003.

[73] B. Zhang, M. Jain, C. Zhao, M. Bruhis, R. Lawcock, K. Ly, Experimental calibration of density-dependent modified Drucker-Prager/Cap model using an instrumented cubic die for powder compact, Powder Technology 204 (1) (2010) 27–41. doi:10.1016/j.powtec.2010.07.003.

[74] J. Almanstötter, A modified Drucker–Prager Cap model for finite element simulation of doped tungsten powder compaction, International Journal of Refrac-

tory Metals and Hard Materials 50 (2015) 290–297. doi:10.1016/j.ijrmhm.2015.02.005.

[75] I. Aydin, B. J. Briscoe, K. Y. Şanlitürk, The internal form of compacted ceramic components: A comparison of a finite element modelling with experiment, Powder Technology 89 (3) (1996) 239–254. doi:10.1016/S0032-5910(96)03188-9.

[76] M. P. Doremus, J. Prado, Model Input data - Failure, in: Modelling of Powder Die Compaction, Springer-Verlag London, 2008, pp. 95–103. doi:10.1007/978-1-84628-099-3.

[77] L. Perez-Gandarillas, Dry granulation process and compaction behavior of granulated powders (doctoral dissertation), 2016.

[78] A. Michrafy, J. A. Dodds, M. S. Kadiri, Wall friction in the compaction of pharmaceutical powders: Measurement and effect on the density distribution, Powder Technology 148 (1) (2004) 53–55. doi:10.1016/j.powtec.2004.09.021.

[79] A. Roberts, The influence of granular motion on the volumetric performance of enclosed screw conveyors, Powder Technology 104 (1999) 56–67. doi:10.1016/S0032-5910(99)00039-X.

[80] L. Pezo, A. Jovanović, M. Pezo, R. Čolović, B. Lončar, Modified screw conveyor-mixers – discrete element modeling approach, Advanced Powder Technology 26 (2015) 1391–1399. doi:10.1016/j.apt.2015.07.016.

[81] Q. Hou, K. Dong, A. Yu, Dem study of the flow of cohesive particles in a screw feeder, Powder Technology 256 (2014) 529–539. doi:10.1016/j.powtec.2014.01.062.

[82] O. Imole, D. Krijgsman, T. Weinhart, V. Magnanimo, B. C. Montes, M. Ramaioli, S. Luding, Reprint of "experiments and discrete element simulation of the dosing of cohesive powders in a simplified geometry", Powder Technology 293 (2016) 69–81. doi:10.1016/j.powtec.2015.07.052.

[83] P. Moysey, M. Thompson, Modelling the solids inflow and solids conveying of single-screw extruders using the discrete element method, Powder Technology 153 (2005) 95–107. doi:10.1016/j.powtec.2005.03.001.

[84] M. Bi, F. Alvarez-Nunez, F. Alvarez, Evaluating and modifying johanson's rolling model to improve its predictability, Journal of Pharmaceutical Sciences 103 (2014) 2062–2071. doi:10.1002/jps.24012.

[85] A. Mazor, L. Perez-Gandarillas, A. de Ryck, A. Michrafy, Effect of roll compactor sealing system designs: A finite element analysis, Powder Technology 289 (2016) 21–30. doi:10.1016/j.powtec.2015.11.039.

[86] Y. Liu, C. Wassgren, Modifications to johanson's roll compaction model for improved relative density predictions, Powder Technology 297 (2016) 294–302. doi:10.1016/j.powtec.2016.04.017.

[87] P. Cundall, O. Strack, A discrete numerical model for granular assemblies, Géotechnique 29 (1979) 47–65. doi:10.1680/geot.1979.29.1.47.

[88] H. Hertz, Über die berührung fester elastischer körper (on contact between elastic bodies), Journal für reine und angewandte Mathematik 92 (1881) 156–171.

[89] N. Brilliantov, F. Spahn, J. Hertzsch, T. Pöschel, A model for collisions in granular gases, Physical Review E 53 (1996) 5382. doi:10.1103/PhysRevE.53.5382.

[90] Liggghts®, http://www.cfdem.com/.

[91] R. G. Keys, Cubic Convolution Interpolation for Digital Image Processing, IEEE TRANSACTIONS ON ACOUSTICS, SPEECH, AND SIGNAL PROCESSING 29 (6) (1981) 1153–1160.

[92] J. A. Parker, R. V. Kenyon, D. E. Troxel, Comparison of interpolating methods for image resampling, IEEE Transactions on Medical Imaging 2 (1) (1983) 31–39. doi:10.1109/TMI.1983.4307610.

[93] A. N. Al-Rabadi, Robust control using lmi transformation and neural-based identification for regulating singularly-perturbed reduced order eigenvalue-preserved dynamic systems, Recent Advances in Robust Control - Novel Approaches and Design Methods, Dr. Andreas Mueller (Ed.), InTech (2011).doi:10.5772/20723.

[94] K. Csordas, P. Kleinebudde, Evaluation of the performance of different types of roll compactors, Powder Technologydoi:http://dx.doi.org/10.1016/j.powtec.2017.04.009.

List of Figures

List of Tables

Nomenclature

Acronyms

ALE	Arbitrary Lagrangian Eulerian
CEL	Coupled Eulerian-Lagrangian
CG	Coarse Grained
DEM	Discrete Element Method
FE	Finite Element
FEM	Finite Element Method
PID	Proportional Integral Derivative
PLC	Programmable Logic Controller

Other Symbols

$[C]$	Damping matrix	[]
$[F]$	External force matrix	[N]
$[K]$	Stiffness matrix	[N/mm2]
$[M]$	Mass matrix	[kg]
α	Nip/gripping angle	[deg]
$\ddot{\vec{u}}$	Displacement	m
Δt_{cr}	Critical time step	$[s]$
δW_{ext}	Total external work	[J]
δW_{int}	Total internal work	[J]

$\dot{\tilde{u}}$	Velocity	$[\frac{m}{s}]$
$\dot{m}_r$	Outlet mass flow rate from roll compactor	[units]
$\dot{m}_s$	Inlet mass flow rate from screw conveyor	[units]
ϵ	Strain vector	[-]
Ω_ζ	Arbitrary reference domain (ALE domain)	
Ω_X	Material domain	
Ω_x	Spatial domain	
$\overrightarrow{\zeta}$	Arbitrary coordinates	
$\overrightarrow{X}$	Lagrangian coordinates	
$\overrightarrow{x}$	Eulerian coordinates	
ρ	Mass density	$[\frac{kg}{mm^3}]$
σ_α	Pressure at angle α	[MPa]
σ_θ	Pressure at angle θ	$[MPa]$
θ	Feeding angle	[deg]
$\tilde{u}$	Displacement	[m]
B	Nodal displacement vector	[m]
c	Speed of sound	m/s
c_s	Screw constant	[-]
D	Gap between rolls	[mm]
D	Roll diameter	[mm]

E	Young's modulus	$[\frac{N}{mm^2}]$
F	Roll force	[N]
N	Interpolation function	[-]
Rd	Ribbon's relative density	[-]
S_1	Inlet roll compactor boundary	[-]
S_2	Contact boundary surface between powder and roll	[-]
S_4	Oulet roll compactor boundary	[-]
t_{n+1}	New time step	[s]
t_n	Old time step	[s]
U	Displacement vector	[m]
v	Fluid velocity	m/s
V_0	Initial velocity of powder	[-]
W	Roll width	[mm]

Appendix

Comparison of vertical stress, σ_{22} on the powder for two different cases of inlet feeding velocity 0.01 m/s (left column) and 0.015 m/s (right column).

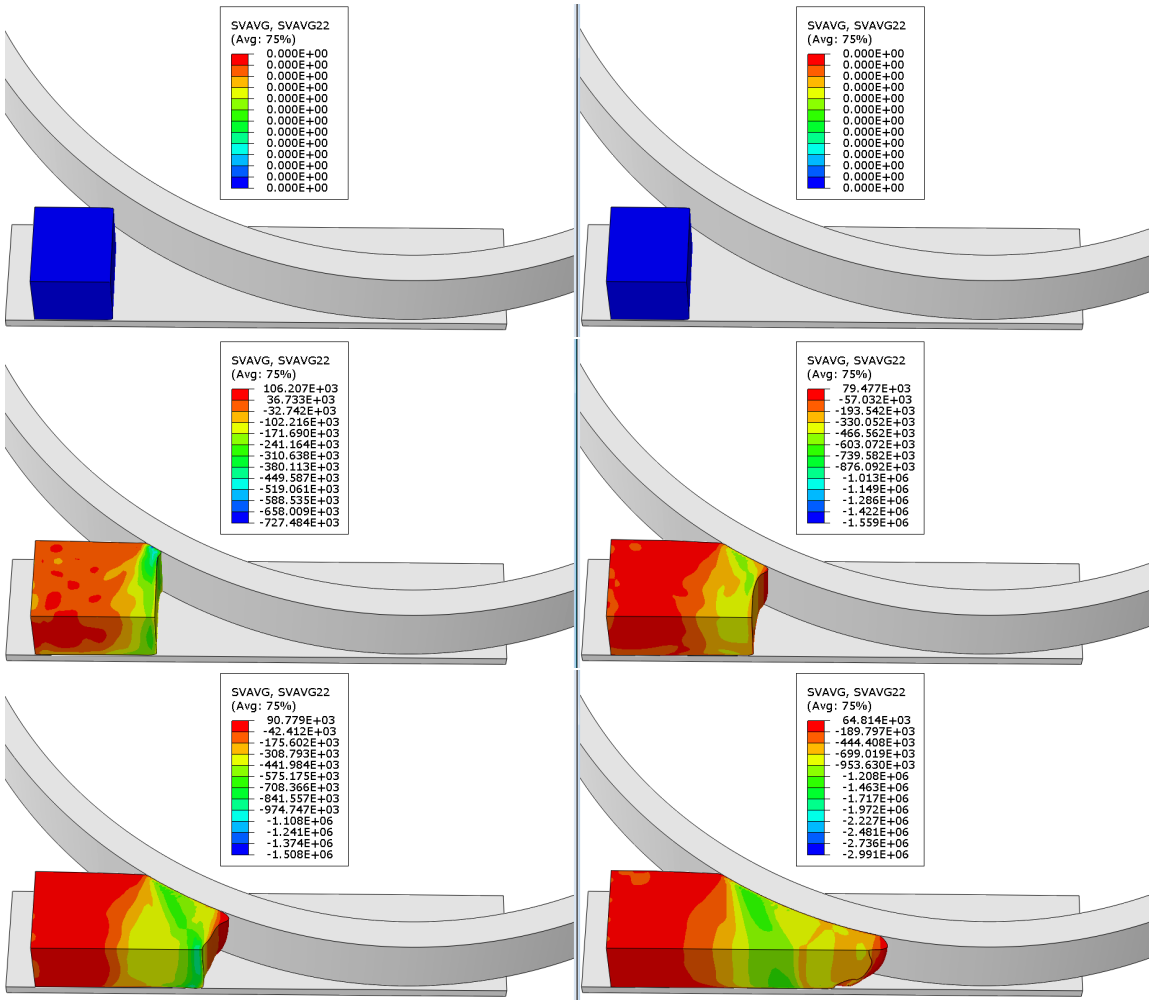

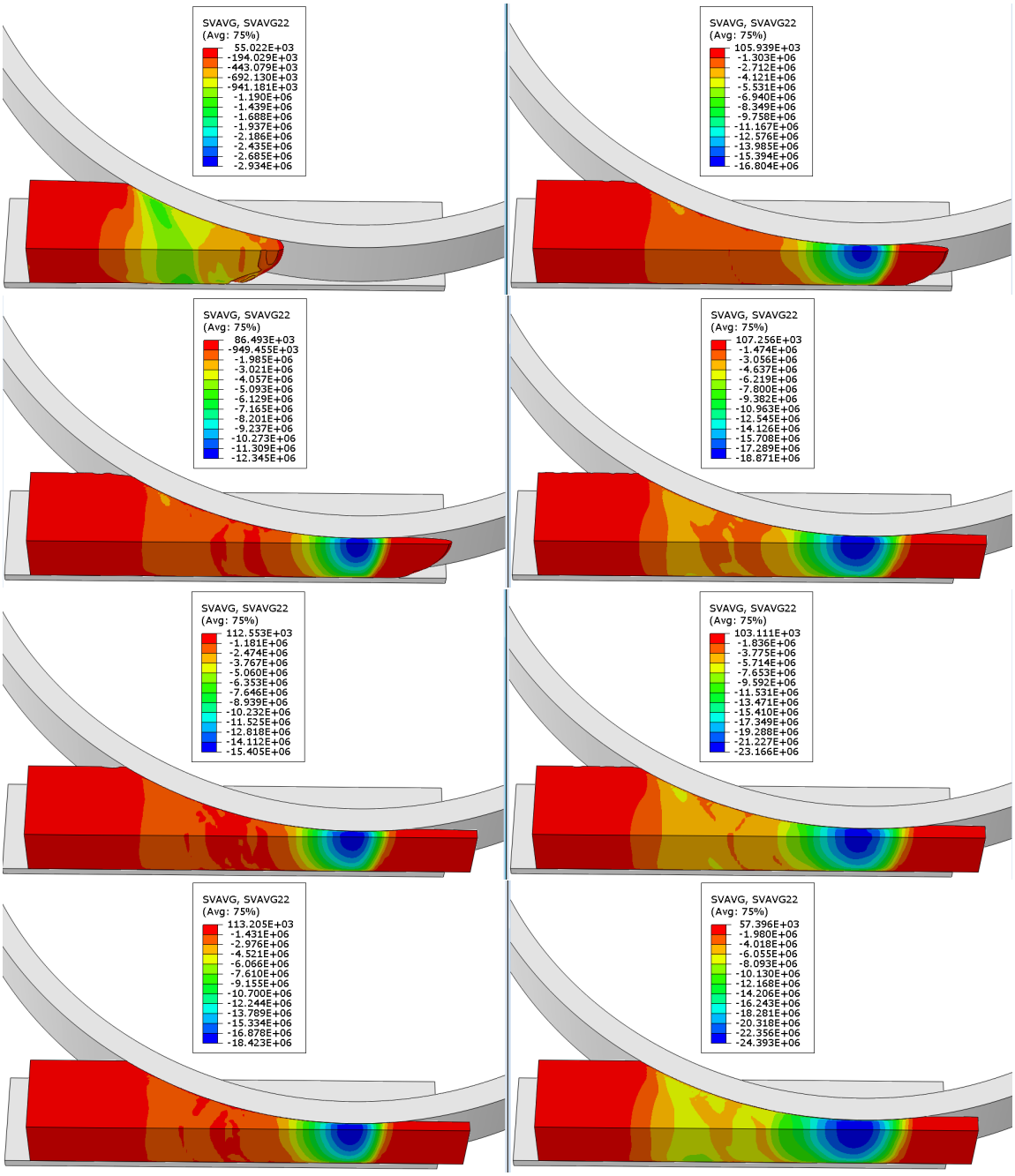

Figure 5.10: Comparison of vertical stress, σ_{22} in CEL FE model

Comparison of powder relative density for two different cases of inlet feeding velocity 0.01 m/s (left column) and 0.015 m/s (right column).

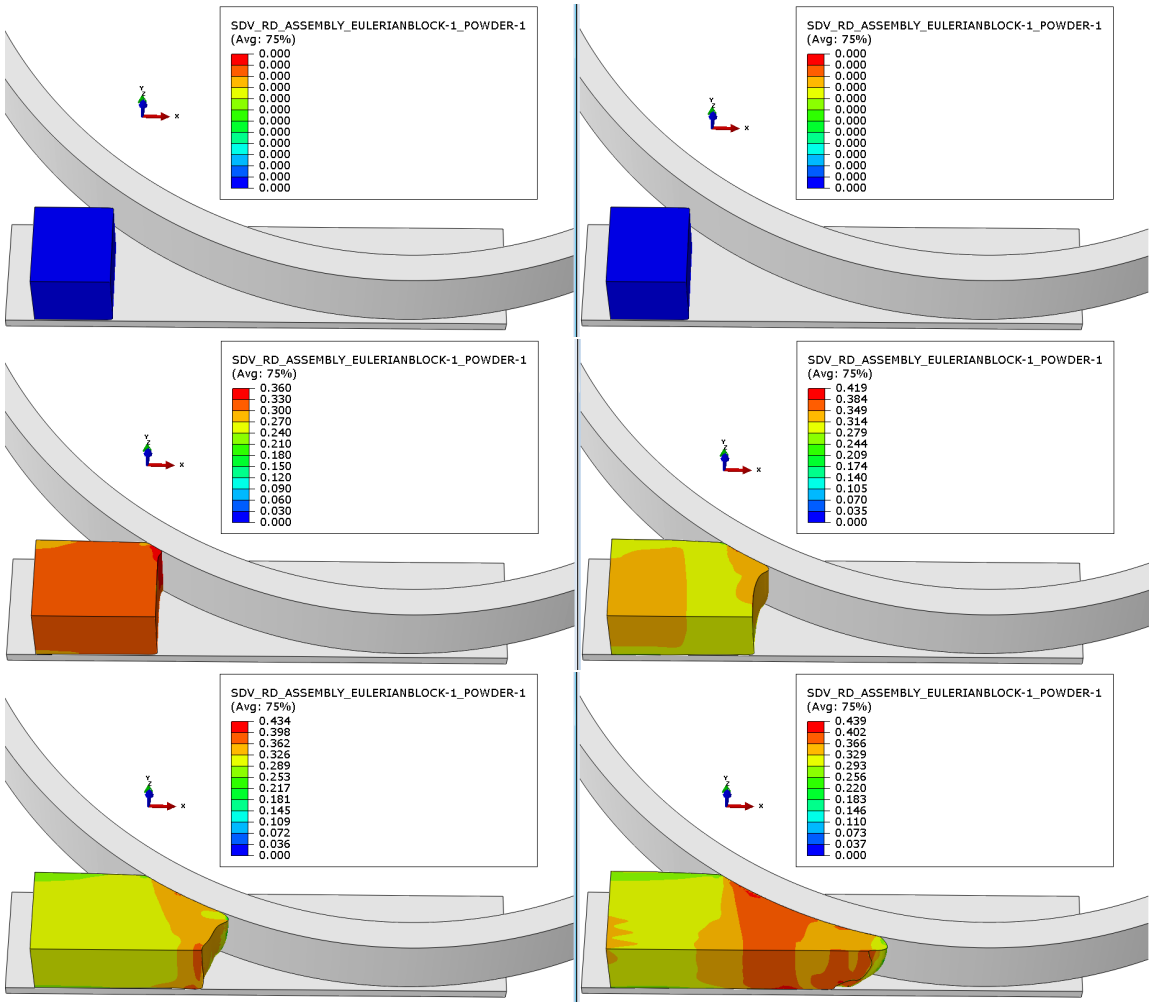

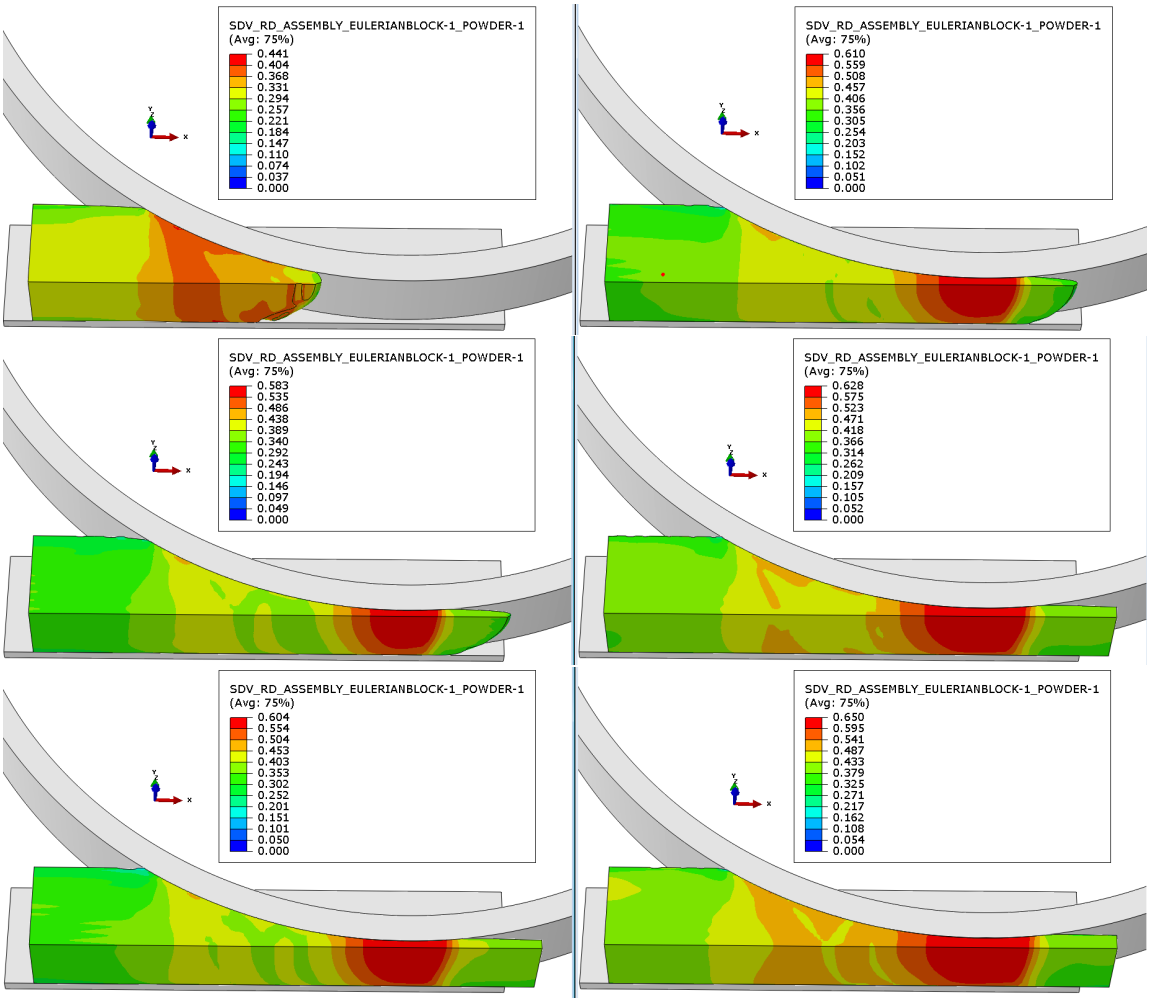

Figure 5.11: Comparison of powder relative density in CEL FE model

Modélisation du compactage à rouleaux par la méthode des éléments finis

Dans l'industrie pharmaceutique, la granulation sèche par compactage à rouleaux est un procédé d'agglomération de poudres en granulés pour améliorer les propriétés d'écoulement nécessaire pour le procédé de compression en matrice. Comprendre le procédé de compactage à rouleaux et optimiser l'efficacité de production est limitée par l'utilisation de l'approche expérimentale à cause du coût élevé des poudres, le temps des essais et la complexité du procédé.

Dans ce travail, une méthode d'éléments finis en 3D, est développée dans le but d'identifier les paramètres critiques du matériau et du procédé pour le contrôle de la qualité de la production. Le modèle de comportement de Drucker-Prager Cap est utilisé pour décrire le comportement en compression de poudres et sa calibration est déterminée à partir des essais standard. Pour surmonter la complexité liée à l'existence de deux mécanismes différents, l'alimentation en poudre par une vis sans fin et le compactage entre les rouleaux, une nouvelle méthode d'interfaçage entre la méthode des éléments discrets (DEM) employée pour décrire l'écoulement dans l'alimentation et la méthode des éléments finis (FEM) utilisée pour le compactage entre les rouleaux est développée. Enfin, pour une modélisation de compactage de rouleaux plus réaliste, prenant en compte la variation de l'entrefer entre les rouleaux, une nouvelle approche de couplage Euler-Lagrange est proposée.

Les résultats de simulations par éléments finis montrent clairement l'effet des différents paramètres du procédé sur les distributions de pression et de densité dans la zone de compactage. En outre, les résultats montrent que l'utilisation de plaques de confinement de la poudre entre les rouleaux, développe une distribution de pression et de densité non homogène dans le compact, avec une densité plus élevée au centre et plus faible aux bords. D'autre part, l'utilisation de rouleaux dont l'un est surmontée d'une jante de confinement, a montré une distribution de propriétés globalement plus uniforme sur la largeur du compact avec des valeurs légèrement plus élevées aux bords qu'au centre. La méthodologie combinant les méthodes DEM & FEM montre clairement une corrélation directe entre la vitesse des particules entraînées par la vis dans la zone d'alimentation et la pression du rouleau. Tous les deux oscillent avec la même période. Cela se traduit par un compact anisotrope avec un profile de densité variant de manière sinusoïdale le long de sa largeur. Afin d'étudier la capacité du modèle à prédire les propriétés des compacts produits par compactage à rouleaux, les prédictions par simulations numériques sont comparées aux données de la littérature et validées par des mesures spécifiques.

Mots-Clés: *Compression de poudres, Méthode des éléments finis, Compactage à rouleaux, Drucker-Prager Cap, Couplage Elements Discrets - Elements Finis méthodes (DEM-FEM), Coupled Eulerian-Lagrangian (CEL)*

This page intentionally left blank.

Modeling of roll compaction process by finite element method

In the pharmaceutical industry, dry granulation by roll compaction is a process of size enlargement of powder into granules with good flowability for subsequent die compaction process. Understanding the roll compaction process and optimizing manufacturing efficiency is limited using the experimental approach due to the high cost of powder, time-consuming and the complexity of the process.

In this work, a 3D Finite Element Method (FEM) model was developed to identify the critical material properties, roll press designs and process parameters controlling the quality of the product. The Drucker-Prager Cap (DPC) model was used to describe the powder compaction behavior and was determined based on standard calibration method. To overcome the complexity involving two different mechanisms of powder feeding by the screw and powder compaction between rolls, a novel combined approach of the Discrete Element Method (DEM), used to predict the granular material flow in the feed zone and the Finite Elements Method (FEM) employed for roll compaction, was developed. Lastly, for a more realistic roll compaction modelling, allowing the fluctuation of the gap between rolls, a Coupled-Eulerian Lagrangian (CEL) approach was developed.

FEM simulation results clearly show the effect of different process parameters on roll pressure and density distribution in the compaction zone of powder between the rolls. Moreover, results show that using a cheek-plates sealing system causes a nonuniform roll pressure and density distribution with the highest values in the middle and the lowest at the edges. On the other hand, the resultant pressure and density distributions with the rimmed-roll obtained higher values in the edges than in the middle and overall a more uniform distribution. The combined DEM-FEM methodology clearly shows a direct correlation between the particle velocity driven by the screw conveyor to the feed zone and the roll pressure, both oscillating in the same period. This translates into an anisotropic ribbon with a density profile varying sinusoidally along its length. To validate the results, the simulations are compared with literature and experimentally measured values in order to assess the ability of the model to predict the properties of the produced ribbons.

Keywords: *Powder compaction, Finite Element Method, Roll compaction, Drucker-Prager Cap, Coupled Discrete Element - Finte Element methods (DEM-FEM), Coupled Eulerian-Lagrangian (CEL)*